Michaela Zagler, B.Eng.

Establishing a Procedure for Transferring Hot Melt Extrusion Processes Based on Physical Similarities

MASTER`S THESIS

to achieve the university degree of

Diplom-Ingenieurin

Master`s degree programme: Advanced Materials Science

submitted to

Graz University of Technology

Supervisor:

Univ.-Prof. Dipl.-Ing. Dr.techn. Franz Stelzer

Institute for Chemistry and Technology of Materials

Co-supervisor:

Dipl.-Ing. Dr. Andreas Witschnigg

Research Center Pharmaceutical Engineering GmbH

Graz, August 2016

AFFIDAVIT

I declare that I have authored this thesis independently, that I have not used other than the declared sources/resources, and that I have explicitly indicated all material which has been quoted either literally or by content from the sources used. The text document uploaded to TUGRAZonline is identical to the present master‘s thesis.

Date

Signature

Abstract

Most of the newly developed active ingredients are crystalline and thus they have a low bioavailability. The adsorption of these substances in the human body therefore is taking place slower. Hot melt extrusion (HME) of pharmaceutical solid dosage forms is a promising option to overcome this issue by producing a solid molecular dispersion of an active pharmaceutical ingredient (API) in a matrix material. Within this master´s thesis a procedure for transferring HME processes is established. The development of new formulations is mainly done on small lab scale extruders due to the expensive APIs. For a later production “scale-up” procedures play an important role in this industry.

The aim of this study is to transfer the HME process from a co-rotating twin screw extruder (D_o = 18 mm) to a smaller one (D_o = 15.6 mm) and thereby receiving intermediate products with similar properties. Via an analysis of the hot melt extrusion process on the model extruder it is shown that only the mass temperature has got a significant (adverse) effect on the dissolution behaviour of the intermediate products. Neither the glass transition temperature nor the content uniformity of the pellets is significantly influenced by the other varying process parameters. While transferring the process, the focus should therefore be mainly on the mass temperature.

The screw configuration of the target extruder is assembled according to the unrolled screw length and the pitch or offset angle of each screw element from the model extruder. The process input parameters are calculated according to the method of Menges and Feistkorn (based on the model theory). The method of Rauwendaal serves as comparison. The thermal properties, dissolution behaviour and content uniformity of the subsequent manufactured intermediate products are investigated and afterwards compared to the values of the respective sample from the model extruder.

By comparing the process output parameters a good correlation of the specific mechanical energy consumption (SMEC) values of the samples from the model extruder and the respective scaled-down samples calculated according to the method of Menges and Feistkorn could be found. Same behaviour can be seen concerning the thermal properties, where the glass transition temperatures of the samples from Menges and Feistkorn are always closer to the ones of the samples from the model extruder (even one identical mean value) than the samples from Rauwendaal are. However, the dissolution behaviour of all samples differs significantly, with a few exceptions. The deviations in the beginning of the testing are caused by the testing method (“paddle”-apparatus). Therefore, a “basket”-apparatus is suggested for future studies of the dissolution behaviour of the binary material system used. The overall lower drug release of the samples from the target extruder is caused by the higher T_{mass} during their HME due to the given boundary conditions. The content uniformity of all intermediate products to be analysed was confirmed.

Kurzfassung

Viele der neu entwickelten Arzneistoffe sind kristallin und haben daher eine geringere Bioverfügbarkeit. Sie werden langsamer vom menschlichen Organismus aufgenommen. Um dieses Problem zu übergehen, stellt die Schmelzextrusion als Verarbeitungsprozess fester, pharmazeutischer Darreichungsformen eine vielversprechende Option dar. Dabei werden aus einem Matrixmaterial und einem Wirkstoff feste molekulare Dispersionen hergestellt. Im Rahmen dieser Masterarbeit wird ein Verfahren entwickelt, um eine Übertragung dieses Prozesses zu ermöglichen. Auf Grund der teuren Wirkstoffe, geschieht die Entwicklung neuer Formulierungen meist auf einer Laboranlage. Für eine spätere kommerzielle Produktion kommt solch einem „Scale-up"-Verfahren in dieser Branche daher eine große Bedeutung zu. Ziel dieser Arbeit ist es, den Schmelzextrusionsprozess von einem gleichläufigen Doppelschneckenextruder (D_o = 18 mm) auf einen Kleineren (D_o = 15.6 mm) zu übertragen. Dabei sollen Zwischenprodukte mit ähnlichen Eigenschaften gewonnen werden. Mit Hilfe der Prozessanalyse am Modell-Extruder wird gezeigt, dass lediglich die Schmelztemperatur einen (unerwünschten) signifikanten Einfluss auf das Freisetzungsverhalten der Zwischenprodukte hat. Die Glasübergangstemperatur und die Verteilung des Wirkstoffs werden hingegen durch keinen der anderen variierenden Prozessparameter beeinflusst. Auf die Temperatur der Schmelze sollte deswegen während des Transferprozesses besonderer Acht gegeben werden.

Die Schneckenkonfiguration des Ziel-Extruders wird anhand der abgewickelten Schneckenlänge und der Steigung bzw. dem Versatzwinkel der einzelnen Schneckenelemente vom Modell-Extruder zusammengestellt. Für die Berechnung der einzustellenden Prozessparameter wird die auf der Modelltheorie basierende Methode von Menges und Feistkorn verwendet. Als Vergleich dazu dient die Methode von Rauwendaal. Die anschließend extrudierten Zwischenprodukte werden bezüglich ihrer thermischen Eigenschaften, ihrem Freisetzungsverhalten und der homogenen Verteilung des Wirkstoffs untersucht und mit den Werten der jeweiligen Proben vom Modell-Extruder verglichen. Eine Gegenüberstellung der Ausgangsparameter zeigt ein gute Übereinstimmung des spezifisch mechanischen Energieeintrags der Proben von Menges und denen des Modell-Extruders. Diese Konformität wiederholt sich bezüglich der thermischen Eigenschaften. Die Glasübergangstemperaturen der Proben von Menges sind stets näher an den Werten des Modell-Extruders (bei einer Probe sogar idente Mittelwerte) als die Proben von Rauwendaal. Das Freisetzungsverhalten aller Proben unterscheidet sich jedoch bis auf einige Ausnahmen deutlich. Der Grund für die anfänglichen Abweichungen liegt an der Testmethodik („Rührer"-Vorrichtung). Daher wird für zukünftige Untersuchungen dieses Materialsystems die „Korb"-Vorrichtung empfohlen. Die allgemein niedrigere Freisetzung der Proben vom Ziel-Extruder liegt an den höheren Schmelztemperaturen während deren Schmelzextrusion, verursacht durch die gegebenen Rahmenbedingungen. Eine homogene Verteilung des Wirkstoffs ist bei allen zu analysierenden Zwischenprodukten gegeben.

Acknowledgement

First, I would like to thank my supervisor Univ.-Prof. Dipl.-Ing. Dr.techn. Franz Stelzer. His door was always open whenever I had a question about my master´s thesis, especially regarding the chemical aspects.

My special thanks go to Dipl.-Ing. Dr. Andreas Witschnigg for his extraordinary support and guidance through my entire thesis. His valuable comments and remarks were very helpful.

Moreover, I want to thank Dipl.-Ing. Josip Matić, Dipl.-Ing. Julia Kruisz and Dipl.-Ing. Dr. Simone Eder for their support. I would also like to thank the Extrusion and Lab Team at RCPE for their help and, in particular, for the great working atmosphere. It was always a pleasure.

Finally, I want to thank my family who always stand behind me and supported me throughout my years of study. This would not have been possible without you.

Table of Contents

List of Figures

List of Tables

List of Abbreviations

Abbreviation	Meaning
a	Distance of screw shaft axes
A	Area
a, b, c, d	Model law exponents (single screw extruder)
AMS	Applied Manufacturing Science
API	Active pharmaceutical ingredient
A_s	Surface area
AV	Acceptance value
Br	Brinkman number
c	Concentration
c_{max}	Maximum concentration
c_p	Specific heat capacity (p = const.)
CU	Content uniformity
c_V	Specific heat capacity (V = const.)
D	Screw Diameter; Diffusion coefficient
dC/dt	Rate of dissolution
D_i	Core diameter of the screw
D_o	Outer diameter of the screw
DoE	Design of experiments
DSC	Differential scanning calorimetry
FEM	Finite element method
h	Channel depth; thickness of diffusion layer
H	Heating capacity; Enthalpy
HME	Hot melt extrusion
HPLC	High-performance liquid chromatography
i	Number of flights
K	Die conductance
k	Consistency factor; acceptability constant (CU-test)
L	Length
l, m	Material exponents
m	Flow exponent; mass
M	Reference value (CU-test)
$\dot{m}$	Melt throughput
M_D	Torque
MV	Mean value
M_w	Molecular weight
n	Screw speed; viscosity exponent
n. a.	Not available
P	Drive power
p	Pressure
PEG	Polyethylene glycol
Ph. Eur.	European Pharmacopoeia

PVAc	Polyvinyl acetate
PVCL	Polyvinyl caprolactam
$\dot{q}$	Specific heat flow density
Q	Heat quantity
R	Radius of tube
R_C	Biggest radius of the cone
r_C	Smallest radius of the cone
RCPE	Research Center Pharmaceutical Engineering GmbH
R_i	Inner radius of annular die gap
R_o	Outer radius of annular die gap
RP-HPLC	Reversed phase high-performance liquid chromatography
rpm	Revolutions per minute
RT_{max}	Maximum residence time
RTD	Residence time distribution
s	Pitch
SD	Standard deviation
SME	Specific mechanical energy
SMEC	Specific mechanical energy consumption
SPH	Smoothed particle hydrodynamics
T	Temperature
t	Residence time
T_{degr}	Degradation temperature
T_g	Glass transition temperature
T_m	Melting temperature
T_{mass}	Melt/mass temperature
T_r	Room temperature
TSE	Twin screw extruder
T_w	Wall temperature
U	Circumference
v	Circumferential speed
V	Volume
$\dot{V}$	Volume flow
$\dot{V}_D$	Pressure flow
V_{free}	Free volume
$\dot{V}_S$	Drag flow
$\bar{X}$	Mean value
α	Heat transfer coefficient
$\dot{\gamma}$	Shear rate
Δp	Pressure loss
ΔT_H	Temperature homogeneity (melt)
η, $\eta_{\_0}$	Viscosity, Dynamic viscosity
λ	Thermal conductivity
π_i	Characteristic quantity
ρ	Density
ϕ	Fluidity
ω, Ψ, x, ε, ξ, κ	Model law exponents (twin screw extruder)

1 Introduction

Hot melt extrusion (HME) is a novel continuous processing technology in the pharmaceutical industry, where molecular dispersions of an active pharmaceutical ingredient (API) in a matrix material are produced. Besides of being an efficient process, HME enhances the bioavailability of pharmaceutical dosage forms of poorly soluble APIs and is therefore able to control or further modify the release of the dispersed drug [1].

The development of new formulations is usually done at laboratory scale in order to save tons of expensive API. For later commercial production the scale-up procedure of a HME process plays an important role in the pharmaceutical technology. Since both the formulation of the material system and the process conditions are affecting the product quality attributes of the solid dosage forms, a transfer of a hot melt extrusion process requires proper considerations [2]. Furthermore, it is necessary to distinguish between three different “scenarios” [3]:

- Increasing the production output by increasing the batch size using the same extruder
- Increasing the production output by increasing the feed rate (and changes to other process input parameters) using the same extruder
- Increasing the production output by increasing the feed rate (and changes to other process input parameters) using another extruder with larger dimensions.

In the plastics industry scale-up/scale-down procedures are common practice, especially for single screw extruders. Regarding the scale up of HME processes only some guidelines already exist, but none of them yet regards the whole process (extruder and die dimensions, screw configuration and process conditions). This leads to the objective of this thesis, where a suitable transfer method for HME processes based on physical similarities shall be established.

2 The Objectives of the Master Thesis

In the scope of this master`s thesis a procedure for transferring a hot melt extrusion (HME) process from an 18 mm co-rotating twin screw extruder (TSE) to a 16 mm co-rotating TSE shall be established, where the properties of the intermediate products of both processes should be as identical as possible. Since both extruders already exist, the scale-down procedures are limited by the variation of the process input parameters and the screw configuration.

First of all, the HME process on the model extruder (*Pharma Extruder ZSK 18* from *Coperion GmbH*) will be investigated in general to find out which process input parameters affect the process/product performance the most and to find the best settings. Subsequently, the screw configuration of the target extruder (*PHARMALAB 16* twin-screw extruder from *Thermo Fisher Scientific Inc.*) will be assembled and the process input parameters will be calculated according to existing transfer methods in the plastics industry.

As material system Fenofibrate and Soluplus® (1:9) are used. By means of a strand pelletizer intermediate products will be obtained. These pellets are characterized afterwards. By comparing the process output parameters, the thermal properties, the dissolution behaviour and the content uniformity of the pellets extruded on both extruders, it shall be shown if the transfer procedure carried out is suitable.

3 Theoretical Basis

3.1 Hot melt extrusion process

As an introduction, this chapter provides a small overview of the hot melt extrusion (HME) process and its applications in the pharmaceutical industry.

3.1.1 Extrusion process

The extrusion process itself is well-known and has been developed since the 19th century, especially in the plastics industry [2]. Within the pharmaceutical industry this process, however, only obtained attention since the last two decades in the manufacturing of pharmaceutical dosage forms, like capsules, pellets, tablets, films and implants [4].

During the HME process, a blend of an active pharmaceutical ingredient (API) and a matrix system (e.g. polymer) are molten and mixed by means of heated barrels and the specific mechanical energy input introduced by a rotating screw (greater contribution – 80 %), whereby a solid dispersion is formed. Furthermore, the melt is conveyed towards a die, which shapes the material leaving the extruder. Excipients, like plasticisers, diluents, stabilizers and antioxidants, can also be added to the material blend and may enhance its process capability and further properties [2]. The main difference between a commercial plastics extruder and a pharmaceutical one are the parts of the extruder, which are in direct contact with the melt [4]. These parts have to fulfil certain regulatory requirements, e.g. the metallurgy must not be reactive, additive or absorptive with the extruded material [4].

Generally, an extrusion process line consists of the following parts: dosing units and a hopper (material feeding; optional side feeding with additional dosing unit), the extruder, a downstream processing unit and a monitoring system. The core part of the process line – the extruder – will be described in more detail below.

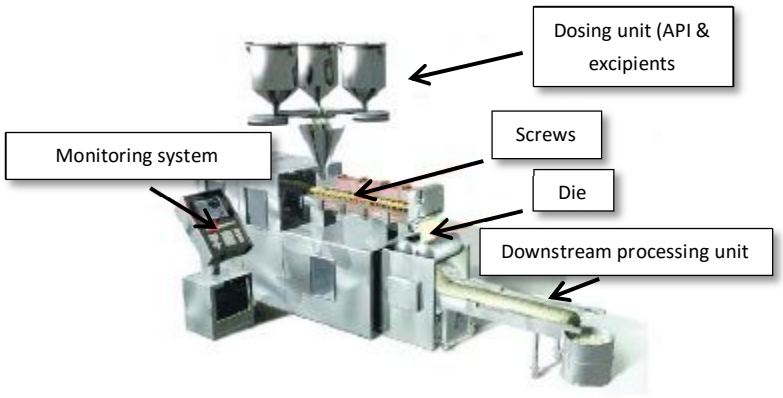

Figure 1: HME process line (adopted from [5])

Extruder types

The extruder itself consists of one or two rotating screws inside stationary barrels. At the end of the last barrel there is a die, which shapes the extruded material. This die can either have a cylindrical exit cross section (e.g. for pellets and solid rods), a slit exit cross section (e.g. for films) or an unregularly profile (e.g. for window profiles). An annular die gap is for example used for cable sheathing.

Single screw extruders are primarily used for melting and pressure build up, since their mixing capability is limited [6]. The mixing capabilities of twin screw extruders (TSEs) are much better and thus these types are the preferred approach for the pharmaceutical production, since one wants to obtain a well- dispersed mixture of API and excipients [1]. TSEs consist, as the name suggests, of two screws, which can either rotate in the same (co-rotating TSEs) or opposite direction (counter-rotating TSEs) and the screws can be non-intermeshing or fully intermeshing. The fully intermeshing and self-wiping co-rotating TSE is the most popular one, because they can be operated at high screw speeds, which implies high output rates, while maintaining good mixing and conveying properties [4]. The backflow of the material is minimized and the material bed is broken by the flights of the screw, thus there exists no continuous bed along the extruder [7]. Furthermore, the self-wiping design minimizes the non-movement of the material, thus it prevents localized overheating within the extruder [4]. The term “self-wiping” means that the flight of one screw wipes the root of the other screw and thereby emptying the compartment. This type of extruder is also used within this thesis.

Screw design

Regardless of the number of screws inside a barrel, every extruder consists of the following three sections in principle: a feeding, a compression (mixing and melting) and a metering zone (see Figure 2).

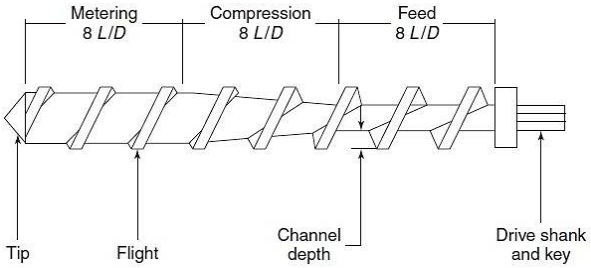

Figure 2: Different sections of a single screw extruder [8]

In the feeding zone the pressure is kept very low by a large pitch and/or channel depth in order to guarantee a constant feeding of the material blend. After the feeding zone, the channel depth and the pitch are decreased and thereby the pressure is increasing. At the same time, the heated barrel elements cause melting of the material system. Thus, the material blend is well mixed, homogenized and compressed in the compression zone [5]. The energy from the barrel heaters (20 %) and the heat generated by friction (80 %), as the material is sheared between the rotating screw and the wall of the stationary barrel, contribute to the

melting of the blend ([4], [5]). At the end of the compression zone, the remaining solid bed is ideally molten. The final section, the metering zone, stabilizes the melt and ensures that the product has a uniform thickness and shape [1].

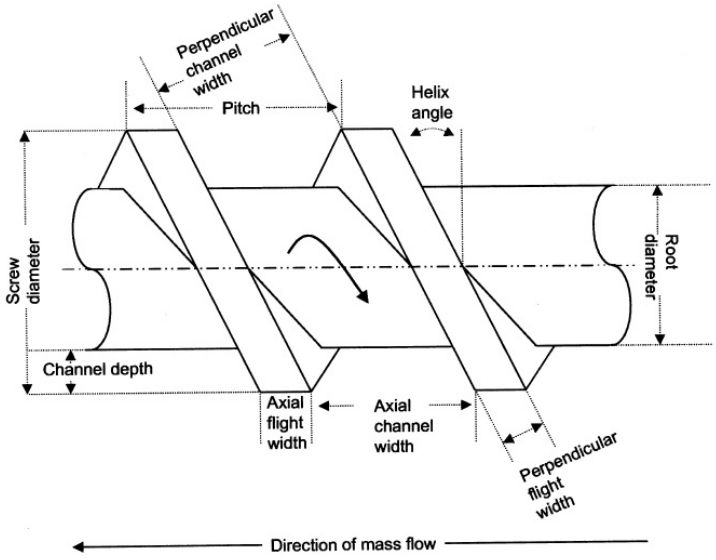

Figure 3: Screw geometry and important terms [5]

In the case of twin screw extruders (especially co-rotating ones) the screw is often segmented and there are many different elements, which can be used for assembling a certain screw configuration in order to optimize it for a particular application. The individual elements have a constant pitch and channel depth. The definition of these screw dimensions are shown in Figure 3. Dimensions like the pitch and the length of the respective elements are often given in terms of the L/D ratio, where L stands for the length and D for the (outer) screw diameter. An additional dimension, the unrolled screw length Z, can be calculated as follows:

$$Z = \frac{L}{sin\ \varphi} \quad with \quad \varphi = \tan^{-1}\left(\frac{s}{\pi \cdot D}\right) = [rad] \tag{1}$$

where s stands for the pitch of the screw element and φ for the pitch angle. This dimension is used within this thesis as scale-factor for assembling the screw configuration of the “target extruder”.

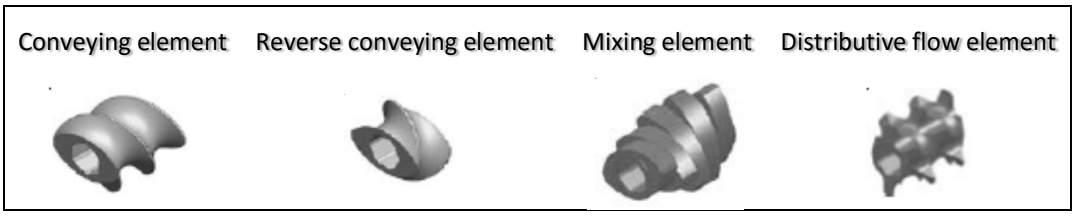

Figure 4: Screw elements of a *Thermo Fisher Scientific Pharma 16 HME* [9]

Figure 4 shows some screw elements, which can be used at the *Pharma 16 HME* (D = 15.6 mm) from *Thermo Fisher Scientific*, the “target extruder” of this thesis. Conveying elements are used in feeding, conveying and venting sections and vary in length and pitch. Elements with a smaller pitch convey the material faster than the ones with a bigger pitch, thus more pressure is build up. Reverse conveying elements convey the material in the counter direction and

therefore they are often used at the end of a mixing section in order to increase the residence time and filling rate of the material within this part of the extruder. Mixing elements, like a kneading block (see Figure 4), shear the material, whereby wide kneading disks (1/2 L/D) introduce higher shear rates into the material and narrow disks (1/8 L/D) improve dispersive mixing [8]. The offset of the kneading disks determines the conveying and mixing characteristics, too. The bigger the offset angles, the lower the conveying and the bigger the mixing properties. Distributive flow elements have a notched outer diameter and are thus not self-wiping. Within these elements the distributive flow dominates over the shear flow (low-energy mixing) [8].

3.1.2 Solid dispersions

Besides HME, the most relevant processes for manufacturing solid dispersions, in particular, solid molecular dispersions are hot spin mixing, co-evaporation, co-precipitation, freeze-drying, roll-mixing and embedding by means of spray drying [5]. The main advantage of a solid dispersion is the modulation of undesirable API properties, such as poor aqueous solubility, inducing higher bioavailability and faster dissolution [10]. Bioavailability is a measure for the absorption of an active pharmaceutical ingredient in the blood circulation [11].

A classification in order to identify solid dispersions in pharmaceutical research is shown in the table below [8]:

Table 1: Classification of solid dispersions (adopted from [8])

	Glassy suspension	**Crystalline suspension**	**Glassy solution**
Drug	amorphous	crystalline	amorphous
Matrix	amorphous	amorphous	amorphous
DSC signals	2 T_gs (matrix and drug)	T_g (matrix) + T_m (drug)	1 T_g

The goal of every drug product development is to obtain a stable API-excipient system, which maximizes the therapeutic potential of the API and facilitates its bioavailability. In order to achieve this goal, one has to understand the physicochemical behaviour and interactions between its constituents. The functionality of the end product is mainly determined by the properties of the (polymer) matrix material. There is a distinction between thermoplastic polymers regarding the release properties. For achieving an immediate release of the drug, one needs to use polymers like polyethylene glycol (PEG), polyvinylpyrrolidone (PVP), Vinylpyrrolidone/vinylacetate copolymer (Kollidon® VA) or PEG6000/vinylcaprolactam/ vinylacetate copolymer (Soluplus®). A sustained release of the drug is obtained by using polymers like ethylene vinyl acetate (EVA), Poly(L-lactic acid) (PLA) or silicone - or as an alternative lipid matrices. Since the physical/chemical stability and the availability of diverse forms are bigger in the crystalline state, the majority of APIs is available in that state. However, amorphous drugs would have better dissolution behaviour. [5], [8]

Within this master thesis a solid dispersion of the amorphous copolymer Soluplus® and the crystalline, lipid regulating drug Fenofibrate is prepared by means of the hot melt extrusion process.

3.1.3 Advantages and disadvantages

HME offers several advantages over other pharmaceutical production processes ([1], [2], [4], [5], [8], [10], [12]):

- Continuous process, which allows a fast production (high throughput rates) and product change with real time release (e.g. near infrared-spectroscopy)
- Increase of API bioavailability, especially for poorly soluble drugs ("40% of all new molecular entities have poor bioavailability" [4])
- Solvent-free process → no need of subsequent, time-consuming drying steps
- Taste masking for bitter APIs
- Wide range of available dosage forms, depending on the die and/or post processing steps (e.g. strand pelletizing or milling)
- Compared to the spray-drying process, more uniform dispersion due to the mixing and agitation imposed by the rotating screw(s) → de-aggregation of suspended particles in the melt → good content uniformity (CU)

However, HME faces also some disadvantages. Due to the high processing temperatures and the viscous energy dissipation, degradation of the API and excipient may occur during the process. Thus HME is limited in the selection of suitable APIs and excipients. Either one chooses a polymer that can be processed at relatively low processing temperatures or one chooses a drug, which is not that thermally labile, since all constituents must be thermally stable during the extrusion process. Another drawback is the high investment cost for the HME equipment. [2], [4], [8]

3.1.4 Applications in the pharmaceutical industry

Despite the several advantages of the HME process mentioned above, this technique is not yet a common manufacturing method for drug delivery systems – the number of pharmaceutical products on the market is limited [8]. Available commercial products are for example:

- *Kaletra* tablets, a protease inhibitor (APIs: lopinavir and ritonavir, excipient: Meltrex) from *Abbott GmbH*, which are used for the treatment of human immunodeficiency virus (HIV) infections [13]
- *Nurofen (Meltlets lemon)* - fast dissolving tablets from *Reckitt Benckiser Group plc.* with ibuprofen as API [14]
- *Nuvaring®* - a contraceptive vaginal ring from *MSD SHARP & DOHME GmbH* (APIs: etonogestrel and ethinylestradiol; excipients: EVA copolymer and magnesium stearate) [15]

Douroumis [8] further mentions the application of tablets for gastro-retentive controlled release systems. In general, HME applications shall fulfil the following two properties: solubility and bioavailability enhancement of the new poorly water-soluble APIs and the sustainment of drug release over an extended period of time ([2], [8]).

Work and research in this field needs still to be done, nonetheless, there are interesting new aspects published in the literature, yet – such as fast dispersing systems with foam like structures, in-situ salt formation and nanoparticles released from molecular dispersions processed by HME [5].

3.2 Scale-up/Scale-down – State of the art

The term "scale-up" is understood as the transfer from a laboratory system to an industrial production plant. By carrying out tests on the model, one gets information about the design and dimensioning of the industrial plant. "Scale-down" means the reverse procedure. If any problems occur during the production, it is possible to find the causes for them at a smaller scale by means of several model trials.

The following chapter gives insight into the basis of scale-up/-down procedures as well as into existing methods for single and twin screw extruders, including their dies.

3.2.1 Dimensional analysis

Technical and chemical problems can be described by mathematical relations. If these relations should be generally valid, they have to be formulated dimensionless. This has to be done with the help of the seven basic dimensions, namely: *M* for mass, *L* for length, *T* for time, *Θ* for thermodynamic temperature, *N* for amount of substance, *I* for electric current and I_v for light intensity. Other physical parameters, like velocity, are derived from these: v [$L\ T^{-1}$]. [16]

Regarding one specific problem, all parameters influencing the problem (should be mutually linearly independent) and the target parameter which is being searched, have to be listed at first. Afterwards, the relation between these parameters has to be formulated dimensionless, forming the basis for the π-theorem: *Every physical relation between n parameters can be reduced to a relation with only m = n – r dimensionless groups (Π_i- quantities) that are independent of each other,* whereby r stands for the rank of the dimensional matrix. [16], [17]

The relevant parameters are then used to set up a dimensional matrix. Table 2 shows an example of a dimensional matrix. The columns are the parameters and the rows the dimensions. The residual matrix should consist of the target parameter, important material and process parameters. By transferring the core matrix into a unity matrix by means of linear transformations of the rows, the Π_i- *quantities* are built. The nominator consists of one parameter of the residual matrix and the denominator consists of the parameters of the unity matrix with their respective exponents. [18], [19]

Table 2: Example of a dimensional matrix

	ρ	d	v	Δp	q
mass M	1	0	0	1	0
time T	3	-1	-2	1	-3
length L	0	0	-1	-2	-1
	core matrix			residual matrix	

After determining the Π_i- *quantities*, trials on the model device can be carried out and evaluated. The Π_i- *quantities* have to be varied by changing one input parameter. The respective other Π_i- *quantities* have to be hold constant during the measurement. [20]

The Π_i- *quantities* are scale-invariant and the basis for the theory of model, which says that two models are equal, if they are geometrically similar and all their Π_i- *quantities* have the same values [21]. Therefore, the scaled-up/-down device should have the same Π_i- *values* as the model device in order to guarantee their similarity.

3.2.2 Scale-up/scale-down of single screw extruders

There are many scale-up/scale-down strategies for single screw extruders that have been proposed in the past by different researchers ([22]–[29]). These methods are especially applied in the plastics industry. In the following, some of these common strategies including the model theory, which is the basis of all these methods, will be described.

Model theory

The aim of the model theory is the transfer of the process parameters and screw geometry from an optimised laboratory extruder to a production machine (or vice versa). It is based on the dimensional analysis (see 3.2.1) [24]. In order to guarantee that both extruders are equal their Π_i- *quantities* have to be the same. The first two dimensionless quantities shown in Table 3 are derived from energetic similarity of both extruders [29]. The others represent geometric and operating data.

Table 3: Set of $\boldsymbol{\pi_i}$ - *quantities* for a single screw extruder with $\boldsymbol{B_{1-4}}$ = constants (adapted from [29])

$\boldsymbol{\Pi_i}$**- *quantities***
$\pi_1 = \frac{P}{\dot{m} \cdot c_v \cdot (T_m - T_r)}$
$\pi_2 = \frac{H}{\dot{m} \cdot c_v \cdot (T_m - T_r)}$
$\pi_3 = \frac{L}{B_1 \cdot D^a}$
$\pi_4 = \frac{h}{B_2 \cdot D^b}$

$$\pi_5 = \frac{n}{B_3 \cdot D^c}$$

$$\pi_6 = \frac{s}{B_4 \cdot D^d}$$

Where P is the drive power of the motor, $\dot{m}$ is the melt throughput, c_v is the specific heat capacity of the melt at a constant volume, T_{mass} is the mass temperature, c is the ambient temperature, H is the heating capacity, h is the channel depth of a screw element and n is the screw speed of the extruder. Figure 5 shows the power balance of an extruder, which gives the dimensionless quantities π_1 to π_2. The energies introduced are the heating capacity H of the heated barrel elements, the power of the motor P and the energy stored in the material system, which is fed into the extruder ($\dot{m} \cdot c_v \cdot T_r$).

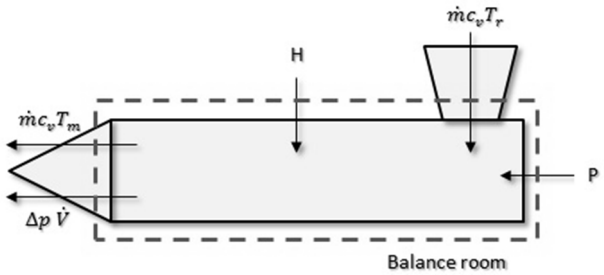

Figure 5: Power balance of an extruder (adapted from [30])

By means of this set of Π_i- *quantities*, which have to be held constant during scale-up/scale-down, the model laws can be generated. These laws picture the ratio of the respective geometry, extruder or process parameters as a function of the extruder diameter ratio plus one exponent, whereby the subscript "*0*" stands for the model extruder [29].

$$General\ equation\colon\ \frac{A}{A_0} = \left(\frac{D}{D_0}\right)^{exp} \tag{2}$$

The first four laws in Table 4 show the geometric and screw speed parameters of the extruder. They are independent from each other and can be applied to the scale-up/-down for a conventional extruder as well as for a grooved-fed one, which has got improved conveying characteristics. The other laws differ depending on which extruder is transferred. In the following, the focus will be on the model laws of conventional extruders.

Table 4: Model laws for a conventional single screw extruder (adapted from [29])

A	**Exponent**
L	a
h	b
n	c
S	d
$\dot{\gamma}$	$1 + c - b$

$\mathrm{T_m} - T_r$	$\frac{1}{1+\mathrm{l}}[1+\mathrm{a}-\mathrm{b}-\mathrm{d}+\mathrm{m}(1-\mathrm{b}+\mathrm{c})]$
p	$\frac{1}{1+\mathrm{l}}[1+\mathrm{a}-\mathrm{b}-\mathrm{d}+\mathrm{m}(1-\mathrm{b}+\mathrm{c})]$
$\dot{\mathrm{m}}$	$1+b+c+d$
P	$1+b+c+d+\frac{1}{1+\mathrm{l}}[1+\mathrm{a}-\mathrm{b}-\mathrm{d}+\mathrm{m}(1-\mathrm{b}+\mathrm{c})]$
H	$1+b+c+d+\frac{1}{1+\mathrm{l}}[1+\mathrm{a}-\mathrm{b}-\mathrm{d}+\mathrm{m}(1-\mathrm{b}+\mathrm{c})]$
M_D	$1+b+d+\frac{1}{1+\mathrm{l}}[1+\mathrm{a}-\mathrm{b}-\mathrm{d}+\mathrm{m}(1-\mathrm{b}+\mathrm{c})]$
$\bar{t}$	$a-c-d$
$\dot{q}$	$-a+b+c+d+\frac{1}{1+\mathrm{l}}[1+\mathrm{a}-\mathrm{b}-\mathrm{d}+\mathrm{m}(1-\mathrm{b}+\mathrm{c})]$
ΔT_H	$-\frac{2}{3}-a+2b+\frac{2}{3}c+d+\frac{1}{1+\mathrm{l}}[1+\mathrm{a}-\mathrm{b}-\mathrm{d}+\mathrm{m}(1-\mathrm{b}+\mathrm{c})]$

As an example of how the other laws are derived, the model law of the shear rate is deduced below. With the general relation for the shear rate

$$\dot{\gamma} \sim \frac{v}{h} \sim \frac{D \cdot n}{h} \tag{3}$$

follows with $n \sim D^c$ and $h \sim D^b$:

$$\dot{\gamma} \sim D^{1+c-b} \tag{4}$$

The model laws illustrated in Table 4 contain six exponents, whereby the exponents *m* and *l* can be determined from the viscosity curve of the material to be processed [24]:

$$l = -\frac{\log\left(\frac{\eta_2}{\eta_1}\right)}{\log\left(\frac{T_2}{T_1}\right)};\ \dot{\gamma} = const. \tag{5}$$

$$m = 1 + \frac{\log\left(\frac{\eta_3}{\eta_2}\right)}{\log\left(\frac{\dot{\gamma}_3}{\dot{\gamma}_2}\right)};\ T = const. \tag{6}$$

In order to carry out a full scale-up/scale-down of an extrusion process, the four remaining exponents need to be determined by means of sensible technical or constructional boundary conditions [29]. As an example for a constructional boundary condition a constant L/D-ratio could be mentioned. In this case, the exponent *a* would be one.

Existing scale-up/scale-down methods

In the following section, some existing scale-up/-down methods for single screw extruders will be described. Carley and McKelvey [28] suggest scale-up rules for two geometrically similar melt extruders. All dimensions are *x* times larger than the one of the smaller extruder, where *x* is the scale-up factor. If the extruders are run at the same screw speed and process the same

material, the output and power consumption will increase by the cubic power of *x* [28]. Furthermore, the pressure increases, the mass temperature and the shear rate remains equal in the case of geometrically similar extruders.

Rauwendaal [22] believes, however, that this theory will lead to undesirable performance of plastication extruders, especially for those processes with low Brinkman numbers. The Brinkman number (Br) is the ratio of the dissipated energy and the discharged heat [31]:

$$Br = \frac{\eta_0 * n^2 * D^2}{\lambda * (T_w - T_{m)}} \quad (7)$$

At low Brinkman numbers the feeding rate increases much faster than the melting rate, ideally, they should match. According to Rauwendaal, another major problem is the ratio of barrel surface area to throughput, which decreases strongly in scale-up [22]. Thus it is more difficult to conduct heat into or away from the polymer melt. In his opinion, the three most critical process parameters, which have to be kept constant during the scale-up, are the ratio of barrel surface area to throughput, the specific mechanical energy consumption (SMEC) and the increase of the solids conveying, melting and feeding rates [22]. Whereas the SMEC is obtained by dividing the power consumption by the throughput [32]. He therefore suggests two new scale-up methods. Both methods keep the SMEC constant and guarantee high throughput rates [22]:

1) Ratio of barrel surface area to throughput = constant (works well for high Br)
2) Melting rate = feeding rate (works well for low Br)

Nevertheless, the most commonly used scale-up method is the one of Maddock [22]. He increases the channel depth by the square root of the diameter ratio, while the screw speed is decreased by the square root [23]. Concerning this method, there are two main problems, which result in poor melt quality and a higher mass temperature in the scaled-up extruder [23]. The first problem is because of the larger increase of the feeding rate at low Br compared to the melting rate. The second problem is due to the rise of the specific energy consumption while scale-up. Chung [23] therefore presents a balanced scale-up method to avoid these problems. This is done by increasing the L/D-ratio of the compression section of the larger extruder in order to increase the melting capacity. The mass temperature is reduced by increasing the channel depth (balanced scale-up exponent: $0.5 < S < 1.0$) more than in the common scale-up method (exponent: 0.5). However, Chung shows that the melting capacity in his balanced method is still not as big as the output rate. Thus a scale-up of more than two times the diameter ratio is not recommended [23].

3.2.3 Scale-up/scale-down of twin screw extruders

There are as well as for single screw extruders also existing scale-up/-down methods for twin screw extruders (TSEs), which will be described in the following section ([3], [6], [30], [32]–[35]). Since the extruders, used for the trials in this thesis, are co-rotating ones, the focus will be on methods for co-rotating TSEs. Nevertheless, the method of Menges and Feistkorn [30] is

mentioned too. It is the only known method that allows a fully worked out scale-up/scale-down of TSEs. In addition to the calculation of the process parameters of the target extruder, its geometry parameters are calculated as well. By means of the model theory the scientists scaled down an 85 mm counter-rotating, tightly intermeshing extruder to a 58 mm counter-rotating extruder and to a 34 mm counter-rotating one. Polyvinylchloride was processed.

The dimensionless quantities shown in Table 5 are derived from energetic similarity of both extruders, similar flow conditions and heat transfer ([25], [30]).

Table 5: Set of $\boldsymbol{\Pi_i}$- *quantities* for an extruder (adapted from [25])

Similarity	$\boldsymbol{\Pi_i}$**- *quantities***
Specific drive power	$\pi_1 = \frac{P}{\dot{m} \cdot c_v \cdot (T_m - T_r)}$
Specific heating capacity	$\pi_2 = \frac{H}{\dot{m} \cdot c_v \cdot (T_m - T_r)}$
Pressure build up	$\pi_3 = \frac{p}{\rho \cdot c_v \cdot (T_m - T_r)}$
Mixing effect	$\pi_4 = \frac{\dot{V}_D}{\dot{V}_S}$
Heat transfer	$\pi_5 = \frac{\alpha \cdot h}{\lambda}$
Thermal homogeneity	$\pi_6 = \frac{\lambda \cdot \Delta T_H \cdot D \cdot L}{\dot{m} \cdot c_p \cdot (T_m - T_r) \cdot h}$

It must be mentioned here that Langecker [25] uses the same set of Π_i- *quantities* and model laws for the scale-up/scale-down of single screw extruders. The only difference between both stated model laws is its enlargement by Menges and Feistkorn. They add the relation of the difference between the respective screw diameter and the distance between the screw shaft axes *(D-a)*.

The model laws for a counter-rotating TSE are shown in Table 6. They follow the general equation (2).

Table 6: Model laws for a counter-rotating TSE (adapted from [30])

A	**Exponents**
L	$1+\omega$
(D – a)	Ψ
h	Ψ
n	-x
S	ε
$\dot{\gamma}$	$-(\psi + x - 1)$

$\mathrm{T_m} - T_r$	$\xi(\psi + \mathrm{x} - 1)$
p	$\xi(\psi + \mathrm{x} - 1)$
ṁ	$\varepsilon + \psi - x + 1$
P	$\varepsilon + \psi - x + 1 + \xi(\psi + \mathrm{x} - 1)$
H	$\varepsilon + \psi - x + 1 + \xi(\psi + \mathrm{x} - 1)$
M_D	$\varepsilon + \psi - x + 1 + \xi(\psi + \mathrm{x} - 1)$
$\bar{t}$	$\omega + x - \varepsilon + 1$
$\dot{q}$	$\psi + \varepsilon - x - \omega - 1 + \xi(\psi + \mathrm{x} - 1)$
ΔT_H	$2\psi + \varepsilon - x - \omega - 1 + \xi(\psi + \mathrm{x} - 1)$
i	0

The exponents of the model laws are linked via the viscosity of the processed material. From the comparison of the viscosity exponents, which are derived from the general viscosity equation and the equation of the dissipated energy [25],

$$\kappa(\psi + x - 1) = \varepsilon + 2\psi + x - 3 - \omega + \xi(\psi + x - 1) \tag{8}$$

the flight depth exponent can be written as follows [30]:

$$\psi = \frac{3 - \varepsilon - \kappa + \omega + \xi}{2 - \kappa + \xi} - x \cdot \frac{\xi + 1 - \kappa}{2 - \kappa + \xi} \tag{9}$$

The exponents κ and ξ can be determined by means of the viscosity curves of the processed material [30]:

$$\kappa = -\frac{ln\frac{\eta}{\eta_0}}{ln\frac{\dot{\gamma}}{\dot{\gamma}_0}}; T = const. \tag{10}$$

$$\xi = -\frac{ln\frac{T_m}{T_{m0}}}{ln\frac{\dot{\gamma}}{\dot{\gamma}_0}}; \eta = const. \tag{11}$$

After carrying out trials on the scaled down extruders (according to model laws), Menges and Feistkorn compared the process parameters of the model extruder and the target extruders (calculated and determined ones). The output parameters of the target extruder are in good agreement with the calculated ones, especially the drive power, heating capacity and melt throughput [30]. These results show that the model laws shown in Table 6 can be applied for the scale-up/scale-down of counter-rotating TSE.

Kohlgrüber [6] does not provide an explicit procedure for scaling up/down co-rotating TSEs. Instead, he gives some guidance on which parameters and conditions to focus on. He states that both extruders need to be geometrically and energetically similar and that they need to be processed with comparable parameters. Geometric similar means that the extruders have a similar D_o/D_i-ratio and number of flights and, in addition, the screw geometry parameters are dimensioned with respect to the screw diameter [6]. Energetic similar means that both extruders have similar power density (M_d/a^3), which is defined as the ratio of maximum torque of the screw M_d to the cube of the distance a of both screw shaft axes [6]. Further, Kohlgrüber lists some conditions, which should be kept constant during scale-up/scale-down of TSEs [6]:

- *Average shear rate* ensures comparable material treatment. With similar D_o/D_i-ratio, the screw speed *n* stays the same. If the ratio is not the same, *n* must be adjusted.
- *Melt pressure* in front of the die, because it has a huge impact on the mass temperature and product quality.
- *Residence time*
- *Specific heating*

The last two conditions are also mentioned by Thiry et al. [35] as key parameters of scale-up in their review paper of pharmaceutical extrusion. The residence time and the specific mechanical energy (SME) need to be held constant by adapting the process parameters, like feed rate, barrel temperatures, screw speed and screw configuration.

Dreiblatt [3] suggests three different scale-up methods for hot melt extrusion processes. Depending on which factor limits the process (volume, power or heat transfer) the proper method has to be chosen. The SMEC, mass temperature, residence time distribution (RTD) and the average shear rate are again considered as critical process parameters, which have to be held constant during scale-up. The three different methods are listed below [3]:

- Volume scale-up (limiting factor: free volume or residence time)
  The throughput of the larger extruder (index: 2) can be determined with the following relationship:

$$\dot{m}_2 = \left(\frac{V_{free2}}{V_{free1}}\right) \cdot \dot{m}_1 \tag{12}$$

  If the D_o/D_i- and the L/D-ratio of both extruders are similar, the ratio of free volume can be calculated as follows:

$$\frac{V_{free2}}{V_{free1}} = \left(\frac{D_2}{D_1}\right)^3 \tag{13}$$

  Moreover, if the D_o/D_i-ratio, the L/D-ratio and the screw speed of both extruders are similar, a constant average residence time, shear rate and filling ratio are obtained.

- Power scale up (limiting factor: SMEC)
  If the HME process consumes all of the available power, the specific mechanical energy input into the material gets the limiting factor:

$$SMEC\ (kWh/kg) = \frac{Torque\ (Nm/shaft) \cdot 2 \cdot n\ (1/min) \cdot \%Torque}{9550\ \cdot \dot{m}(kg/h)} \tag{14}$$

  Since the SMEC is maintained constant during scale-up, the maximum achievable throughput of the larger extruder (index: 2) is calculated as follows:

$$\dot{m}_{\,2,max.} = \left(\frac{Available\ power_2}{SMEC_1}\right) \tag{15}$$

- Heat transfer scale-up (limiting factor: heat transfer from barrel)
  The inner barrel surface area of the larger extruder can be determined with the relationship below to the condition that the D_o/D_i-ratio is similar:

$$Inner\ barrel\ surface\ area_2 = \left(\frac{D_2}{D_1}\right)^2 \cdot Inner\ barrel\ surface\ area_1 \tag{16}$$

  This method, however, is rarely applied in the pharmaceutical industry as the most energy is introduced via dissipation (shearing effect).

Rauwendaal [32] suggests scaling the throughput of a larger, geometric similar co-rotating TSE (index: 1) as follows:

$$\frac{\dot{m}_1}{\dot{m}_2} = \frac{D_1 \cdot\ n_1}{D_2 \cdot\ n_2} \tag{17}$$

Keeping the SMEC constant during scale-up/scale-down is desirable again. If the extrusion process is heat transfer limited, the throughput has to be calculated differently [32]:

$$\frac{\dot{m}_1}{\dot{m}_2} = \frac{{D_1}^2 \cdot\ n_1}{{D_2}^2 \cdot\ n_2} \tag{18}$$

If the average shear rate is kept constant during scale-up (see (19)), the screw speed of the larger extruder (index: 1) can be adjusted as follows [32]:

$$\dot{\gamma}_{ave} = K \cdot n = \frac{\pi \cdot\ D \cdot n}{h_{ave}} = const. \tag{19}$$

$$K_1 \cdot\ n_1 = K_2 \cdot\ n_2 \ \text{ with } \quad K = \frac{\pi \cdot D}{h_{ave}} \tag{20}$$

K is determined by the screw geometry of each extruder. If one wants to achieve the same performance of the mixing elements of both extruders, their degree of fill hast to be equal. In this case, the throughput of the larger extruder (index: 1) is calculated as follows [32]:

$$\frac{\dot{m}_1}{\dot{m}_2} = \frac{V_{e1}}{V_{e2}} = \frac{V_{free1} \cdot\ n_1}{V_{free2} \cdot\ n_2} \tag{21}$$

The effective volume of each extruder V_e is the product of the respective internal free volume V_{free} and the screw speed n. This is a possibility to determine the throughput of a larger extruder, which is not geometric similar to the model extruder.

3.2.4 Scale-up/scale-down of extrusion dies

The principal task of every extrusion die is to shape the melt into a (semi-)finished product. The die has a huge influence on the geometry and the properties of the resulting product and should not be neglected while scaling up/down an extrusion process.

In front of the die, at the inlet, there is a pressure build up. The so-called die head pressure determines the throughput of the extruder since the melt has to overcome it. If the pressure changes, the throughput changes and so do the dimensions of the extruded product [36]. Therefore, the pressure loss Δp in the die of the model extruder should be the same as the one of the target extruder. Another important parameter, which influences the product properties, is the temperature development in the die. The increase in temperature in the extrusion die due to the dissipation energy of the melt and the pressure loss, can be calculated as follows [37]:

$$\Delta T = \frac{\Delta p}{\rho \cdot c_p} \tag{22}$$

Michaeli [37] compiles in his book basic equations of flow processes in die channels with circular, rectangular and annular gap cross sections. The basis for the calculation of the flow processes are the conservation laws for mass, momentum and energy [37]. In order to dissolve these laws some assumptions need to be made. These assumptions include, among others, steady laminar flow of the melt, wall adhesion, a constant density of the melt and the disregard of gravity and in- and outlet effects [37].

Using the derived equations of the volume flow and the power-law model after *Ostwald* and *de Waele* ([37], [39]):

$$\dot{\gamma} = \phi \cdot \tau^m \tag{23}$$

$$\eta = k \cdot \dot{\gamma}^{n-1} \quad \text{with } k = \phi^{-\frac{1}{m}} \quad \text{and } n = \frac{1}{m} \tag{24}$$

one obtains the following relation between the pressure loss and the volume flow in the die, where *K* is the die conductance and depends on the die geometry (see Table 7):

$$\dot{V} = K \cdot \phi \cdot \Delta p^m \tag{25}$$

Table 7: Die conductance values of pseudoplastic materials (adopted from [37])

Geometry	Die conductance K
Tube	$K = \frac{\pi \cdot R^{m+3}}{2^m \cdot (m+3)} \cdot \left(\frac{1}{L}\right)^m$
Annular gap	$K = \frac{\pi \cdot (R_a + R_i) \cdot (R_a - R_i)^{m+2}}{2^{m+1} \cdot (m+2)} \cdot \left(\frac{1}{L}\right)^m$
Slit	$K = \frac{B \cdot H^{m+2}}{2^{m+1} \cdot (m+2)} \cdot \left(\frac{1}{L}\right)^m$ $(\mathrm{B/H} > 20)$

Cone	$K = \frac{\pi}{(m+3)\cdot 2^m} \cdot \left[\frac{3\cdot\left(\frac{R_C}{r_C}-1\right)}{m\cdot L\cdot\left(1-\left(\frac{r_C}{R_C}\right)^{3/m}\right)}\right]^m \cdot {r_C}^{m+3}$
Irregular profile	$K = \frac{2\cdot A^{m+2}}{(m+3)\cdot L\cdot U^{m+1}} \cdot \left(\frac{1}{L}\right)^m$ *(Approximation formula!)*

If several die geometries are connected in series the total pressure loss is the sum of the pressure losses of each die segment *i*, whereas the volume flow through each segment *i* is constant. The total die conductance is calculated as follows [40]:

$$\frac{1}{K} = \left(\sum_i \frac{1}{K_i^{1/m}}\right)^m \tag{26}$$

In order to return to the scale-up/scale-down of extrusion dies and its objective, namely receiving (semi-) finished products with similar properties – by processing the same material (equal material parameters), equal die conductance of both dies and an equal melt throughput, one obtains a similar pressure loss and temperature increase of the melt while passing the respective die.

Potente and Kramme [38] scaled up an annular die gap by means of the theory of model (see 3.2.2). First, they broke down the die into basic geometric elements (cylindrical bores and annular gaps) and then they established scale-up rules for each element that satisfy both full and partial similarity. If the inner and outer diameter and the length of the target die can be varied, full similarity is obtained. This, however, cannot always be realised in practice because there may be already certain boundary conditions like a constant outside diameter. As key parameters, which should be kept constant during die scale-up/scale-down in order to guarantee identical product properties, they consider the pressure loss Δp, the melt throughput $\dot{m}$ and the deformation γ. [38]

They analysed the calculated flow parameters (e.g. pressure drop) of the scaled up die by finite element methods (FEMs) with the program POLYFLOW and compared them to the ones of the model die. Good conformity could be shown.

3.3 Design of experiments

Design of experiments (DoE) is used to get as much information about a process/product as possible by carrying out as few efficient trials as necessary [41]. A further objective is to understand which input variables affect the process/product performance the most and besides find the best settings for these variables to obtain satisfactory output(s) [42]. DoE investigates the whole factor space evenly. Each factor is shifted several times at different boundary conditions, so that a clear allocation of the causes of the effects is possible [43].

Thereby, the success of each designed experiment is based on good planning, appropriate choice of design and statistical analysis of the gained data [44].

First of all, it is necessary to understand the process behaviour, its inputs (parameters) and outputs (e.g. quality characteristics of a product). This is done best by creating a general model of the process (see Figure 6). On the left side all controllable parameters, which affect the process, are listed. Below, the either uncontrollable or unknown parameters, like ambient conditions or material variations, are listed. On the right side one can find the performance characteristics of the process/product (output(s)), which have to be continuous quantities [43].

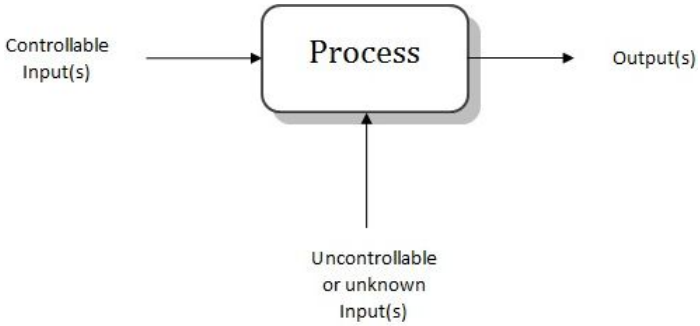

Figure 6: General model of a process

The parameters, which shall be included in the designed experiment, are called *factors*, whereby not all of them have to be varied. Some factors could be kept constant, but they are monitored as well. There are two types of factors: qualitative (discrete) and quantitative (continuous) ones [45]. Their different settings are called *levels*. The output(s) are defined as *responses*.

The most common used experimental designs in production companies are full and fractional factorial designs [46]. In the scope of this thesis the full factorial design is used. This design method is especially useful in the early stages of experimental work, if the factors are less than or equal 4, since it consists of all possible combinations of the levels of all factors [46]. The number of trials N, which are called *runs*, for the investigation of n_f factors at k levels is:

$$N = k^{n_f} \tag{27}$$

If there are too many factors that influence the process/product performance, then the fractional factorial design has to be applied, because the number of experiments will burst resources available. By means of an orthogonal experiment design, main and interaction effects can be investigated [47].

3.4 Thermal analysis – Differential scanning calorimetry

Differential scanning calorimetry (DSC) is a method to analyse the thermal behaviour of materials. This knowledge is essential, because the performance of HME products in terms of dissolution, bioavailability and stability depends strongly on their thermal properties [8]. The device measures changes in the heat flows as a function of a controlled temperature programme [48].

The measuring cell of such a calorimeter consists of a sample cell and an empty reference cell. The temperature difference ΔT of both cells is measured by thermocouples, which are installed at the bottom, where the crucibles are fixed at (see Figure 7).

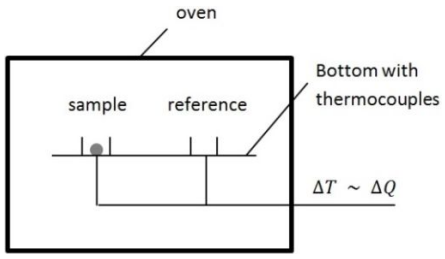

Figure 7: Measuring cell (adopted from [49])

If a sample is heated, chemical and physical conversions are taking place, which may run either exothermic (energy is released in the form of heat; $\Delta H < 0$) or endothermic (energy is absorbed in the form of heat; $\Delta H > 0$). This arising temperature difference between the sample and the reference (air) is proportional to the relative heat flow [49]. By means of the supplied heat quantity

$$\Delta Q = m \cdot c_p(T) \cdot \Delta T \tag{28}$$

the specific heat capacity c_p and the enthalpy H of the sample can be determined as a function of temperature [48].

The figure below shows a typical DSC curve of a semi-crystalline polymer. The glass transition, re-crystallization and melting temperature of the polymer can be determined by such a curve. In order to melt the crystalline segments of polymers a certain enthalpy quantity ΔH is needed. This is shown by an endothermic peak in the curve (see Figure 8).

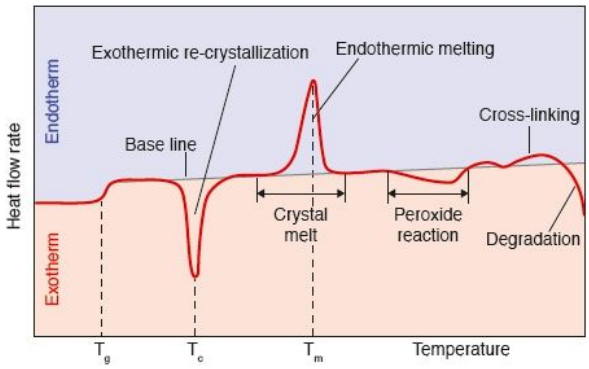

Figure 8: Typical DSC heat flow of a semi-crystalline polymer [50]

By means of DSC measurements also the miscibility of the API-excipient system can be determined. If the components are miscible, the homogeneously dispersed system shows changes in melting endotherms and, regarding the glass transition temperature, a single concentration-dependent T_g shows up [8]. The differentiation between a solid dispersion and a solid solution is also possible by means of DSC curves. If the HME product consists of a solid dispersion, the API is present both in a crystalline and an amorphous state and if it consists of a solid solution, the API is only present in the amorphous state [2].

3.5 Drug release

The dissolution of HME products – solid dosage forms - is tested according to the European Pharmacopoeia (Ph. Eur. 2.9.3), in order to evaluate the drug release of the embedded API as a function of time [51]. This testing method is essential, if one wants to evaluate the effects of the HME process parameters on the final product properties. In particular, one wants to know if the criteria of an immediate release dosage form or either a sustained release one is met [8]. The theoretical background of the dissolution behaviour of an API is given by the modified *Noyes-Whitney equation* [52], stated by Brunner [53] and Nernst [54] what is known as the *Nernst-Brunner equation*:

$$\frac{dC}{dt} = \frac{D \cdot A_s}{V \cdot h}(C_s - C_t) \tag{29}$$

where $\frac{dC}{dt}$ is the rate of dissolution, D is the diffusion coefficient, A_s is the surface area of the sample, V is the volume of the dissolution medium, h is the thickness of the diffusion layer, C_s is the concentration of the API in the dissolution medium or the concentration of its saturated solution and C_t is the API concentration at time t ([52], [55], [56]). Hence, there are several parameters, which influence the dissolution behaviour of the drug.

During testing, specimens are withdrawn at a specific time interval and afterwards analysed by means of a suitable assay method. Within this thesis the API contents of the respective samples are determined via high performance liquid chromatography (HPLC). This assay method is described in more detail below.

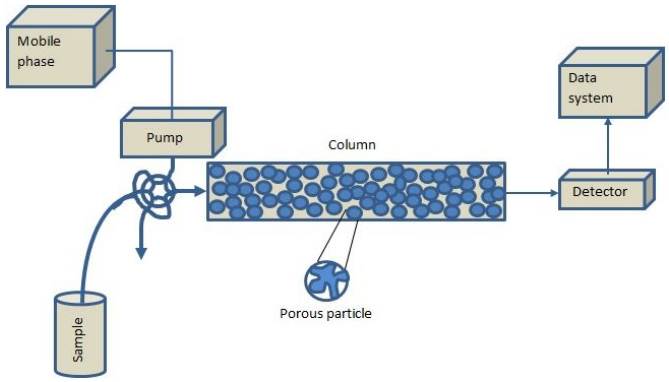

Figure 9: Components of a HPLC system

In general, chromatographic analyses are based on the different interactions of the individual components of a material system between a stationary and a mobile phase. By means of a HPLC device (see Figure 9) liquid samples are analysed. The stationary phase is a column filled with adsorbent particles, which are either polar (e.g. SiO_2) or apolar (e.g. chemically modified SiO_2). The choice of the mobile phase depends on the sample, since it should be completely dissolved in it. From the retention time, which is a measure of the magnitude of the interaction between the sample and the stationary phase, the individual components can be determined. Furthermore, the signal intensity provides information about the concentration of the respective components.

4 Experimental part

4.1 Model Extruder

This chapter contains the used materials and methods, in order to analyse the hot melt extrusion process on the model extruder - a co-rotating, fully intermeshing twin screw extruder with a diameter of 18 mm (*Pharma Extruder ZSK 18* from *Coperion GmbH*). In the end of this chapter the results of the trials and the characterization methods are discussed. Furthermore, the runs which were subsequently transferred on the target extruder are listed.

4.1.1 Trials and characterization methods

4.1.1.1 Design of experiments

In a first step, a flow diagram was developed to analyse the HME process on the model extruder. Figure 10 shows the parameters influencing the HME and which will be considered during the transfer procedure. On the left side all controllable input parameters are listed. Below, the material properties and ambient conditions are listed. These parameters are uncontrollable or may vary during extrusion. On the right side one can find the output parameters of the process.

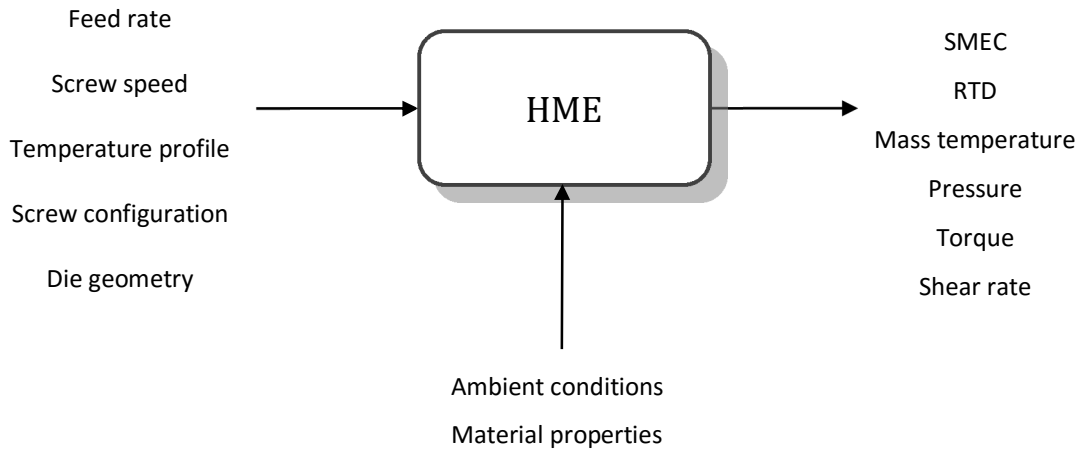

Figure 10: Flow diagram of the HME process

A full factorial DoE was set up (see Table 8) to see which input parameters affect the process/product performance the most and, besides to find the best settings. The feed rate, the screw configuration and the die geometry were set constant.

Table 8: Process DoE

Run	n [rpm]	Temperature profile [°C]	Feed rate [kg/h]	Screw configuration [-]
1	120	60/80/100/100/100/110/110/110/110/120	2	AMS-18_1.0

2	200	60/80/100/100/100/110/110/110/110/120	2	AMS-18_1.0
3	600	60/80/100/100/100/110/110/110/110/120	2	AMS-18_1.0
4	1000	60/80/100/100/100/110/110/110/110/120	2	AMS-18_1.0
5	120	60/80/115/115/115/125/125/125/125/135	2	AMS-18_1.0
6	200	60/80/115/115/115/125/125/125/125/135	2	AMS-18_1.0
7	600	60/80/115/115/115/125/125/125/125/135	2	AMS-18_1.0
8	1000	60/80/115/115/115/125/125/125/125/135	2	AMS-18_1.0
9	120	60/80/130/130/130/140/140/140/140/150	2	AMS-18_1.0
10	200	60/80/130/130/130/140/140/140/140/150	2	AMS-18_1.0
11	600	60/80/130/130/130/140/140/140/140/150	2	AMS-18_1.0
12	1000	60/80/130/130/130/140/140/140/140/150	2	AMS-18_1.0

4.1.1.2 Trials

In this section the materials, machinery and settings, which had been used to produce the intermediate products for pharmaceutical dosage forms on the model extruder, are listed.

Materials

The intermediate products consist of a binary material system. As active pharmaceutical ingredient (API) Fenofibrate, 2-[4-(4-Chlorobenzoyl)phenoxy]-2-methylpropanoic acid isopropyl ester (empirical formula: $C_{20}H_{21}ClO_4$), was chosen. The structural formula of the poorly water-soluble API is shown in Figure 11. Fenofibrate is a lipid regulating drug, since it increases the high density lipoprotein levels by reducing cholesteryl ester transfer protein expression [57]. Hence, the risk of heart diseases is minimized and strokes are prevented [58]. Further properties of Fenofibrate are shown in Table 9.

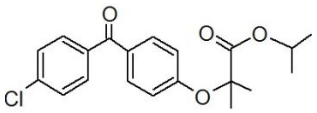

Figure 11: Structural formula of Fenofibrate

As matrix material the polymer Soluplus®, an acetic acid ethenyl ester polymer with 1-ethenylhexahydro-2H-azepin-2-one and alpha-hydro-omega-hydroxypoly(oxy-1,2-ethanediyl) graft, was chosen. The structural formula of this graft copolymer is shown in Figure 12. The amphiphilic chemical structure of Soluplus® (PEG: hydrophilic backbone; PVCL, PVAc: lipophilic side chains) enables a good interaction with drugs as a matrix polymer in order to form solid dispersions and it enables a good solubility of solid dosage forms in aqueous media [59]. Hence, it has the ability to increase the bioavailability of poorly water-soluble drugs, such as Fenofibrate. Additional properties of Soluplus® are summarized in Table 9.

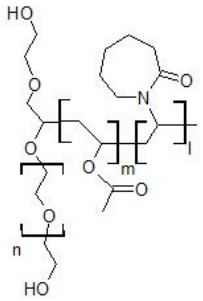

Figure 12: Structural formula of Soluplus®

Table 9: Properties of the used materials according to their data sheets and literature ([2], [59]–[62])

Material	Producer	Type	T_g [°C]	T_m [°C]	T_{degr} [°C]	ρ [kg/m³]	M_w [g/mol]	Appearance
PVCL-PVAc-PEG graft copolymer	BASF	Soluplus®	70	-	250	500-600	90,000-140,000	Powder (white to light yellow colour)
Fenofibrate	Sigma-Aldrich	F6020	-20.0	80.5	n. a.	n. a.	360.83	Powder (white colour)

For the RTD-measurements, the dye *Allura Red AC* from *Sigma-Aldrich* (80% dye content) was used, because this colour is well visible regarding the evaluation of the video recordings of the polymer strand coming out of the die.

Machinery

The binary material system was weighed via a balance and afterwards mixed in a three-dimensional shaker mixer. The properties of these two devices are shown in the table below:

Table 10: Properties of the balance and the mixer (RCPE) ([63], [64])

Machine	Producer	Type	Accuracy [g]	Max. mixing volume [l]
Balance	Sartorius AG	Combics 1 plus	0.1	-
Mixer	WAB AG Maschinenfabrik	Turbula® T 2 F	-	2

Table 11 shows the respective parts of the extrusion line:

Table 11: Extrusion line (RCPE)

Machine	Producer	Type
Twin screw loss-in-weight feeder	Coperion K-TRON GmbH	K-PH-CL-SFS-KT20
Twin screw extruder	Coperion GmbH	Pharma-Extruder ZSK 18
Die	Coperion GmbH	1 cavity, Ø 1.5 mm
Conveyor belt*	GEPPERT Band GmbH	-
Strand pelletizer	Maag Automatik GmbH	PRIMO 60 E

*strand was cooled via compressed air

Settings and procedure

Preparation of physical mixtures

The polymer matrix material Soluplus® and the API Fenofibrate were weighed in the ratio 9:1 by the balance *Combics 1 plus* from *Sartorius AG*. Afterwards the binary material system was mixed at 60 Hz for 10 minutes via the three-dimensional shaker mixer *Turbula® T 2 F* from *WAB AG Maschinenfabrik* in order to guarantee a uniform distribution of both powders. This physical mixture (premix) was fed into the extruder via the twin screw loss-in-weight feeder *K-PH-CL-SFS-KT20* from *Coperion K-TRON GmbH*.

Hot melt extrusion

The co-rotating twin screw *Pharma-Extruder ZSK 18* from *Coperion GmbH* with an outer screw diameter of 18 mm was used for the hot melt extrusion of the intermediate products. Further extruder parameters are listed in Table 12:

Table 12: Properties of the *Pharma-Extruder ZSK 18* (model extruder) [65]

Machine	Producer	Type	D_o [mm]	D_o/D_i	L [mm]	Power density [Nm/cm³]	n_{max} [rpm]	$M_{d, max}$ [Nm]
TSE	Coperion GmbH	Pharma-Extruder ZSK 18	18	1.55	740	10.13	1200	2 · 34.2

In order to calculate the die conductance *K* of the model extruder, the die was broken down into 6 elements (see Figure 13), for which a respective formula of the die conductance exists. The die element “6” is not visible in the cross-sectional view, since it is an exchangeable insert and can be changed depending on the desired die outlet diameter.

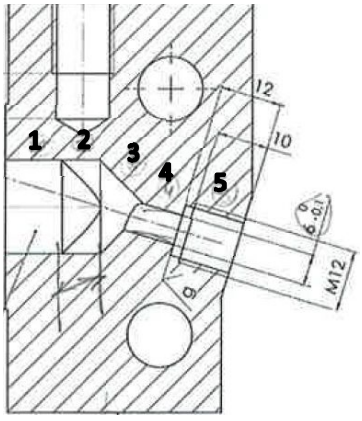

Figure 13: Cross-sectional view of the die with 5 of the 6 elements (model extruder)

With the flow exponent (m = 1.61812) of the binary material system, which was previously determined by means of the rheometer *MCR 301* from *Anton Paar GmbH*, the die conductance of each die element was calculated. Table 13 shows an overview of the results.

Table 13: Die conductance values K_i of the respective die elements (model extruder) [37]

Die element	Geometry	Formula	With:	K_i
1	Irregular profile	$K = \frac{2 \cdot A^{m+2}}{(m+3) \cdot L \cdot U^{m+1}} \cdot \left(\frac{1}{L}\right)^m$	B = 33.2 mm, H = 18.2 mm, L = 11 mm, A = 534.2 mm², U = 87.29 mm	$K_1 = 3.38 \cdot 10^{-8}$
2	Conical rectangular	$K = \frac{H^{m+2} \cdot (B_1 - B_2)^m \cdot (-1+m)^m}{2^{m+1} \cdot (m+2) \cdot (-L \cdot m)^m \cdot m^m} \cdot \frac{1}{\left(B_2^{\frac{-1+m}{m}} - B_1^{\frac{-1+m}{m}}\right)^m}$	B1 = 33.2 mm, B2 = 14.29 mm, H = 18.2 mm, L = 7.5 mm	$K_2 = 7.10 \cdot 10^{-7}$
3	Cone	$K = \frac{\pi}{(m+3) \cdot 2^m} \cdot \left[\frac{3 \cdot \left(\frac{R_C}{r_C} - 1\right)}{m \cdot L \cdot \left(1 - \left(\frac{r_C}{R_C}\right)^{3/m}\right)}\right]^m \cdot {r_C}^{m+3}$	L = 7.0 mm, R_c = 9.1 mm, r_c = 3.0 mm	$K_3 = 1.62 \cdot 10^{-8}$
4	Tube	$K = \frac{\pi \cdot R^{m+3}}{2^m \cdot (m+3)} \cdot \left(\frac{1}{L}\right)^m$	L = 6.4 mm, R = 3.0 mm	$K_4 = 1.76 \cdot 10^{-9}$
5	Tube	$K = \frac{\pi \cdot R^{m+3}}{2^m \cdot (m+3)} \cdot \left(\frac{1}{L}\right)^m$	L = 22.8 mm, R = 3.0 mm	$K_5 = 2.25 \cdot 10^{-10}$
6	Tube	$K = \frac{\pi \cdot R^{m+3}}{2^m \cdot (m+3)} \cdot \left(\frac{1}{L}\right)^m$	L = 2.4 mm, R = 0.75 mm	$K_6 = 1.42 \cdot 10^{-11}$

Afterwards, the total die conductance was calculated according to equation (26), since the individual die elements are connected in series [40]:

$$K_{model\ extruder} = 9.86 \cdot 10^{-12}$$

The screw configuration used for the trials on the model extruder is shown in Figure 14 and Table 14. Every screw element is categorized by a serial number starting with *8018-XX*. In front of the serial number its dimensions are given. Conveying (see Figure 14, green colour) and mixing elements are indicated with their pitch and length in mm (e.g. 24/12 means that their pitch is 24 mm and their length is 12 mm). Kneading blocks (KB) are indicated with the offset angle of the kneading discs, the number of kneading discs and the total length of the block in mm (e.g. KB45/5/16). The screw consists of two kneading zones (blue and grey colour) and one distributive mixing zone (orange colour). Two conveying elements with a small pitch (0.66 D and 0.44 D) are positioned at barrel zone 10 - the end of the screw – in order to build up the necessary pressure in front of the die. This screw configuration was chosen, because it is a classical approach for HME. The kneading block in the front (barrel element 2) melts the binary material system, whereas the subsequent kneading blocks (barrel element 4 and 5) are responsible for the dispersive mixing of the melt, especially the KB with an offset angle of 90° (higher pressure generation). In order to guarantee a homogenous melt, a distributive mixing element with a subsequent reverse conveying element (enlarges the residence time of the

melt in the mixing element) is placed at barrel element 8. The large conveying section in the end enables degassing of the melt.

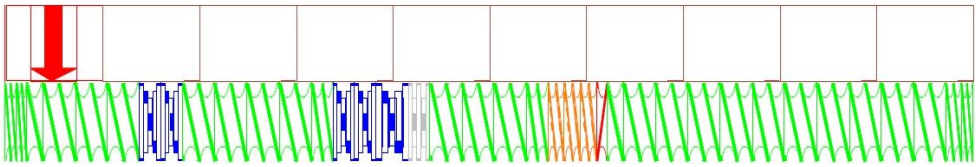

Figure 14: Screw configuration of the model extruder (green: conveying elements, blue and grey: kneading blocks, orange: distributive mixing elements, red: reverse conveying element)

Table 14: Screw configuration of the model extruder

Screw configuration AMS-18_1.0
2 x 8/8 - 8018-XX.21-008/008-12
1 x 24/12 - 8018-XX.21-024/012-12
3 x 24/24 - 8018-XX.21-024/024-12
2 x KB45/5/16 - 8018-XX.26-405/016-12
4 x 24/24 - 8018-XX.21-024/024-12
1 x 16/16 - 8018-XX.21-016/016-12
2 x KB45/5/16 - 8018-XX.26-405/016-12
1 x KB45/5/24 - 8018-XX.26-405/024-12
1 x KB90/5/16 - 8018-XX.26-905/016-12
3 x 24/24 - 8018-XX.21-024/024-12
1 x 16/16 - 8018-XX.21-016/016-12
3 x SME 12/12 - 8018-XX.92-373/012-76
1 x 16/8 LH - 8018-XX.51-016/008-12
1 x 24/12 - 8018-XX.21-024/012-12
10 x 24/24 - 8018-XX.21-024/024-12
1 x 12/12 - 8018-XX.21-012/012-12
1 x 8/8 - 8018-XX.21-008/008-12

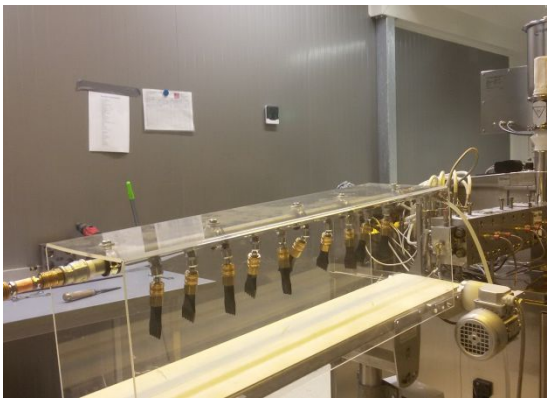

Figure 15: Extrusion line (RCPE)

As already mentioned in section 4.1.1.1, all samples (premix of Fenofibrate and Soluplus® in the ratio 1:9) were extruded at a constant feed rate of 2 kg/h. The screw configuration and die geometry were the same for all samples. Further extrusion parameters were set according to the design of experiments (see Table 8 and Table 15):

Table 15: HME process parameters of the trials on the model extruder

Run	Temperature profile [-]	screw speed [rpm]
1	1	120
2	1	200
3	1	600
4	1	1000
5	2	120
6	2	200
7	2	600
8	2	1000
9	3	120

10	3	200
11	3	600
12	3	1000

Table 16 shows the respective barrel/die temperatures of the three different temperature profiles, which are abbreviated “1”, “2” and “3” in this thesis. Barrel zone 1 – the feeding zone – was not heated in order to avoid powder sticking to the barrel walls.

Table 16: Temperature profiles of the trials on the model extruder

Temperature profile	**Temperature (set) [°C]**										
	Barrel zone										*Die*
	1	**2**	**3**	**4**	**5**	**6**	**7**	**8**	**9**	**10**	**11**
1	-	60	80	100	100	100	110	110	110	110	120
2	-	60	80	115	115	115	125	125	125	125	135
3	-	60	80	130	130	130	140	140	140	140	150

Before the extrusion of the intermediate products could be started, the extruder was driven at a low screw speed. As soon as air bubbles were visible (mainly at high screw speeds) in the polymer strand leaving the die, an atmospheric venting was installed. In these cases, barrel element 8 was left open (see Figure 16, marked in red). At the end of the extruder a conveyor belt was installed, where the strand was cooled via air (see Figure 15). A strand pelletizer was used to obtain the intermediate products (pellets).

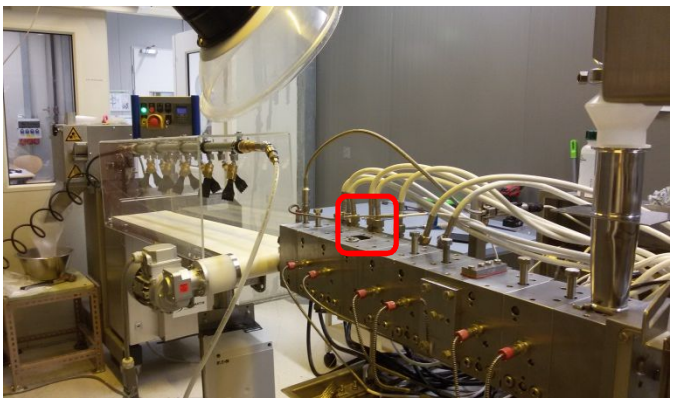

Figure 16: Extrusion line (2) – open barrel element 8 is marked in red (RCPE)

Optical RTD measurements

In order to investigate the residence time distribution (RTD) of the binary material system at the respective process setting, each run was carried out again with the addition of the dye *Allura Red AC* from *Sigma-Aldrich*. The RTD is an important process output parameter since it has a significant influence on the product performance. For these measurements the digital camera *FINEPIX HS25EXR* from *Fujifilm Corporation* was attached to a tripod and placed in front of the extruder, thereby recording the coloured strand coming out of the die (see Figure

17). A sheet of white paper was fixed at the die outlet in order to improve the visibility of the strand.

Figure 17: Set-up for optical RTD measurements

The camera captured 29 single images per second, which were afterwards analysed by means of a *MATLAB®* code (in-house tool from *RCPE GmbH*). The residence time of the coloured pigments within the extruder was investigated by measuring the a-value of the strand in comparison to a defined background area (white sheet) over time. The a-value is one of the three axes of the three-dimensional CIE LAB colour space (see Figure 18). The more red pigments are in the strand, the higher its a-value gets.

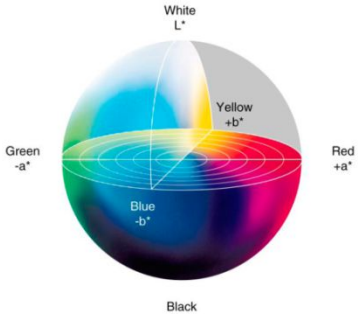

Figure 18: CIE LAB colour space [66]

4.1.1.3 Characterization methods

Differential scanning calorimetry

In order to determine the thermal properties of the intermediate products (pellets) a differential scanning calorimetry (DSC) was carried out. The samples were tested by the *DSC 204 F1 Phoenix®* from *NETZSCH-Gerätebau GmbH* with an automatic sample changer under a nitrogen atmosphere (flow rate: 50.0 ml/min) in triplicates (n = 3).

Before starting the measurements, each sample was ground by means of ceramic mortars and put under the discharging bar *R50* from *Eltex Elektrostatik GmbH*, because the material was statically charged. Hence material handling was much easier afterwards. About 10 mg of each sample, including the physical mixture, was accurately weighed in a pierced aluminium crucible (25 µl) using the analytical balance *XPE205DR* from *Mettler-Toledo*. The specimens (except the physical mixture) were heated from 0°C to 200°C at a rate of 10°C/min, followed by

a cooling ramp towards 0°C at a rate of 40°C/min and a final heating ramp up to 200°C at a rate of 10°C/min. The physical mixture (premix) was cooled down from 200°C to 0°C at a different rate, namely 10°C/min. The heating rates did not differ from the sample ones. Afterwards the gained data was evaluated by the software Proteus® 6.1.0. from *NETZSCH*.

Particle size analysis

The 3D dynamic image analyser *PartAn*^{3D} from *Microtrac Inc*. was used to determine the surface area of the intermediate products, because this parameter influences the dissolution behaviour of the API.

Figure 19: 3D dynamic image analyser *PartAn3D* from *Microtrac Inc.*

About 2 g of each sample were poured into the feeder. A vibrating ramp fed the pellets towards the opening of the device (see Figure 19, marked by a red arrow), where a camera (position: 89.5 mm) took 100 images per second of the intermediate products falling down. The measured surface areas of the numerous pellets were then averaged for each sample.

Dissolution test

In order to determine the release profile of the API of the intermediate products, dissolution tests were carried out according to the European Pharmacopoeia 8.0 – 2.9.3. Dissolution test for solid dosage forms with apparatus 2 (paddles) [51]. Solid dosage forms are according to the definition of Ph. Eur., tablets or capsules. The samples (triplicate, n = 3) were investigated by means of the dissolution testing device *DT 820 LH* from *ERWEKA GmbH* at a paddle speed of 100 rpm (see Figure 20). The water bath around the vessels, filled with 750 ml of the dissolution medium, kept the temperature at 37.0°C ± 0.5°C.

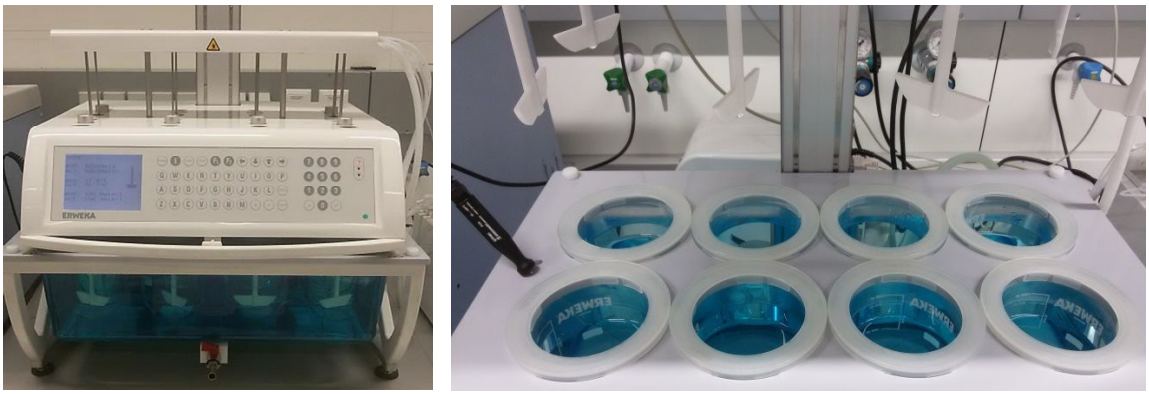

Figure 20: Dissolution testing device : closed (left) and open (right)

0.1 M hydrochloride acid fuming 37 % *ROTIPURAN®* from *Carl Roth GmbH + Co. KG* was used as dissolution medium. Before the samples were placed in the vessels, about 500 mg each had to be weighed by the analytical balance *SI-234A* (accuracy = 0.0001 g) from *Denver Instrument.* As the device was closed, the measurement could be started. Within the specified time intervals - 10, 20, 30, 40, 50, 60, 90 and 120 minutes – 100 µl of the samples were withdrawn and pipetted into brown glass vials, which were filled with 900 µl of the mobile phase before. The mobile phase consists of acetonitrile *Chromasolv® grade* from *Sigma-Aldrich Co. LLC.* and distilled water (pH = 2.5) in the ratio 8:2. The pH value of the acidic water was adjusted by means of ortho-phosphoric acid (10%) from *AppliChem GmbH*, *FiveEasy™* pH Meter from *Mettler-Toledo* and the magnetic stirrer *MR Hei-Standard* from *Heidolph Instruments GmbH & Co. KG*.

After 2 hours the dissolution test was finished and the withdrawn specimens were analysed via the HPLC *1260 Infinity LC System* from *Agilent Technologies* in order to determine the concentration of Fenofibrate dissolved in the medium at the respective time point. The HPLC was equipped with a photo diode array detector and the column *Luna C18(2)* from *Phenomenex Inc.,* where octadecyl silane ligands are bound to the silica particle surface thus causing a very hydrophobic phase and a non-polar endcapping eliminates silanol interaction [67]. As already mentioned above, acetonitrile and acidic water (pH = 2.5) in the ratio 8:2 was used as hydrophilic mobile phase, therefore the assay method is a reversed phase chromatography (RP-HPLC). A calibration line with 5 suitable standard concentrations in the range from 3 µg/ml to 30 µg/ml was prepared for quantification before each analysis (injection volume: 40 µl). Further setting parameters of the HPLC system are listed in the table below.

Table 17: HPLC settings for dissolution testing

Flow [ml/min]	1
Detection wave length [nm]	286
Column temperature [°C]	40
Sample temperature [°C]	20
Injection volume [µl]	80

Content uniformity test

The uniformity of the intermediate products was investigated using RP-HPLC as analytical method. According to the European Pharmacopoeia the “uniformity of dosage units” is defined as *“the degree of uniformity in the amount of the active substance among dosage units”* [68]. In order to determine, if the individual API contents of the samples are within the acceptance value (AV) of 15.0, about 5 mg of each sample (n = 10) were weighed by the analytical balance *SI-234A* (accuracy = 0.0001 g) from *Denver Instrument* and dissolved in 10 ml of mobile phase, which was prepared according to the section *Dissolution test* above. RP-HPLC analysis was performed as described in the section above, whereby the concentrations of the standards

were in the range from 30 µg/ml to 150 µg/ml (injection volume: 40 µl; injection volume of the specimens: 5 µl). The results were afterwards evaluated according to the European Pharmacopoeia – section 2.9.40 Uniformity of Dosage Units, after which the acceptance value is calculated as follows:

$$AV = |M - \bar{X}| + k \cdot s \tag{30}$$

where M is a reference value that depends on the mean value $\bar{X}$ of the individual API contents, k is the acceptability constant (if n = 10 → $k = 2.4$) and s is the sample standard deviation (SD). If the mean value $\bar{X}$ is in-between 98.5 % and 101.5 % of the total API content, *M* is equal to the mean value. The reference value *M* is 98.5 % if $\bar{X}$ < 98.5 % and for $\bar{X}$ > 101.5 % *M* is 101.5 %.

4.1.2 Results and discussion

This chapter contains the results of the HME process on the model extruder and of the characterization methods of the intermediate products as well as their discussion.

4.1.2.1 Influence of input parameters on output parameters

The effect of the varying process input parameters (screw speed and temperature profile of the extruder) on the output parameters are discussed in this section. Table 18 lists the twelve samples and their respective process parameters. Regarding the output parameters, the focus was on the mass temperature, the SMEC and the RTD, because these three parameters have the greatest influence on the product performance and are also scale-independent ([35], [69]).

Table 18: Effect of input parameters on output parameters

Run	Temperature profile [-]	screw speed [rpm]	T_{mass} [°C]	p_m [bar]	M [%]	SMEC [kWh/kg]	RT_{min} [s]	RT_{max} [s]
1	1	120	117	60.7	38.7	0.165	79	320
2	1	200	118	18.0	36.0	0.258	52	203
3	1	600	124	7.0	36.0	0.774	45	166
4	1	1000	127	1.0	32.0	1.146	27	131
5	2	120	133	22.7	25.2	0.108	73	318
6	2	200	133	18.0	27.0	0.193	72	194
7	2	600	135	3.0	31.0	0.666	47	148
8	2	1000	142	0.0	30.0	1.074	43	146
9	3	120	149	5.5	16.0	0.069	73	302
10	3	200	154	1.0	19.0	0.136	71	184
11	3	600	153	0.5	25.4	0.546	43	141
12	3	1000	154	0.1	26.8	0.959	42	135

Effect on the mass temperature

Figure 21 shows the influence of the temperature profile and the screw speed *n* on the mass temperature T_{mass} for the twelve samples. Regarding the four samples 1 - 4, which have been extruded at the temperature profile “1”, it can be seen that their T_{mass} increases by increasing

the screw speed due to dissipation. Sample 1 shows a T_{mass} of 117°C (n = 120 rpm), whereas sample 4 (n = 1000 rpm) has already a T_{mass} of 127°C – an increase of 10°C. By increasing the screw speed, the shear rate increases and thus the dissipated heat energy rises. Hence, the mass temperature of the binary material system is elevated. This effect is also visible concerning sample 5 – 8.

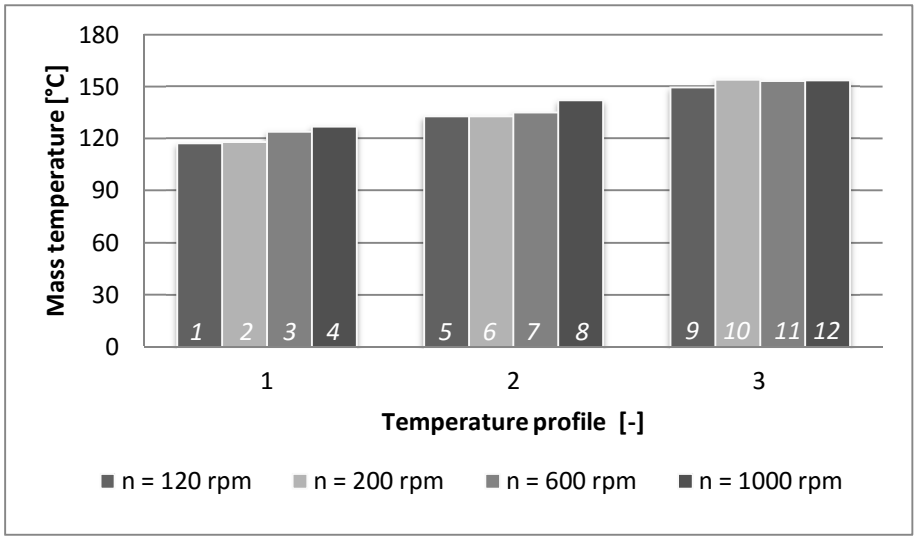

Figure 21: Influence of the varying input parameters on T_{mass}

While comparing the change of T_{mass} as a function of the temperature profile, it has to be considered that the measured mass temperature is mainly in the range of the die temperature set (see Table 16), because the temperature sensor is mounted at barrel element 10 which is next to the die element. The die temperature at temperature profile "2" was, as an example, set to 135°C and the T_{mass} of sample 5 - 8 fluctuates around this value. Their mass temperatures are 133°C, 133°C, 135°C and 142°C respectively. The T_{mass} s of sample 9 – 12 also fluctuates around the die temperature of the temperature profile "3", which was set to 150°C. Their mass temperatures are 149°C, 154°C, 153°C and 154°C respectively. However, the actual mass temperature is significantly higher than the one measured, since the sensor does not extend into the melt.

Effect on the specific mechanical energy consumption

The influence of the screw speed and the temperature profile on the SMEC is shown in Figure 22, whereby the specific mechanical energy consumption was calculated according to equation (14). A significant influence of the screw speed *n* is visible, which had been expected since the SMEC is directly depending on *n* (see equation (14)). This effect occurs at every temperature profile set. Sample 1 was extruded at a screw speed of 120 rpm and the resulting SMEC is 0.165 kWh/kg, whereas the SMEC at sample 4 (n = 1000 rpm) is 1.146 kWh/kg. This is an increase of the SMEC by a factor of about 7.

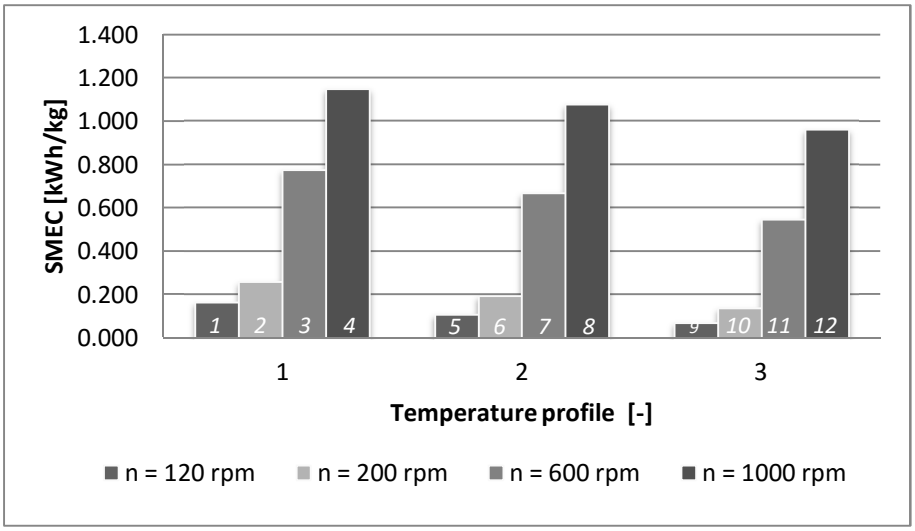

Figure 22: Influence of the varying input parameters on SMEC

When comparing the samples, extruded at the same screw speed and with different temperature profiles, it can be seen that the SMEC decreases with a higher temperature profile. Sample 3 was extruded at temperature profile "1" and the SMEC is 0.774 kWh/kg, whereas the SMEC at sample 7, which was extruded at temperature profile "2", is 0.666 kWh/kg. The screw speed of both samples was set at 600 rpm. This decrease in SMEC is due to the decreasing torque required *M [%]*.

The SMEC is also directly depending on this process output parameter (see equation (14)). By increasing the temperature profile the mass temperature rises and thus the viscosity of the material system decreases. Hence, less torque is needed to convey the melt towards the die at the defined screw speed.

Effect on the residence time distribution

As already mentioned in section 0, the optical RTD measurements were evaluated by means of a MATLAB® code (in-house tool from *RCPE GmbH*). Figure 23 shows, as an example, the residence time distribution of sample 5. The strand reaches its maximum a*-value after 123 s (time point: C) of the beginning of the RTD measurement.

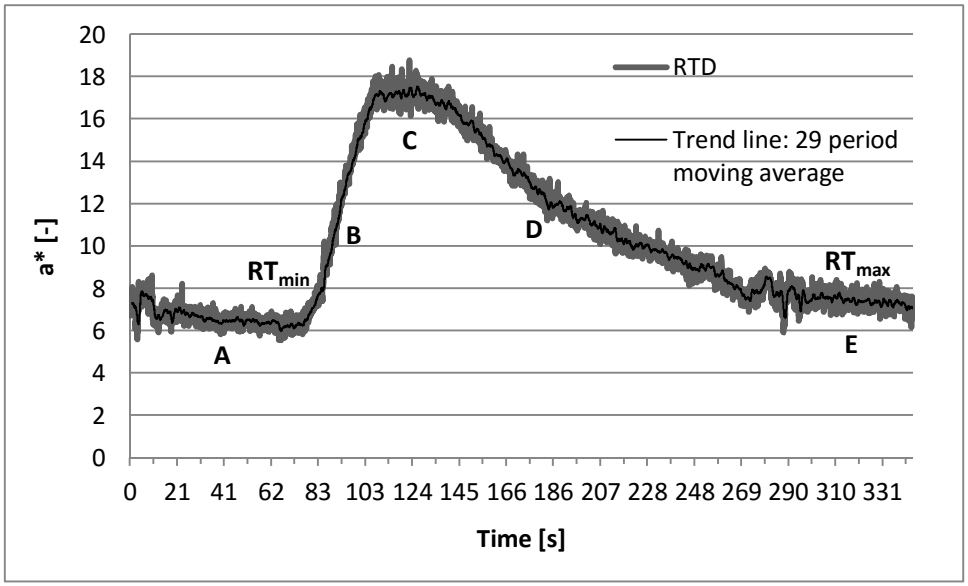

Figure 23: Residence time distribution of sample 5

Figure 24 shows the recorded strand leaving the extrusion die at time points A (40 s), B (90 s), C (123 s), D (180 s) and E (320 s). The reddish colouration with time can well be seen.

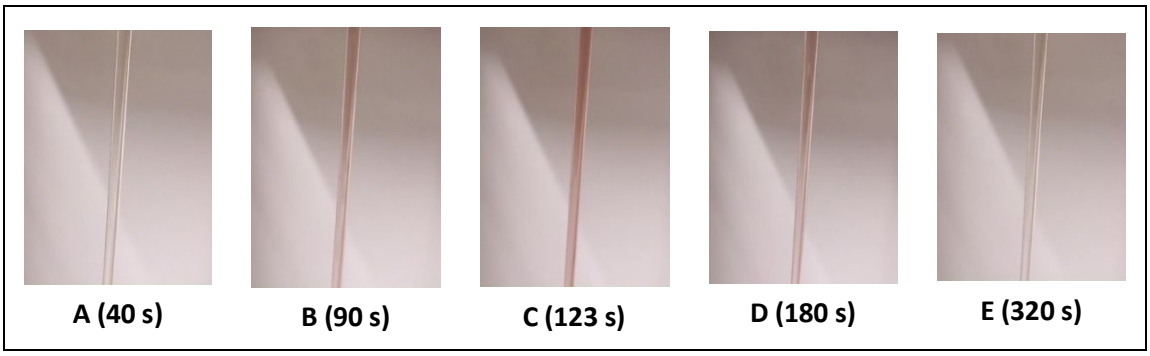

Figure 24: Recorded strand of sample 5 at the respective time points A, B, C, D and E

The maximum residence time RT_{max} of the binary material system for all twelve samples is shown in Figure 25 as a function of the temperature profile and the screw speed *n*. At the samples, which had been extruded at temperature profile "1", it can be seen that by increasing the screw speed from 120 rpm to 1000 rpm the maximum residence time decreases from 320 s to 131 s. This correlation between the screw speed and RT_{max} is also visible at the other two temperature profiles. This effect has been expected, since at higher screw speeds the material is conveyed faster through the extruder and thus the residence time decreases.

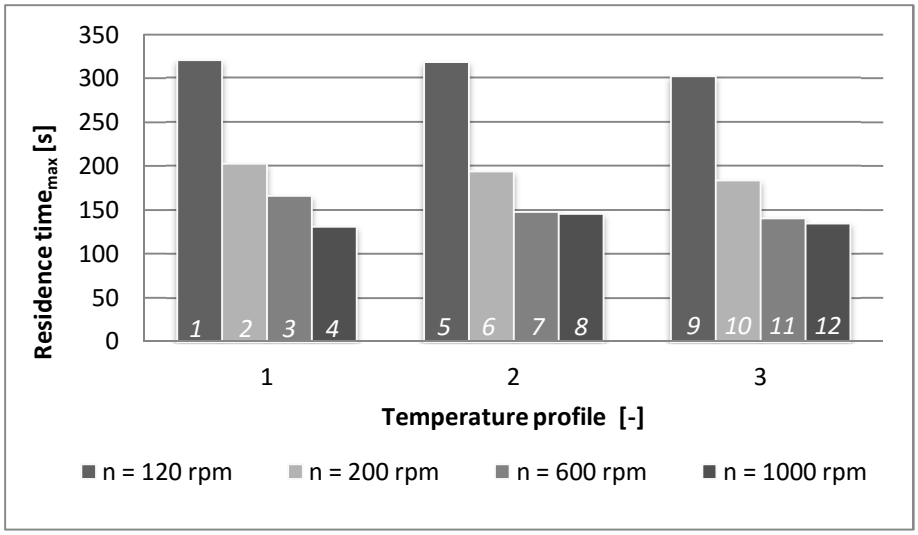

Figure 25: Influence of the varying input parameters on RT_{max}

The maximum residence time of sample 11 differs only slightly from the one of sample 12 (ΔRT_{max} ~ 6 s). Both samples were extruded at temperature profile "3" and at a screw speed of 600 rpm and 1000 rpm, respectively. These process parameters led to a mass temperature of about 154°C (see Table 18), where the viscosity of the melt is such low that there is no resistance towards the material passing the extruder, therefore the RT_{max} cannot be significantly reduced further.

When comparing RT_{max} of the samples, which have been extruded at the same screw speed but at different temperature profiles, there is just a small influence recognizable. By increasing the temperature profile RT_{max} decreases. Sample 2 was extruded at temperature profile "1" and at a screw speed of 200 rpm. Its maximum residence time within the extruder is 203 s, whereas the one of sample 6 (temperature profile "2", n = 200 rpm) is 194 s. That is a decrease of 9 s. However, there is one exception. Regarding sample 4, 8 and 12, their screw speed was set at 1000 rpm and their temperature profile varied from "1" to "3". In that case, the maximum residence time does not decrease with a higher temperature profile (see Figure 25). The reason for that has already been explained earlier.

4.1.2.2 Differential scanning calorimetry

DSC measurements were performed to analyse the thermal properties of the intermediate products. Since the influence of different process settings on the thermal properties should be investigated, only the first heating curve of the samples was evaluated. The results are shown in Table 19.

Table 19: DSC results of the intermediate products produced on the model extruder (1st heating curve; n = 3)

Sample [-]	T_g ± SD [°C]	Δc_p ± SD [J/(g*K)]
1	49.4 ± 0.6	0.60 ± 0.03
2	51.7 ± 1.0	0.81 ± 0.03
3	50.0 ± 1.0	0.71 ± 0.03

4	49.1 ± 0.3	0.59 ± 0.03
5	47.3 ± 0.6	0.73 ± 0.09
6	50.6 ± 0.1	0.60 ± 0.02
7	49.6 ± 0.5	0.60 ± 0.06
8	49.5 ± 0.5	0.52 ± 0.03
9	49.3 ± 0.7	0.62 ± 0.05
10	48.9 ± 0.4	0.57 ± 0.04
11	49.0 ± 0.8	0.58 ± 0.09
12	48.7 ± 0.3	0.53 ± 0.02

The glass transition of the samples is in the range from 48.7°C to 51.7°C. However, sample 5 has got a T_g of 47.3°C. In general, there is no significant influence of the specific mechanical energy consumption (SMEC), the mass temperature and neither of the varying residence time distribution of the melt within the model extruder on the T_g visible. Looking at sample 1-4, where the mass temperature increases from 117°C to 127°C, the SMEC rises from 0.165 kWh/kg up to 1.146 kWh/kg and the maximum residence time RT_{max} decreases from 320 s to 131 s - all those changes in process parameters do not have a significant influence on the glass transition of the intermediate products. There is no increase/decrease visible regarding sample 1 to 4. This is also the case for the samples 5-8 and 9-12, where the process parameters change in the same manner, but the glass transition temperature does not show any significant shift again. There is no influence of changing process parameters on the T_g.

The DSC thermogram of sample 3 is shown in Figure 26. The blue curve represents the first heating run. A glass transition occurs at 49.8°C and in the range from the melting temperature of Fenofibrate (T_m = 80.5°C) there is a weak peak visible. This indicates that there is some crystalline API in the pellets. These crystalline parts form a crystalline suspension with the matrix material (see Table 1). It has to be mentioned here, that the DSC measurement of sample 3 was carried out 18 weeks after extrusion. Recrystallization of Fenofibrate after a certain storage period of HME pellets was also reported in literature [70]. Kalivoda et al. extruded pellets of the binary material system Soluplus/Fenofibrate in the ratio 3:1. After 10 weeks and 26 weeks of storage, crystalline Fenofibrate was detected in the DSC curves and in the X-ray diffractograms, respectively [70]. Whereas directly after extruding the HME pellets, no crystalline API could be detected in the characterization results. As the glass transition temperature of the sample lies in-between the glass transition of the individual components (T_g (Fenofibrate) = -20.0°C, T_g (Soluplus®) = 70°C), the presence of a glassy solution is concluded [8]. Looking at the second heating run (red curve) the glass transition occurs at 43.2°C. It is shifted to lower temperatures. No crystalline API is detectable in the second heating curve.

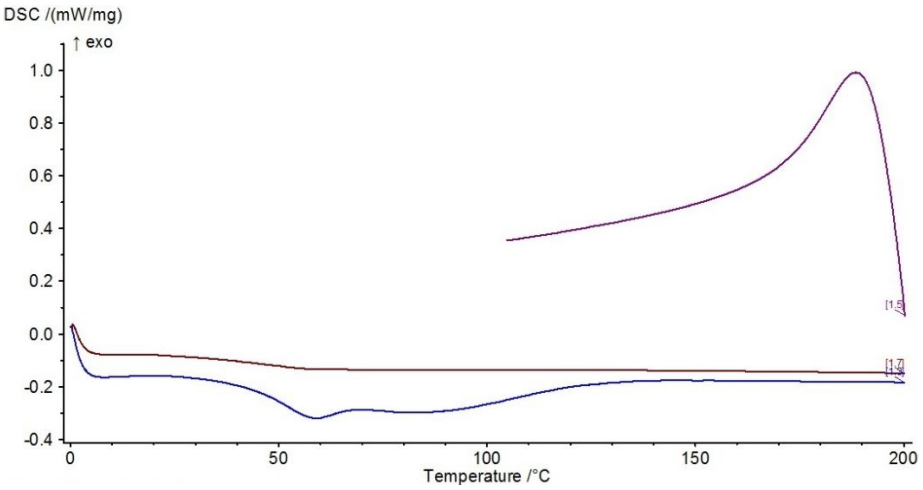

Figure 26: DSC thermogram of sample 3. The blue curve shows the 1st heating run, the purple one shows the cooling ramp and the red one shows the 2nd heating run.

Figure 27 shows the DSC thermogram of the physical mixture (premix) of Soluplus and Fenofibrate, which has been extruded on the model extruder. The first heating run is displayed by the blue curve. The glass transition of Soluplus® is shifted to a lower temperature, namely to 64.5 °C (according to the data sheet T_g = 70°C). This plasticizing effect of Fenofibrate was also shown in literature [71]. It has further to be mentioned that the glass transition of the graft copolymer Soluplus® is difficult to determine due to its wide shape. The melting peak of the crystalline API Fenofibrate has got its maximum at 82.0°C and an area of 7.358 J/g. The overlap of the T_g of Soluplus® and the T_m of Fenofibrate, however, hinders an exact determination of the enthalpy of melting of the API. The second heating curve shows only one glass transition of the physical mixture at 49.6°C and no melting peak of the API. This indicates that heating the premix up to 200°C in an aluminium pan is sufficient to generate a glassy solution of the binary material system. Nevertheless, there is certainly a difference between this solution and the one generated during the HME process. This is already recognizable by comparing their T_gs (2nd heating cycle). There is a difference of more than 6 degree Celsius.

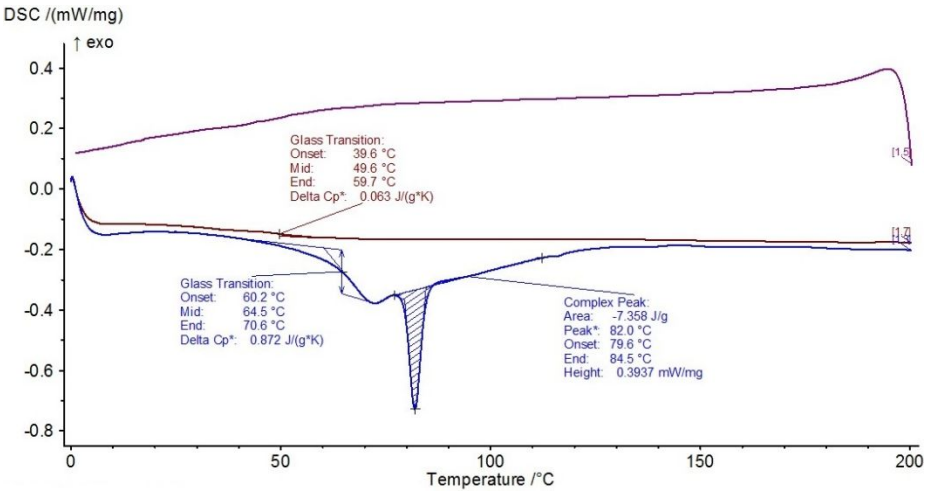

Figure 27: DSC thermogram of the physical mixture Soluplus and Fenofibrate (9:1) of the model extruder. The blue curve shows the 1st heating run, the purple one shows the cooling ramp and the red one shows the 2nd heating run.

Effect of mass temperature on thermal properties

Since the comparison of the glass transition temperatures of all 12 samples showed no significant influence by T_{mass}, SMEC and RT_{max}, the following section contains a comparison of the courses of the 1st heating cycles. Figure 28 shows the first heating run of sample 3, 7 and 10 whose mass temperatures varied.

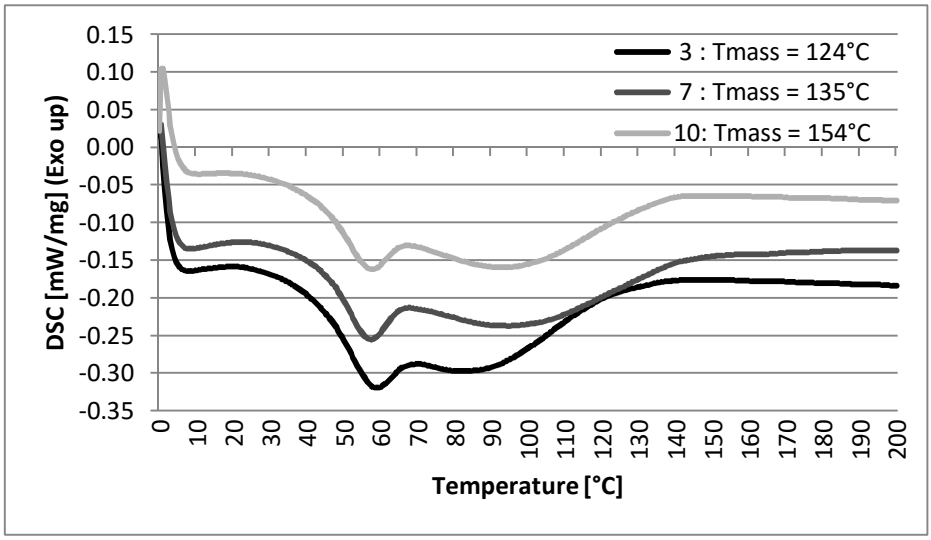

Figure 28: DSC thermogram of sample 3, 7 and 10 (1st heating cycle)

At the glass transition of sample 3 (T_{mass} = 124°C), most energy is needed to soften the material. The height of the glass transition Δc_p is 0.71 J/(g*K), whereas the glass transition of sample 10 has a Δc_p of 0.57 J/(g*K) (see Table 19). This indicates that the higher the mass temperature of the sample, the less energy is needed to create a melt in a second step. At higher temperatures during HME, it is likely that some polymer chains might start to degrade and thus the molecular weight decreases.

Furthermore, the elongated melting peak of sample 3 in the range of the T_m of Fenofibrate is slight narrower than the ones of sample 7 and 10. These samples had a mass temperature of 135°C and 154°C, respectively.

Effect of specific mechanical energy consumption on thermal properties

Figure 29 shows the first heating runs of sample 6, 7 and 8. During HME their SMEC values were 0.193 kWh/kg, 0.666 kWh/kg and 1.074 kWh/kg, respectively. The shape of those three DSC curves looks quite similar. Regarding their Δc_p values, sample 8 has got the lowest one (Δc_p = 0.52 J/(g*K)). Compared to sample 6, whose SMEC value is almost less than 20 % of the one from sample 8, Δc_p decreases by 13 %. By increasing the SMEC and therefore increasing the mechanical impact on the material, Δc_p decreases.

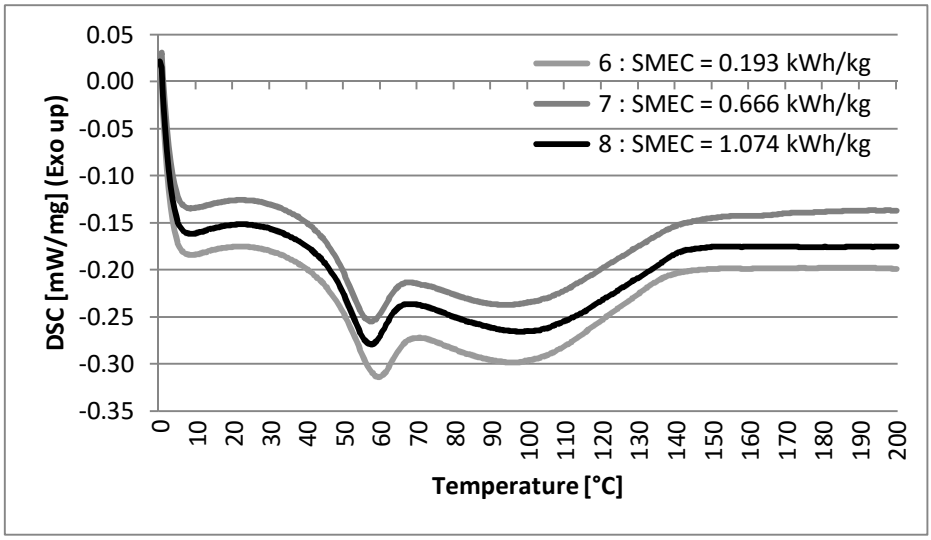

Figure 29: DSC thermogram of sample 6, 7 and 8 (1st heating cycle)

Effect of RTD on thermal properties

The first heating run of sample 4, 7 and 10 is shown in Figure 30. These samples differ in their maximum residence time within the extruder. Sample 10 remained the longest in the TSE, its RT_{max} is 184 s and its Δc_p value of the glass transition is 0.57 J/(g*K). It is, compared to the Δc_p values of sample 4 and 7, the lowest one. However, the difference is just 0.02 J/(g*K) (to sample 4) and 0.03 J/(g*K) (to sample 7) and therefore not significant. In general, the shape of the curves looks similar.

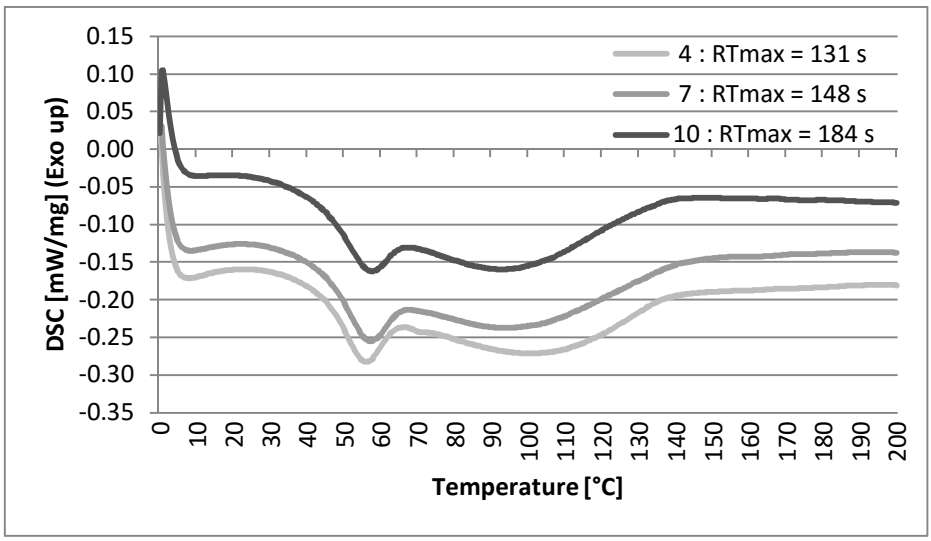

Figure 30: DSC thermogram of sample 4, 7 and 10 (1st heating cycle)

4.1.2.3 Particle size analysis

The results of the particle size analysis via the 3D dynamic image analyser *PartAn*^{3D} from *Microtrac Inc.* are shown in Table 20. It lists the mean surface area of each sample, which has been extruded on the model extruder. The mean surface areas of sample 1, 5 and 9 are significantly higher than the ones of the other samples. Their surface area is almost twice the surface area of the others. For example, the pellets of sample 1 (n = 120 rpm; temperature

profile 1) have got a mean surface area of 12.16 mm², whereas the pellets of sample 2 have got a mean surface area of 6.79 mm² (n = 200 rpm; temperature profile 1).

Table 20: Mean surface are of the samples (model extruder)

Sample [-]	Mean surface area [mm²]
1	12.16
2	6.79
3	7.61
4	7.12
5	11.42
6	6.89
7	6.67
8	5.11
9	11.33
10	5.75
11	5.69
12	5.80

The samples 1, 5 and 9 have been extruded at a screw speed of 120 rpm and thus the viscosity of the polymer strand leaving the die was higher than the one of the other samples (n > 120 rpm). As the viscosity of the polymer strand was getting lower (higher screw speeds are causing higher shear rates), the haul-off speed of the conveyor belt and the strand pelletizer had to be increased due to the sagging of the strand, which results in pellets with smaller cylindrical lengths and smaller mean surface areas.

4.1.2.4 Dissolution test

The investigation of the dissolution behaviour of the intermediate products that have been extruded on the model extruder is illustrated in Table 21:

Table 21: Initial dissolution rate and maximum concentration of dissolved API of each sample (n = 3, model extruder)

Sample [-]	Initial dissolution rate ± SD [µg/(ml*min)]	c_{max} ± SD [µg/ml]	t_{max} [min]
1	3.36 ± 0.17	69.57 ± 4.18	120
2	4.06 ± 0.11	72.76 ± 2.17	90
3	3.66 ± 0.17	74.77 ± 0.99	120
4	3.71 ± 0.31	70.73 ± 0.36	120
5	3.16 ± 0.20	76.02 ± 2.36	90
6	3.41 ± 0.83	71.47 ± 2.51	120
7	4.78 ± 0.29	74.63 ± 4.97	90
8	4.51 ± 0.94	79.24 ± 5.30	120
9	2.93 ± 0.71	75.96 ± 4.77	90
10	3.88 ± 0.40	68.72 ± 7.21	60
11	2.48 ± 0.58	70.31 ± 1.75	120
12	3.63 ± 0.38	69.60 ± 4.14	50

After 10 minutes the largest amount of API was dissolved in the dissolution medium at sample 7. Its initial dissolution rate is 4.78 µg/(ml*min). At the beginning of the measurements, already 70 % of the total API content is dissolved in the medium. Sample 11 has got the lowest initial dissolution rate, namely 2.48 µg/(ml*min) which equals 37 % of the total API content in the pellets. The samples 1, 5 and 9 have also got low initial dissolution rates. They are in the range from 2.93 to 3.36 µg/(ml*min). Their low values are caused by their large particle sizes (see Table 20). According to equation (29) the dissolution rate decreases by increasing the particle size due to a lower surface area to volume ratio [70].

The maximum concentration c_{max} of dissolved Fenofibrate is reached by sample 8. After 120 minutes 79.24 µg/ml were dissolved in the dissolution medium (118 % of total API content). Looking at the other samples, the maximum concentration of dissolved Fenofibrate was mostly reached after 90 or 120 minutes. Thus, it is concluded that the intermediate products have got an immediate-release behaviour. Immediate-release dosage forms are those who release (more than) 85 % of their total API content within 30 minutes of dissolution testing [72].

In the following section the influence of the scale-independent parameters (mass temperature, SMEC and RTD) on the dissolution behaviour of the pellets will be discussed.

Effect of mass temperature on drug release

In order to analyse the effect of the mass temperature on the dissolution profile of the samples, Figure 31 depicts 3 samples which had different mass temperatures during their HME. The effect of particle size on the dissolution behaviour is eliminated, because samples with similar particle sizes have been chosen for this comparison (see Table 20). This was also ensured at the two following discussions about the influence of the respective process output parameters on the drug release of the intermediate products.

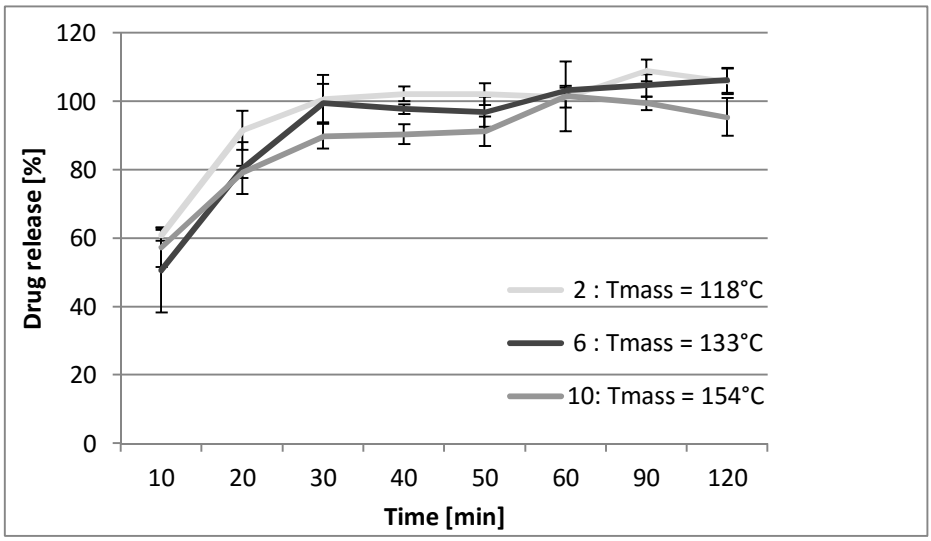

Figure 31: Dissolution profiles of sample 2, 6 and 10 (n = 3)

The initial dissolution rate of sample 2 (T_m = 118°C), sample 6 (T_m = 133°C) and sample 10 (T_m = 154°C) is in the range from 3.41 µg/(ml*min) to 4.06 µg/(ml*min). Until 30 minutes of dissolution testing, there is no significant difference between the drug releases of those three

samples. However, after 30 minutes, the release profile of sample 10 was shifted to lower values of API release. After 40 minutes of dissolution testing, sample 10 released 90 % of the total API content, whereas the drug release of sample 2 and 6 was 103 % and 98 % of the total API content, respectively. Thus, it is concluded that a change in the mass temperature during extrusion of about 35°C does influence the dissolution behaviour of the intermediate products significantly. It is assumed that shorter polymer chains are likely to enclose the API better (micelle formation of Soluplus in aqueous media [59]) and therefore the drug release decreases.

Effect of SMEC on drug release

Figure 32 shows the dissolution profiles of sample 3, 4 and 6. These samples varied in their SMEC during the extrusion process on the model extruder. While sample 4 and 6 differ in their SMEC values almost about 1 kWh/kg, their dissolution profile shows no significant difference. The initial dissolution rate of sample 6 is 3.41 µg/(ml*min) and the one of sample 4 is 3.71 µg/(ml*min). That is a difference of 0.3 µg/ml and regarding their standard deviations it is negligible.

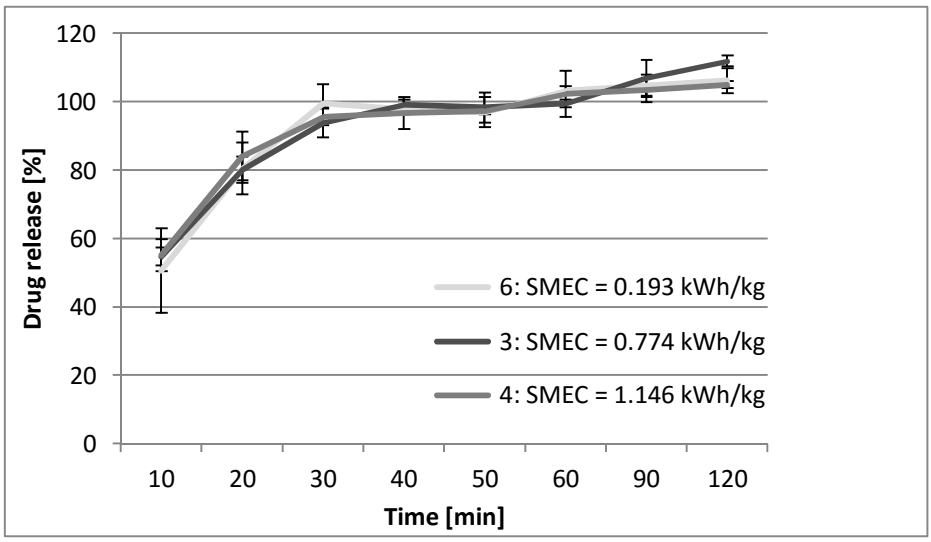

Figure 32: Dissolution profiles of sample 3, 4 and 6 (n = 3)

Both samples reached the maximum concentration of dissolved Fenofibrate after 120 minutes of dissolution testing. The values are in the range from 71.47 µg/ml to 70.73 µg/ml dissolved API in the dissolution medium. Therefore, it is concluded that the SMEC has no significant influence on the dissolution profile of the intermediate products.

Effect of RTD on drug release

Sample 2, 3 and 4 vary in their residence time within the model extruder. Looking at their dissolution profiles, there is, however, no significant influence of the residence time on the dissolution behaviour of the intermediate products (see Figure 33). The standard deviations of all 3 samples coincide with each other over the entire dissolution testing time.

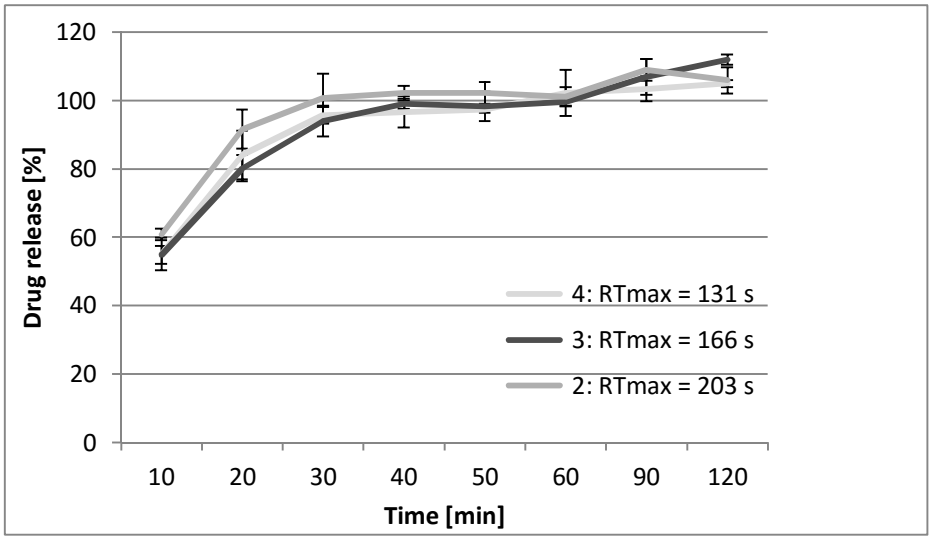

Figure 33: Dissolution profiles of sample 2, 3 and 4 (n = 3)

Their initial dissolution rate is in the range from 3.66 µg/(ml*min) to 4.06 µg/(ml*min) and their maximum concentration of dissolved API is in the range from 70.73 µg/ml to 74.77 µg/ml. The maximum concentration of dissolved Fenofibrate was reached by sample 3 after 120 minutes (c_{max} = 74.77 µg/ml). For sample 2 the maximum amount of Fenofibrate was already dissolved after 90 minutes. It has to be mentioned that all values are within the standard deviation range.

4.1.2.5 Content uniformity test

The evaluation of the content uniformity tests is shown in Figure 34. All samples fulfil the criteria according to the Ph. Eur. – section 2.9.40 *Uniformity of Dosage Units*, after which the acceptance value (AV) of a dosage unit has to be below 15.0 (L1 value). Hence the uniformity of the intermediate products is confirmed (see Figure 34).

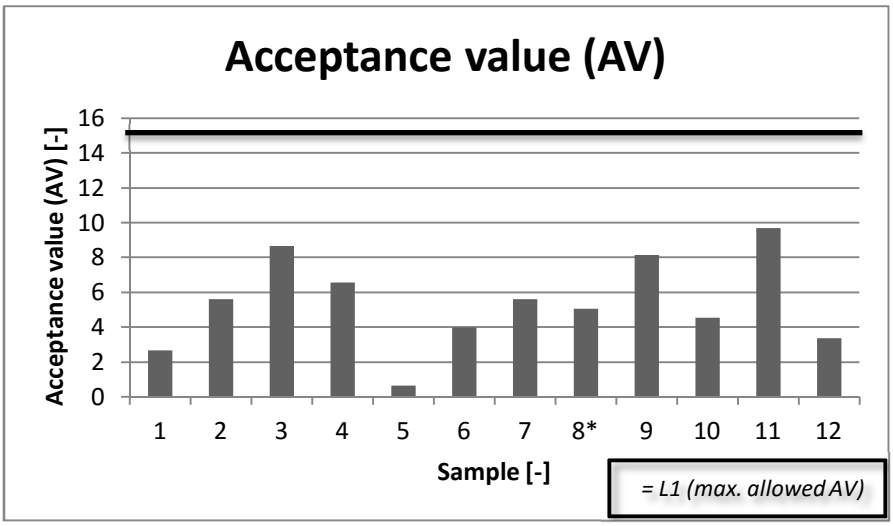

Figure 34: Acceptance values of the intermediate products from the model extruder (*n = 9; the other samples: n = 10)

Sample 5 has got the smallest acceptance value, namely 0.6. The acceptance value of sample 1 is also very low (AV = 2.7) compared to the AVs of the other samples. The smaller the AV, the more uniform the API content is distributed in the 10 specimens of each sample. Sample 1 and 5 were both extruded at a screw speed of 120 rpm and thus the residence time of the binary material system within the model extruder was longer than of the samples that have been extruded at higher screw speeds (see Figure 25). A higher residence time of the material may contribute to a better mixing of the melt. Thus, a more homogeneously melt is obtained, where the API is better dispersed in the matrix material. However, it must be noted that the AV of sample 9, which was also extruded at a screw speed of 120 rpm is comparably high (AV = 8.1).

The mass temperature has no influence on the content uniformity (CU) of the intermediate products. While the temperature rises from 117°C (sample 1) up to 154°C (sample 12), there is no correlation between an increasing mass temperature and the content uniformity of the samples visible (see Figure 34).

Looking at the content uniformity of the samples 1 – 4, it seems that an increasing SMEC has got an effect on the AV. The SMEC of sample 1 is 0.165 kWh/kg and its AV is 2.7. Whereas the SMEC of sample 4 is 1.146 kWh/kg and its AV has got a value of 6.5. This is an increase in the acceptance value of 140 %, which means that the API is less uniform dispersed in the pellets of sample 4. But when regarding sample 9, which has got a comparatively high acceptance value of 8.1 and at the same time a relatively low SMEC of 0.069 kWh/kg, this assumption is contrary. As the specific mechanical energy consumption during the extrusion of sample 9 is even lower than the one of sample 1 (SMEC = 0.165 kWh/kg), it becomes apparent that the SMEC shows no effect on the AVs of the intermediate products.

4.1.3 Summary

All samples could be extruded on the *Pharma Extruder ZSK 18* from *Coperion GmbH* according to the trial set-up (see Table 8) without any serious problems occurring. However, during the runs with high speed screws, such as 600 and 1000 rpm, melt accumulated at the die outlet. Figure 35 shows the strand of sample 8, which was extruded at a screw speed of 1000 rpm. This accumulation did not appear at lower screw speeds where a continuous strand left the die (see Figure 36, sample 6 with n = 200 rpm). Furthermore, at high screw speeds and/or with temperature profile “3”, the binary material system starts to degrade (see Figure 35, yellowish colour of the polymer strand of sample 8). Since the degradation temperature of Soluplus® is about 250°C, Fenofibrate might be the reason for the yellowish colour of the strand coming out of the die [2].

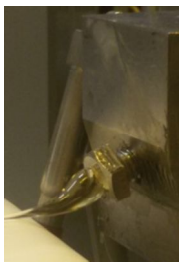

Figure 35: Strand of sample 8

Figure 36: Strand of sample 6

The mass temperature of the binary material system was mainly influenced by the temperature profile of the extruder (see Figure 21). Sample 1, as an example, has a T_{mass} of 117°C and the mass temperature of sample 5 is 133°C – an increase of 16°C. Both samples were extruded at the same screw speed (n = 120 rpm) but the temperature profile was different. By way of comparison: increasing the screw speed of the extruder and holding the temperature profile constant, the T_{mass} increases less. Sample 3 was extruded at a screw speed of 600 rpm and at the same temperature profile "1" as sample 1. The mass temperature of sample 3 is just 7°C higher than the one of sample 1. However, it was concluded that the effect of the temperature profile on the mass temperature is mainly due to the fact that the temperature sensor is mounted at barrel element 10, which is next to the die element (see Table 16).

The specific mechanical energy consumption was significantly influenced by the screw speed (see Figure 22). This effect has been expected since the SMEC directly depends on *n* (see equation (14)). By increasing the screw speed from 120 rpm to 1000 rpm, the SMEC rises from 0.165 kWh/kg (sample 1) to 1.146 kWh/kg (sample 4). In contrast, the temperature profile has not that big influence on the SMEC. By increasing the temperature profile of the extruder and thus the mass temperature, the SMEC decreases. This effect is caused by the decreasing amount of torque needed to convey the melt towards the extruder die at the defined screw speed (see equation (14)). As the material system has got a higher temperature, the viscosity gets lower and less torque is required.

The evaluation of the RTD video recordings showed that the residence time of the binary material system within the model extruder is mainly influenced by the screw speed and hardly by the temperature profile. Regarding sample 5 and 8, which have been extruded at temperature profile "2", it is obvious that by increasing the screw speed from 120 rpm to 1000 rpm, the maximum residence time decreases from 318 s to 146 s. The RTD results also demonstrated that the difference in RT_{max} of sample 11 and 12 is only 6 s. Both samples were extruded at high screw speeds (600 and 1000 rpm) and at temperature profile "3". These process parameters led to a mass temperature of about 154°C (see Table 18), which is critical for the binary material system since the strand leaving the die had a yellowish colour. Furthermore, melt accumulated at the die outlet and the viscosity of the material was such low, that the pressure sensor "measured" just 0.5 and 0.1 bar, respectively. These indicators show that the highest temperature profile ("3"), in combination with fast screw speeds, is not favourable in order to guarantee a continuous hot melt extrusion process of the binary

material system. However, even as the temperature profile “1” and “2” were set, high screw speeds caused a critically low viscosity of the melt, which can be recognized by low melt pressure values (see Table 18).

The DSC thermograms of sample 1 – 12 look more or less similar. However, the SMEC and in particular the mass temperature have got an influence on the height (Δc_p) of the glass transition of the samples. By an increase of the mass temperature from 124°C to 154°C, Δc_p decreases by almost 20 %. At an SMEC of 0.193 kWh/kg (sample 6) the Δc_p value is 0.60 J/(g*K), whereas it is 0.52 J/(g*K) at an SMEC of 1.074 kWh/kg. That is an decrease of 0.08 J/(g*K) (13 %). This indicates, that the higher the mass temperature and the SMEC of a sample, the less energy is later needed to form a melt. If the material is subjected to higher temperatures and mechanical impact during HME, some polymer chains might start to degrade and thus the molecular weight decreases.

In general, the 1st heating cycle of sample 1-12 shows one glass transition in the range from 48.7°C to 51.7°C (exception: sample 5, see Table 19) and in the range of the melting temperature of Fenofibrate (T_m = 80.5°C) a weak melting endotherm. This indicates a recrystallization of the API during storage, which was also reported by Kalivoda et al. [70]. The 2nd heating cycle shows only one glass transition in the range from 40.8°C to 45.5°C (exception: sample 10 – T_g = 51.7°C). Apart from sample 10, the glass transition temperature is shifted to the left compared to the one of the 1st heating cycle. Nevertheless, both T_gs (1st and 2nd heating run) are always in-between the T_gs of the individual components (see Table 9), thus the presence of a glassy solution is evidenced. Furthermore, the absence of crystalline Fenofibrate in the 2nd heating cycle of the premix indicates, that heating it up to 200°C in an aluminium pan is sufficient to generate a glassy solution of the binary material system. Regarding the change of the scale-independent output parameters (mass temperature, SMEC and RTD) and their influence on the glass transition temperature of the intermediate products, no correlation could be found.

No correlation was found between the varying scale-independent parameters SMEC and RTD and the dissolution behaviour of the intermediate products, too. However, the mass temperature of the samples during HME influences the drug release. High mass temperatures have an adverse effect on the dissolution behaviour. It is assumed that shorter polymer chains are likely to enclose the API better (micelle formation of Soluplus in aqueous media [59]) and therefore the drug release decreases. In general, the evaluation of the dissolution tests has shown that the pellets have got an immediate-release behaviour of the active pharmaceutical ingredient [72]. After 30 minutes of dissolution, (more than) 85 % of the total Fenofibrate content of the samples was released. The only exception is sample 11 whose drug release was only 76 % after 30 minutes of measuring. Sample 11 reached a drug release of 85 % after 40 minutes of dissolution.

By the evaluation of the content uniformity tests according to the European Pharmacopoeia – section 2.9.40 *Uniformity of Dosage Units*, the uniformity of all intermediate products

extruded on the model extruder could be confirmed. Their acceptance values are all below the maximum allowed AV "*L1*", which has a value of 15.0. A definite correlation between the varying scale-independent parameters of the HME (mass temperature, SMEC and RTD) and the content uniformity of the pellets could not be shown.

In summary, it can therefore be said that the HME on the model extruder with high screw speeds (600 rpm and 1000 rpm) and/or at temperature profile "3" is critical, regarding the process output parameters (mass temperature and pressure) and the processability, since it was difficult to pull off the low-viscous strand. However, the scale-independent parameters (T_{mass}, SMEC and RTD) did not have an effect on the glass transition temperature. It was the amount of energy required (Δc_p) to soften the material in a subsequent processing step, which decreases with an increasing mass temperature and SMEC. Furthermore, the mass temperature was the only scale-independent parameter that had a significantly influence on the dissolution behaviour of the intermediate products. As the processability of the intermediate products plays an important role, especially with regard to a subsequent commercial production of pharmaceutical dosage forms, and the mass temperature showed an influence on the dissolution behaviour and the thermal properties of the pellets, it was decided to transfer only the run 1, 2, 5 and 6 (see Table 8) from the model to the target extruder.

4.2 Target Extruder

Within this master`s thesis the HME process on the *Pharma Extruder ZSK 18* from *Coperion GmbH* is transferred to the *PHARMALAB 16* twin-screw extruder from *Thermo Fisher Scientific Inc.*, located at *Applied Manufacturing Science (AMS)* in Poznan (Poland). This stainless steel TSE, hereafter called "target extruder", has got an outer screw diameter of 15.6 mm and hence a scale-down procedure is carried out in this case.

This chapter presents the scale-down methods chosen, the set-up and execution of the trials on the target extruder in Poznan and, furthermore, the results of the characterization of the intermediate products are given and discussed.

4.2.1 Appropriate scale-down methods

As appropriate scale-down methods, the existing method from Menges and Feistkorn [30] as well as the one from Rauwendaal [32] were chosen (see 3.2.3). The first one allows a complete scale-down of the extrusion process, whereas at the second one the critical process parameters, such as the shear rate $\dot{\gamma}$ and the SMEC, are hold constant during the transfer.

With the knowledge that a complete scale-down of the HME process is not possible, since both extruders already exist, the method of Menges and Feistkorn was nevertheless applied. It serves as comparison to the method from Rauwendaal, which is not based on the model theory (see 3.2.2) and thus it is theoretically not well-founded. How the process input parameters of the target extruder were calculated via the respective scale-down method is shown in the following section.

Calculation of the process input parameters:

As already mentioned in chapter 4.1.3, the run 1, 2, 5 and 6 from the model extruder (see Table 15) were transferred to the target extruder. In order to carry out the trials at *AMS* in Poznan, the process input parameters had to be calculated first. Table 22 shows a comparison of the specifications of the model and target extruder. Many of these parameters were used for subsequent calculations.

Table 22: Specifications of the model and target extruder ([65], [73])

Specifications	Unit	Pharma-Extruder ZSK 18	PHARMALAB 16
Barrel length	L/D	40/1	40/1
Barrel length (L)	mm	720	624
Barrel bore diameter	mm	18.2	16
Screw diameter (D_o)	mm	18	15.6
Root diameter (D_i)	mm	11.6	9

Diameter radio (D_o/D_i)	-	1.55	1.73
Channel depth (h)	mm	3.2	3.3
Center-line spacing (a)	mm	15	12.5
Maximum torque per screw	Nm	34.2	12
Power density	Nm/cm^3	10.13	6.144
Maximum screw speed	rpm	1200	1000
Barrel cross section area	mm^2	495.33	378.257
Screw cross section area	mm^2	154.877	103.77 *conveying* 87.148 *mixing and kneading*

Menges and Feistkorn [M]

As already mentioned in chapter 3.2.3, the method of Menges and Feistkorn is based on the model theory. In order to calculate the screw speed and the feed rate of the target extruder a boundary condition had to be set, because exponent x was unknown. In this case, an identical shear rate of the HME process on the model and target extruder was determined as boundary condition. Therefore its exponent *"- (Ψ + x – 1)"* had to be zero. By the values of the exponent *x* and the three exponents *ω*, *Ψ* and *ε* obtained from the given length *L*, the centre-line spacing *a*, the channel depth *h* and the pitch *S* of the model and target extruder, the screw speed and feed rate of each scaled-down run was determined. Table 23 shows the respective parameters of the model and target extruder (subscript "0") used for the calculation steps mentioned above.

Table 23: Geometry and process parameters of the model and target extruder (subscript "0"), which have been used for the HME transfer according to the method of Menges and Feistkorn

A	**Exponent**		**D/D_0**	**A**	**A_0**	**A/A_0**
L	1+ω	ω = 0	1.15	720	624	1.15
(D – a)	Ψ	Ψ* = - 0.23	1.15	3.0	3.1	0.97
h	ψ	Ψ = - 0.22	1.15	3.2	3.3	0.97
$\underline{n}$	-x	x = 1.23	1.15	120 / 200	$\underline{143 / 238}$	0.81
S	ε	ε = 1.99	1.15	1.33	1	1.33
$\dot{\gamma}$	-(Ψ + x – 1)	0	1.15	_	_	1.15
$\underline{\dot{m}}$	ε + Ψ – x + 1	1.53	1.15	2	$\underline{1.6}$	1.20

*This exponent was chosen for further calculations

Rauwendaal [R]

By using the method from Rauwendaal, the average shear rate is kept the same in the model and target extruder. Thus the screw speed of the target extruder (index: 2) was calculated as follows:

$$n_2 = \frac{K_1 \cdot n_1}{K_2} \tag{31}$$

with $K_i = \frac{\pi \cdot D}{h_{ave}}$. The factor K_i depends on the screw geometry of the respective extruder. Since both extruders already exist, the average channel depth h_{ave} and the screw outer diameter D are given (see Table 22).

Table 24: Necessary parameters for the transfer of the HME process according to the method of Rauwendaal

$\boldsymbol{K_1}$ **[-] =**	17.67
$\boldsymbol{K_2}$ **[-] =**	14.85
$\boldsymbol{V_{free1}}$ **[mm³] =**	(495.33 mm² - 2 * 154.877 mm²) * L_1 = 133614.72
$\boldsymbol{V_{free2}}$ **[mm³] =**	(378.257 mm² * L_2) - 2 * ($L_{conveying}$ * 103.77 mm² + $L_{mixing\ and\ kneading}$ * 87.148 mm²) = 111454.17

In order to guarantee the same mixing performance on the model and target extruder, their degree of fill has to be the same. For this purpose, the feed rate of the target extruder was calculated according to equation (32):

$$\dot{m}_2 = \frac{V_{free2} \cdot n_2 \cdot \dot{m}_1}{V_{free1} \cdot n_1} \tag{32}$$

The inner volume V_{free} of each extruder was determined by the subtraction of the respective screw cross section area along the extruder from its barrel cross section area (see Table 24). As already mentioned several times in section 3.2, it is desirable to keep the SMEC constant during a transfer of the extrusion process. In order to see if the extrusion on the target extruder is possible with the calculated input parameters (screw speed and feed rate) and keeping the SMEC constant, the torque of each scaled-down run was determined:

$$Torque\ (\%) = \frac{9550 \cdot \dot{m}\ (kg/h) \cdot SMEC\ (kWh/kg)}{Torque\ (Nm/shaft) \cdot 2 \cdot n\ (1/min)} \tag{33}$$

At a torque of more than 80 %, the feed rate of the target extruder was decreased in order to keep the SMEC and the shear rate constant. This was the case with the runs, which were going to be extruded at temperature profile “1” (see Table 25, marked in grey – initial M_D values in brackets).

Table 25: Process parameters of the target extruder, calculated according to the method of Rauwendaal. Initial M_D values are listed in brackets.

n [rpm]		ṁ [kg/h]		SMEC [kWh/kg]		M_D [%]	
Model extruder	*Target extruder*	*Model extruder*	*Target extruder*	*Model extruder*	*Target extruder*	*Model extruder*	*Target extruder*
120	143	2.0	1.7	0.165	0.165	38.7	78.8 *(92.0)*
200	238	2.0	1.8	0.258	0.258	36.0	77.6 *(85.6)*
120	143	2.0	2.0	0.108	0.108	25.2	59.8
200	238	2.0	2.0	0.193	0.193	27.0	64.2

4.2.2 Trials and characterization methods

4.2.2.1 Trials

In this section the materials, machinery and settings, which have been used to produce the intermediate products for pharmaceutical dosage forms on the target extruder, are listed.

Materials

Since similar product properties of the extruded pellets are a measure of a successful transfer of the HME process, the same binary material system as the one from the model extruder was extruded on the target extruder (see 4.1.1.2 - Materials). For the optical RTD measurements the dye *Allura Red AC* from *Sigma-Aldrich* was used again.

Machinery

The binary material system was weighed via a balance and afterwards mixed in the powder blender *MultiBlend® MB015* from *Pharmatech* (variable blend speed: 3 – 30 rpm) [74]. Table 26 shows the respective parts of the extrusion line.

Table 26: Extrusion line (AMS)

Machine	Producer	Type
Twin screw loss-in-weight feeder	Coperion K-TRON GmbH	K-PH-ML-SFS-KT20
Twin screw extruder	Thermo Fisher Scientific Inc.	*PHARMALAB 16*
Die	Thermo Fisher Scientific Inc.	1 cavity, Ø 1.0 mm
Conveyor belt*	Thermo Fisher Scientific Inc.	-
Strand pelletizer	Thermo Fisher Scientific Inc.	VARICUT

*strand was cooled via compressed air

Figure 37: A part of the extrusion line at AMS

Settings and procedure

Preparation of physical mixtures

The polymer matrix material Soluplus® and the API Fenofibrate were weighed in the ratio 9:1. Afterwards the binary material system was mixed at a blend speed of 15 rpm for 10 minutes via the powder blender *MultiBlend® MB015* from *Pharmatech* in order to guarantee a uniform distribution of both powders. This physical mixture (premix) was afterwards fed into the extruder via the twin screw loss-in-weight feeder *K-PH-ML-SFS-KT20* from *Coperion K-TRON GmbH*.

Hot melt extrusion

The co-rotating twin screw extruder *PHARMALAB 16* from *Thermo Fisher Scientific Inc.* with a screw outer diameter of 15.6 mm was used for the hot melt extrusion of the intermediate products at *AMS*. Further extruder parameters are listed in Table 22.
As already mentioned in chapter 3.2.4, it is desirable that the dies of the model and target extruder have got the same die conductance. This guarantees to obtain intermediate products with the same product performance. Since both extruders, including their dies, already exist it is not possible to construct the die of the target extruder as requested. If a complete transfer of the process would be possible (target extruder does not yet exist), the construction of the target die is an important step towards a successful transfer. However, the die conductance of the target extruder was nevertheless calculated by breaking down the die into 5 elements (see Figure 38), for which a respective formula of the die conductance exists (see Table 27).

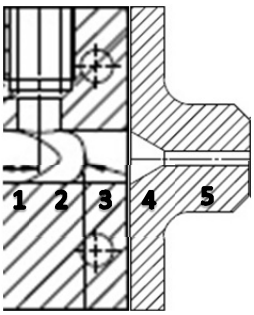

Figure 38: Cross sectional view of the die (target extruder)

Afterwards, the total die conductance was calculated according to equation (26), since the individual die elements are connected in series [40]:

$$K_{target\ extruder} = 9.79 \cdot 10^{-14}$$

Thus the die conductance value of the target extruder is two times the power of ten smaller than the die conductance value of the model extruder ($K_{model\ extruder}$ = 9.86 · 10^{-12}). This difference in *K* causes a greater pressure loss of the melt while passing the die of the target extruder (see equation (25)) and temperature increase due to dissipation.

Table 27: Die conductance values K_i of the respective die elements (target extruder) [37]

Die element	Geometry	Formula	With:	K_i
1	Conical rectangular	$K = \frac{H^{m+2} \cdot (B_1 - B_2)^m \cdot (-1+m)^m}{2^{m+1} \cdot (m+2) \cdot (-L \cdot m)^m \cdot m^m} \cdot \frac{1}{\left(B_2^{\frac{-1+m}{m}} - B_1^{\frac{-1+m}{m}}\right)^m}$	B_1 = 28.5 mm, B_2 = 12.5 mm, H = 10.0 mm, L = 8.0 mm	$K_1 = 6.34 \cdot 10^{-8}$
2	Conical rectangular	see above	B_1 = 12.5 mm, B_2 = 10.0 mm, H = 10.0 mm, L = 9.0 mm	$K_2 = 3.00 \cdot 10^{-8}$
3	Tube	$K = \frac{\pi \cdot R^{m+3}}{2^m \cdot (m+3)} \cdot \left(\frac{1}{L}\right)^m$	L = 7.0 mm, R = 5.0 mm	$K_3 = 1.61 \cdot 10^{-8}$
4	Cone	$K = \frac{\pi}{(m+3) \cdot 2^m} \cdot \left[\frac{3 \cdot \left(\frac{R_C}{r_C} - 1\right)}{m \cdot L \cdot \left(1 - \left(\frac{r_C}{R_C}\right)^{3/m}\right)}\right]^m \cdot {r_C}^{m+3}$	L = 6.0 mm, R_c = 5.0 mm, r_c = 0.5 mm	$K_4 = 4.83 \cdot 10^{-11}$
5	Tube	$K = \frac{\pi \cdot R^{m+3}}{2^m \cdot (m+3)} \cdot \left(\frac{1}{L}\right)^m$	L = 16 mm, R = 0.5 mm	$K_5 = 1.02 \cdot 10^{-13}$

The screw configuration of the target extruder (see Figure 39) was assembled according to the one of the model extruder, whereby the unrolled screw length *Z* (see equation (1)) was used as scale-factor. Due to the significant impact of the screw configuration on the residence time of the material system within the extruder, the configuration is of major importance during the transfer procedure.

Figure 39: Screw configuration AMS-16_1.5 (target extruder)

Regarding the (reverse) conveying and dispersive mixing elements, their pitch in the ratio to the respective screw diameter *D* should be preferably identical. Furthermore, kneading discs should have the same offset angle. Since the portfolio of available screw elements at *AMS* was limited, a screw configuration was assembled that comes as close to the one of the model extruder as possible. In Table 28 the different screw elements of both configurations are listed

and their respective pitch and unrolled screw length *Z* are compared. Kneading blocks are characterized by their offset angle and their total length in L/D.

Table 28: Comparison of both screw configurations (from top to bottom: inlet zone – end of screw)

Element		**Pitch [L/D] or offset angle [°]**		**Z [L/D]**	
Model extruder	*Target extruder*	*Model extruder*	*Target extruder*	*Model extruder*	*Target extruder*
Feed screw	Feed screw	0.44 / 1.33	1	6.35 / 11.94	19.78
Kneading block	Kneading block	45	60	1.78 (total length)	2.5 (total length)
Feed screw	Feed screw	1.33 / 0.89	1	13.65 / 3.26	19.78
Kneading block	Kneading block	45	30	3.11 (total length)	3.75 (total length)
Kneading block	Kneading block	90	90	0.89 (total length)	1.25 (total length)
Feed screw	Feed screw	1.33 / 0.89	1	10.24 / 3.26	14.84
Distributive mixing	Distributive mixing	0.67	1	9.63	6.59
Reverse feed screw	Reverse feed screw	-0.89	-1	1.63	1.65
Feed screw	Feed screw	1.33	1	35.83	39.56
Feed screw	Discharge feed screw	0.67 / 0.44	α	3.21 / 3.17 (total length: 1.11)	1.50 (total length)

Smoothed-particle hydrodynamics (SPH) simulations were carried out by Josip Matić (*RCPE GmbH*) in order to determine the conveying, mixing and pressure generation behaviour of the respective screw elements of the target extruder. This method enables the simulation of free surface flows and mixing processes at complex geometries (here: tightly intermeshing TSEs), since it is a mesh-free method ([75]–[77]). By means of the SPH- and 1D simulation results it could be shown if the assembled screw configuration of the target extruder had to be further optimized. Since the generated temperature profile within the extruder showed no temperature peaks (except in front of the die) and filled kneading blocks were given, the screw configuration AMS-16_1.5 was used for the trials on the target extruder.

Table 29 shows the process set-up of the trials on the target extruder. The process input parameters - screw speed and feed rate - were calculated according to the two existing transfer methods (calculation steps are listed in chapter 4.2.1). The screw and die configuration were not changed during the investigations on the target extruder, like it was the case with the HME on the model extruder.

Table 29: HME process set-up with input parameters according to the respective transfer methods (M: Menges and Feistkorn, R: Rauwendaal)

Run	**Sample**	**Temperature profile [-]**	**screw speed [rpm]**	**feed rate [kg/h]**
1	2_M	1	240	1.6
2	2_R	1	240	1.8

3	1_R	1	140	1.7
4	1_M	1	145	1.6
5	5_R	2	140	2.0
6	5_M	2	145	1.6
7	6_M	2	240	1.6
8	6_R	2	240	2.0

The respective barrel/die temperatures of the two different profiles of the trials on the target extruder are shown in Table 30. Barrel zone 1 – the feeding zone – was not heated in order to avoid powder sticking to the barrel walls. The settings were equal to the temperature profiles on the model extruder. But since the target extruder consists only of 8 barrel elements, the two temperature zones in the middle of the barrel (compared to the temperature profile of the model extruder) were deleted.

Table 30: Temperature profiles of the trials on the target extruder

Temperature profile	**Temperature (set) [°C]**								
	Barrel zone								*Die*
	1	**2**	**3**	**4**	**5**	**6**	**7**	**8**	**9**
1	-	60	80	100	100	110	110	110	120
2	-	60	80	115	115	125	125	125	135

To avoid entrapped air in the polymer strand, an atmospheric venting was installed (barrel element 6 was left open). The strand pelletizer *VARICUT* was used to obtain intermediate products, which could be further analysed. The pellet length was set to 1 mm in order to get pellets with a similar size to the one extruded on the model extruder, which have got an average cylindrical length from 1.0 to 1.5 mm.

Optical RTD measurements

The residence time distribution of the samples, which were extruded on the target extruder, was measured according to the procedure on the model extruder – the same set-up, digital camera *FINEPIX HS25EXR* from *Fujifilm Corporation* and the same dye *Allura Red AC* from *Sigma-Aldrich* were used. The optical RTD measurements of sample 2_M, 2_R, 1_R and 1_M were carried out right after the respective "trial" run and therefore the pellets of each subsequent sample have got a slightly red colour, because there was still some remaining dye in the extruder, which was unfortunately noticed later.

4.2.2.2 Characterization methods

The intermediate products of the HME trials on the target extruder were afterwards characterized by the same methods (DSC, dissolution test and content uniformity) as the intermediate products of the model extruder. This was done in order to enable a comparison of both product properties. For a detailed method description see chapter 4.1.1.3.

4.2.3 Results

4.2.3.1 Differential scanning calorimetry

The evaluation of the DSC graphs of the intermediate products extruded on the target extruder points out the following results:

Table 31: DSC results of the intermediate products produced on the target extruder (1st heating curve; n = 3)

Sample [-]	T_g ± SD [°C]	Δc_p ± SD [J/(g*K)]
1_M	46.6 ± 1.5	0.65 ± 0.11
1_R	45.8 ± 0.5	0.46 ± 0.12
2_M	48.4 ± 0.8	0.54 ± 0.01
2_R	48.3 ± 1.4	0.63 ± 0.10
5_M	47.3 ± 1.2	0.65 ± 0.06
5_R	45.8 ± 0.3	0.46 ± 0.14
6_M	47.1 ± 0.6	0.59 ± 0.02
6_R	46.6 ± 0.9	0.59 ± 0.08

The glass transition temperature of the samples is in the range from 45.8 °C to 48.4 °C (1st heating curve, see Table 31). Sample 2_M and 2_R have got the highest T_g, it is at about 48 °C. These two samples were both extruded at a screw speed of 240 rpm and their feed rate was 1.6 kg/h and 1.8 kg/h, respectively. Looking at the T_gs of the other sample "pairs", such as 1_M and 1_R, and their standard deviations, it can be shown that they do not differ significantly from each other. Sample 1_M has got a T_g of 46.6°C and sample 1_R has got one of 45.8°C, which is a difference of less than one degree (0.8°C). Regarding the standard deviation of sample 1_M (± 1.45°C), this difference is not significant. As an example of the DSC thermograms of the samples extruded with the scaled-down process settings, Figure 40 shows the thermogram of sample 2_R. The blue curve represents the 1st heating run from 0°C to 200°C. At 47.1°C a glass transition is visible. This T_g lies in-between the T_gs of the individual components (see Table 9), which indicates the presence of a glassy solution [78]. To the right of the glass transition of the pellets, there is again an elongated endothermic heat flux visible. But in this case, there is no "small" peak in the range of the melting temperature of Fenofibrate (T_m = 80.5°C) observable. The 2nd heating run (red curve) shows only one glass transition at 47.5°C. There is no melting endotherm visible.

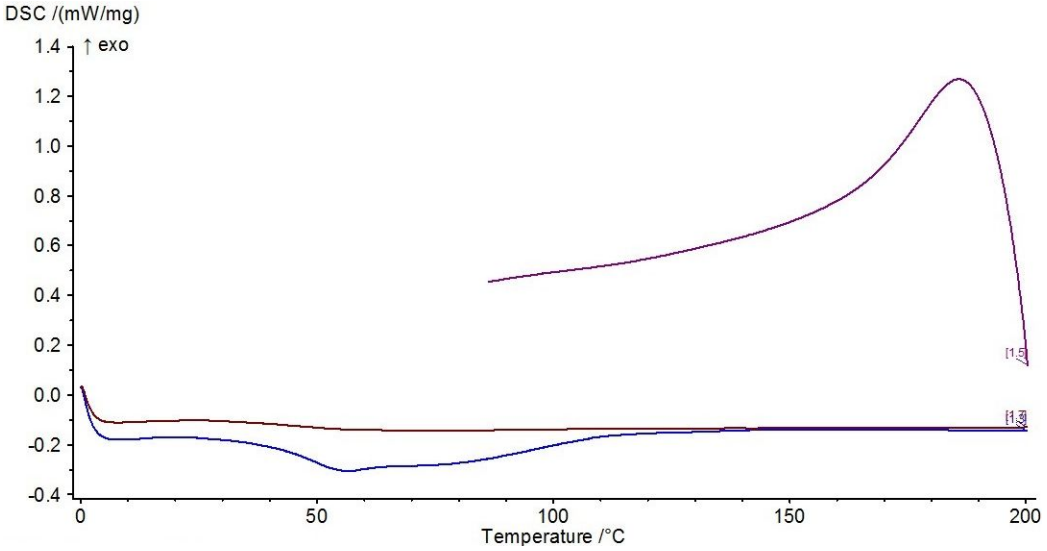

Figure 40: DSC thermogram of sample 2_R. The blue curve shows the 1st heating run, the purple one shows the cooling ramp and the red one shows the 2nd heating run.

Figure 41 shows the first heating run of sample 5_M, 5_R, 6_M and 6_R. These samples were extruded at temperature profile "2" (see Table 29). The course of the curves from sample 5_M and 5_R are nearly identical, whereas the curves from sample 6_M and 6_R differ more. At sample 6_M the melting endotherm next to the glass transition is more elongated.

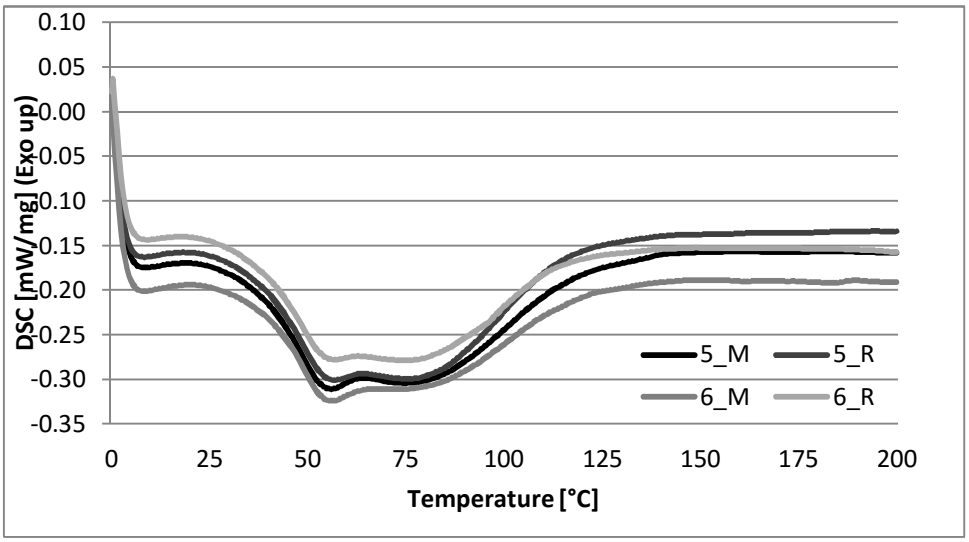

Figure 41: DSC thermograms of sample 5_M, 5_R, 6_M and 6_R (1st heating run)

Figure 42 shows the DSC thermogram of the physical mixture Soluplus® and Fenofibrate (9:1), which was mixed at *AMS*. The cooling ramp of this premix was set, in contrast to the one that was mixed at the *RCPE GmbH*, the same as for the DSC measurements of the pellets. The 1st heating run (blue curve) shows a glass transition at 63.9°C and a melting peak at 82.5°C. These thermal transitions can be assigned to the respective components of the binary material system. The T_g of Soluplus® is although shifted to lower temperatures, because the data sheet states a glass transition of pure Soluplus® at 70°C [59]. This was the case for the physical mixture mixed at the *RCPE GmbH*, too (see 4.1.2.2). There, the T_g of Soluplus® was at 64.5°C and the T_m of Fenofibrate at 82.0°C. This shift in the glass transition temperature is due to the

plasticizing effect of Fenofibrate [71]. The 2nd heating run (red curve) shows only one glass transition at 55.1°C. It lies between the individual T_gs of Soluplus® and Fenofibrate (see Table 9). This again indicates that heating the premix up to 200°C in an aluminium pan is sufficient to generate a glassy solution of the binary material system (see also Figure 27).

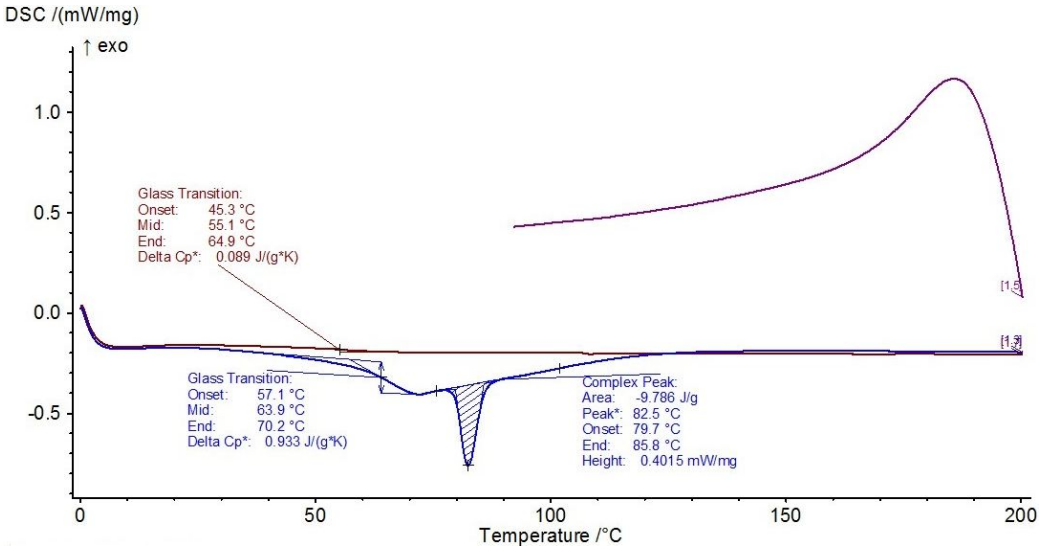

Figure 42: DSC thermogram of the physical mixture Soluplus® and Fenofibrate (9:1) of the target extruder. The blue curve shows the 1st heating run, the purple one shows the cooling ramp and the red one shows the 2nd heating run.

4.2.3.2 Particle size analysis

The particle size analysis results of the pellets gained by the 3D dynamic image analyser *PartAn*^{3D} from *Microtrac Inc*. are shown in Table 32.

Table 32: Mean surface are of the samples (target extruder)

Sample [-]	Mean surface area [mm²]
1_M	6.26
1_R	6.52
2_M	6.37
2_R	6.91
5_M	5.99
5_R	7.04
6_M	6.14
6_R	7.04

The mean surface area of the samples is in the range from 5.99 mm² to 7.04 mm². Since the strand pelletizer was set to a constant pellet length (1 mm) during the HME on the target extruder, the mean surface area of the samples does not differ much compared to the samples that have been extruded on the model extruder (see Table 20).

4.2.3.3 Dissolution test

By testing the dissolution behaviour of the intermediate products extruded on the target extruder, the following results are received:

Table 33: Initial dissolution rate and maximum concentration of dissolved API of each sample (n = 3; target extruder)

Sample [-]	Initial dissolution rate ± SD [µg/(ml*min)]	c_{max} ± SD [µg/ml]	t_{max} [min]
1_M	3.20 ± 0.38	60.74 ± 2.25	30
1_R	1.97 ± 0.34	58.73 ± 4.63	90
2_M	3.43 ± 0.33	64.49 ± 4.39	120
2_R	2.37 ± 0.34	60.36 ± 7.67	90
5_M	2.21 ± 0.16	63.94 ± 7.78	60
5_R	2.68 ± 0.59	57.44 ± 2.82	120
6_M	2.91 ± 0.99	60.02 ± 3.77	60
6_R	3.42 ± 0.25	58.19 ± 3.68	60

Table 33 shows the initial dissolution rate (after 10 minutes of testing) and the maximum concentration of dissolved API of the samples. As already mentioned in chapter 4.2.3.2 the pellets almost have got the same mean surface area (ΔA_s= 1.05 mm²) thus this effect on the dissolution behaviour can be neglected. In the following section the samples will be grouped by the temperature profile set during the HME and their respective drug release will be discussed. The dissolution behaviour of sample 1_M, 1_R, 2_M and 2_R is shown in Figure 43:

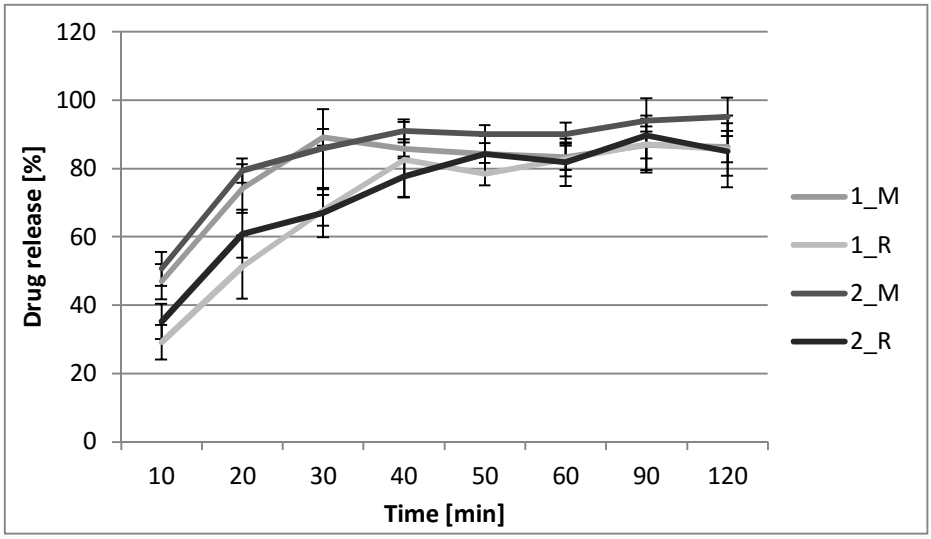

Figure 43: Dissolution profiles of sample 1_M, 1_R, 2_M and 2_R (n = 3)

Looking at the four profiles, it is obvious that the samples whose process settings were calculated according to the transfer method of Menges and Feistkorn (M), have got higher initial dissolution rates (3.20 µg/(ml*min) and 3.43 µg/(ml*min)) than the samples whose process settings were calculated according to the transfer method of Rauwendaal (R) (1.97 µg/(ml*min) and 2.37 µg/(ml*min)). Sample 1_M and 2_M have also got a lower mean

surface area than sample 1_R and 2_R (see Table 32). After 40 minutes of dissolution, the profiles were approaching to each other. At this time, the concentration of dissolved Fenofibrate in the dissolution medium is 58.5 µg/ml, 55.7 µg/ml, 61.7 µg/ml and 52.2 µg/ml, respectively (from 1_M to 2_R). The drug release of sample 2_M is, nevertheless, higher than the one of the other samples until the end of dissolution testing.

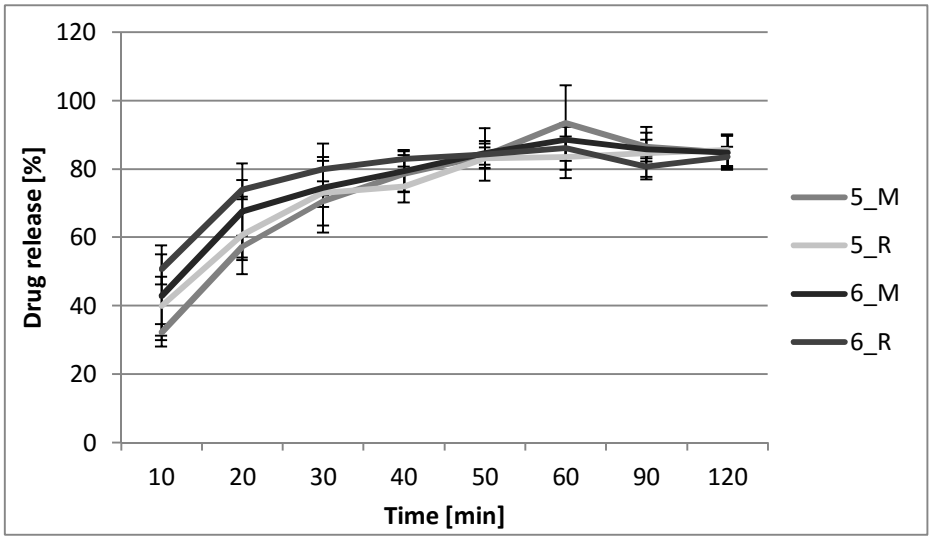

Figure 44: Dissolution profiles of sample 5_M, 5_R, 6_M and 6_R (n = 3, except for sample 6_R after 50 minutes of dissolution: n = 2)

Figure 44 shows the dissolution profiles of sample 5_M, 5_R, 6_M and 6_R. These samples have been extruded at temperature profile "2" (see Table 29). Sample 5_M has got the lowest initial dissolution rate, after 10 minutes just 32 % of the total API content in the pellets was dissolved. Apart from that, the dissolution behaviour of those four samples is similar. Their standard deviations of the dissolved API concentration overlap over the whole testing time and after 40 minutes of testing even their average values were almost the same.

4.2.3.4 Content uniformity test

All samples that have been extruded on the target extruder fulfil the criteria according to the Ph. Eur. – section 2.9.40 *Uniformity of Dosage Units*, after which the acceptance value (AV) of a dosage unit has to be below 15.0 (L1 value). Thus the uniformity of the intermediate products is confirmed (see Figure 45).

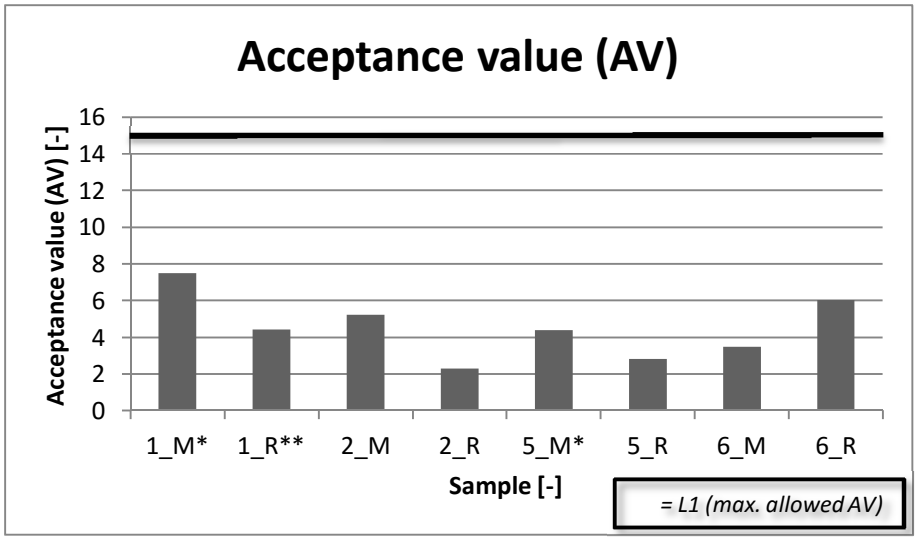

Figure 45: Acceptance values of the intermediate products from the target extruder (*n = 9, **n = 8, the other samples: n = 10)

Sample 2_R has got the lowest AV, namely 2.3. The lower the acceptance value, the more uniform the distribution of the API in the pellets. The other samples have also got low AVs, since they are clearly under the maximum allowed value L1. The AV of sample 1_M (7.5) is nearest to the L1 value.

4.2.4 Summary

The HME process of the intermediate products according to the scaled-down settings (see section 4.2.1) and with the assembled screw configuration *AMS-16_1.5* was possible for all runs. During the extrusion of all samples, a homogeneous strand of the binary material system left the die. The pellets were afterwards characterized by means of DSC analysis, dissolution testing and content uniformity tests. The evaluation of the thermal analysis revealed that during the HME a glassy solution was formed by Soluplus® and the crystalline API Fenofibrate. The 1st heating cycle of the DSC thermograms of all samples shows a T_g in the range from 45.8 °C to 48.4 °C, which is in-between the T_gs of the individual components (see Table 9), and to the right an elongated melting endotherm. Only one glass transition was visible in the 2nd heating cycle of the DSC thermograms. It was shifted to lower temperatures. The only exception is sample 1_M, where the T_g of the second heating run is almost three degrees higher than the one measured in the first heating cycle.

By dissolution testing the drug release behaviour of the intermediate products extruded on the target extruder was investigated. The dissolution profiles of sample 1_M, 1_R, 2_M and 2_R (all temperature profile “1”) show a significant difference in their drug release until 40 minutes of testing, whereby the samples whose process parameters were calculated according to the method of Rauwendaal have got lower dissolution rates (see Figure 43). They reached a drug release of more than 85 % of the total API content just after 90 minutes of dissolution testing. The dissolution profiles of sample 5_M, 5_R, 6_M and 6_R, whereas, are more similar (see Figure 44). These samples have been extruded at temperature profile “2” and their standard

deviations of the dissolved API concentration overlap over the whole testing time. After 40 minutes of dissolution testing even the average values were almost the same. Most of the samples from the target extruder reached the maximum concentration of dissolved Fenofibrate after 60 minutes of testing. However, sample 1_M already reached c_{max}, 60.74 µg/ml, after half an hour of dissolution measurements, which corresponds to 89 % of the total API content.

By the evaluation of the content uniformity tests according to the European Pharmacopoeia – section 2.9.40 *Uniformity of Dosage Units*, the uniformity of all intermediate products extruded on the target extruder could be confirmed. All acceptance values are beneath 8.0, which is 7 size units beneath the maximum allowed AV "*L1*". The highest AV is reached by sample 1_M (7.5). Sample 2_R has got the lowest one (2.3). The smaller the AV of the samples, the more uniform Fenofibrate is dispersed in the pellets.

5 Comparison of Critical Process Parameters and Product Characteristics

By comparing the critical process output parameters and the product characteristics (thermal properties, drug release and CU) of each sample from the HME process on the model extruder and from the respective scaled-down process on the target extruder, it will be shown if the transfer procedure carried out was successful. Furthermore, it will be revealed if the calculation methods from Menges/Feistkorn and Rauwendaal are suitable.

5.1 Critical process parameters

The respective process output parameters of each sample are shown in Table 34 and Table 35. These tables list the HME settings and the output signals, like the mass temperature T_{mass}, pressure p_m, the torque M_D, the SMEC and the minimum/maximum residence time. In the following section, the focus will be on the mass temperature of the binary material system, the SMEC during HME and the residence time distribution. These process output parameters are critical for the product characteristics and, furthermore, scale-independent ([35], [69], [79]).

Table 34: Comparison of the process output parameters of the samples extruded on the model extruder and the samples of the respective scaled-down runs (target extruder)

Sample [-]		**Temperature profile [-]**		**n [rpm]**		**Feed rate [kg/h]**		**p_m [bar]**		**M_D [Nm]**	
Model	*Target*	*Model*	*Target*	*Model*	*Target*	*Model*	*Target*	*Model*	*Target*	*Model*	*Target*
1	1_M	1	1	120	145	2.0	1.6	61	51	27	16
	1_R		1		140		1.7		54		16
2	2_M	1	1	200	240	2.0	1.6	18	43	25	15
	2_R		1		240		1.8		45		15
5	5_M	2	2	120	145	2.0	1.6	23	36	17	11
	5_R		2		140		2.0		40		12
6	6_M	2	2	200	240	2.0	1.6	18	32	19	12
	6_R		2		240		2.0		36		13

Regarding the mass temperature of the samples extruded on the model extruder and their respective scaled-down runs, it becomes apparent that the mass temperature of the samples from the target extruder is always more than 10°C higher than the respective one from the model extruder (see Table 35). The difference in the T_{mass} of sample 1 and 1_M/1_R is even 14°C. The significantly higher mass temperature of the runs carried out at the target extruder is caused by the discharge feed screw elements at the end of the screw configuration *AMS-16_1.5* (see Table 28). These screw elements have a single-start geometry in order to generate the required pressure before the extrusion die [9]. This pressure build-up in front of the die causes the increase in the mass temperature. Furthermore, the die outlet diameter of the

target extruder is 0.5 mm smaller than the die outlet diameter of the model extruder. This difference additionally contributes to the pressure build-up in front of the die. Assessing the samples whose process settings were calculated according to the method of Menges and Feistkorn in comparison to the ones whose settings follow the rules from Rauwendaal, neither the mass temperature of sample 1/2/5/6_M is considerably closer to the T_{mass} of the respective samples from the model extruder nor are sample 1/2/5/6_R.

Table 35: Comparison of the process output parameters of the samples extruded on the model extruder and the samples of the respective scaled-down runs (target extruder)_2

Sample [-]		**T_{mass} [°C]**		**SMEC [kWh/kg]**		**RT_{min} [s]**		**RT_{max} [s]**	
Model	*Target*	*Model*	*Target*	*Model*	*Target*	*Model*	*Target*	*Model*	*Target*
1	1_M	117	131	0.165	0.154	79	66	320	282
	1_R		131		0.139		66		508
2	2_M	118	130	0.258	0.239	52	51	203	450
	2_R		132		0.209		48		448
5	5_M	133	144	0.108	0.102	73	72*	318	153*
	5_R		145		0.088		65*		150*
6	6_M	133	145	0.193	0.186	72	60*	194	150*
	6_R		145		0.159		54*		133*

*measured by means of a stopwatch

However, if the specific mechanical energy consumption (SMEC) of the intermediate products is compared, the SMEC values of the samples from the model extruder correspond well with those of the samples whose process settings were calculated according to the method of Menges and Feistkorn (see Table 35). The closest matching is reached by sample 5 and 5_M. Their SMEC differs only about 0.006 kWh/kg. Thus by calculating the process input parameters according to Menges and Feistkorn, this critical process output parameter can be hold almost constant.

Regarding the RT_{max} values of the samples, there is no correspondence between the intermediate products from the model extruder and their respective scaled-down samples recognizable (see Table 35). In general, the maximum residence time of the samples from the target extruder is longer. Furthermore, their minimum residence time within the extruder is generally shorter. RT_{min} of sample 1_M and 1_R is 66 s, whereas the first pigments left the die not until 79 s of sample 1. The reason for this is obviously the smaller extruder length of the target extruder ($L_{target\ extruder}$ = 624 mm; $L_{model\ extruder}$ = 720 mm). But the minimum residence times of sample 2 and 5 and their scaled-down samples according to Menges and Feistkorn are nevertheless similar. They only differ in 1 second (see Table 35). However, these were not the parameters to investigate. The residence time distribution (RTD) of the melt within the extruder is far more important [79]. The following section, therefore, presents the comparison of the RTD curves of the samples from the model extruder and their respective scaled-down runs. Since the video recordings from the extruded strand of sample 5_M, 5_R, 6_M and 6_R were blurry, the RTD evaluation was not possible. Thus only the residence time distribution of

the other two “sample trios” can be compared. Figure 46 shows the RTD curves of sample 1, 1_M and 1_R. The curve of sample 1 is shifted to the right. Its RT_{min} is more than 10 s longer. Furthermore, the width is wider than the one of the curves from sample 1_M and 1_R. The difference in the maximum a*-value of the samples is due to the varying amount of dye pigments poured into the extruder. In order to avoid this difference for future investigations, a certain amount of dye pigments should be weighed in capsules before and afterwards poured into the extruder.

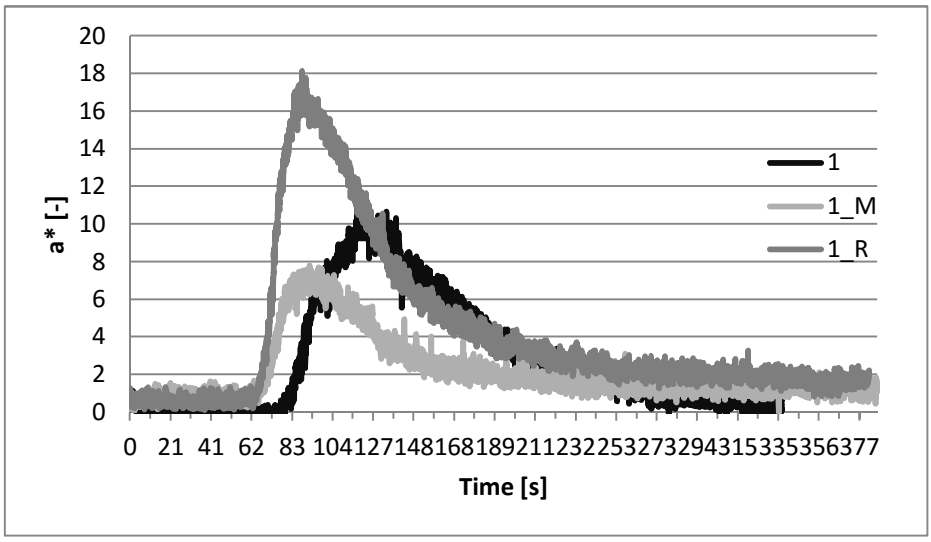

Figure 46: RTD of sample 1, 1_M and 1_R

Figure 47 shows the RTD curves of sample 2, 2_M and 2_R. Their minimum residence time is almost the same. It ranges from 48 s to 52 s. However, the slope of the curve from sample 2_M is obviously smaller. This difference might be caused due to their varying feed rates. The feed rate of sample 2_M was 1.6 kg/h, whereas the one of sample 2 and 2_R was 2.0 kg/h and 1.8 kg/h, respectively. In literature it was reported, that by increasing the feed rate the width of the curve decreases and the slope increases [79]. In this case, the effect on the width of the curves is, however, not recognizable.

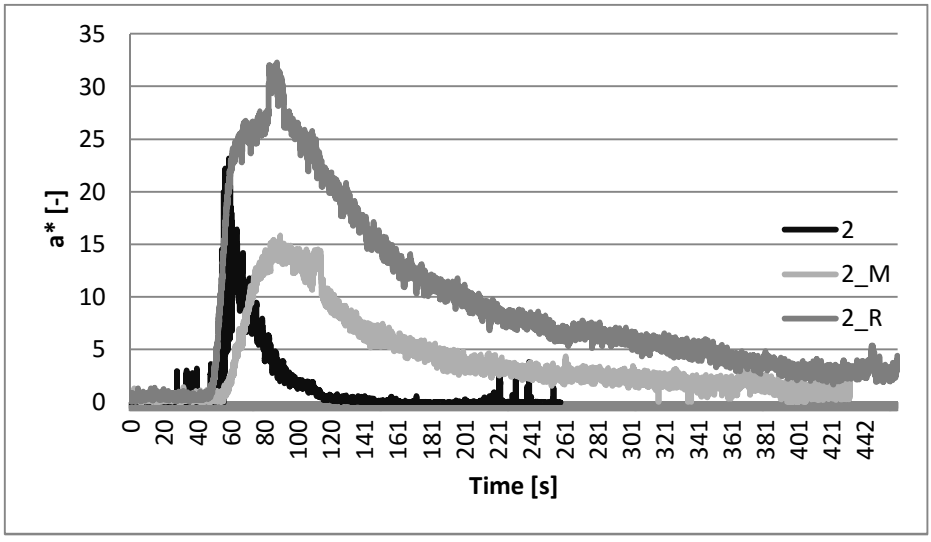

Figure 47: RTD of sample 2, 2_M and 2_R

5.2 Product characteristics

5.2.1 Thermal properties

By comparing the glass transition temperatures of sample 1, 2, 5, 6 and the samples of the respective scaled-down runs, it stands out that those extruded on the model extruder have got a significantly higher T_g (see Table 36). The only exception is sample 5 in comparison to sample 5_M. The intermediate product, which was extruded on the model extruder, has got a T_g of 47.33°C and the one that has been extruded by means of the transferred settings from Menges and Feistkorn has got an identical T_g. It must be noted, however, that the glass transition of sample 5_M has got a standard deviation of more than one degree Celsius.

Table 36: Comparison of the glass transition temperature of sample 1, 2, 5, 6 and the samples of the respective scaled-down runs (1st heating curve, n = 3)

Sample [-]		**T_g ± SD [°C]**		**Δc_p ± SD [J/(g*K)]**	
Model	*Target*	*Model*	*Target*	*Model*	*Target*
1	1_M	49.4 ± 0.6	46.6 ± 1.5	0.60 ± 0.03	0.65 ± 0.11
	1_R		45.8 ± 0.5		0.46 ± 0.12
2	2_M	51.7 ± 1.0	48.4 ± 0.8	0.81 ± 0.03	0.54 ± 0.01
	2_R		48.3 ± 1.4		0.63 ± 0.10
5	5_M	47.3 ± 0.6	47.3 ± 1.2	0.73 ± 0.09	0.65 ± 0.06
	5_R		45.8 ± 0.3		0.46 ± 0.14
6	6_M	50.6 ± 0.1	47.1 ± 0.6	0.60 ± 0.02	0.59 ± 0.02
	6_R		46.6 ± 0.9		0.59 ± 0.08

In the following section each “sample trio” will be considered individually. Every subsequent figure depicts a representative DSC thermogram of a sample, whereby just the first heating cycle is displayed. Figure 48 shows one representative DSC thermogram of sample 1 (blue curve), 1_M (red curve) and 1_R (green curve). The heating curve of sample 1 is significantly shifted to the right. Its T_g is at 48.7°C, whereas the glass transition of sample 1_M and 1_R does take place at a temperature of 46.7°C and 45.8°C, respectively. This change in the glass transition temperature of the samples is caused by their different storage times. Sample 1 was stored for 7 weeks until the DSC analysis were carried out. On the contrary, sample 1_M and 1_R were only stored for 3 weeks. Literature data confirm these findings, as the DSC analysis of HME pellets of Soluplus and Cinnarizine showed that physical aging has occurred after 5 months of storage at 25°C and 0 % relative humidity [80]. During the first two months of investigation the T_g increased almost 5°C and afterwards stagnated, thus the achievement of a final kinetic equilibrium was suggested [80]. Furthermore, enthalpy relaxation occurred in the DSC thermograms, which is the amount of enthalpy that is lost by the sample during the storage period – it reflects its excess enthalpy with respect to its equilibrium state ([81], [82]).
The term “physical aging” is a relaxation phenomenon. Since the sample is rapidly cooled down after leaving the extrusion die, there is not enough time for the polymer chains to arrange in a thermodynamically stable equilibrium - a non-equilibrium system prevails ([82],

[83]). During storage time below T_g the polymer structure relaxes towards the equilibrium by molecular rearrangements (changes in inter-chain packing) and unstable amorphous parts may even crystallize ([81], [83]–[85]). Thus, the performance of amorphous polymers, such as glass transition behaviour and mechanics, may be significantly influenced by physical aging ([82], [84], [85]).

In general, the course of all three curves looks similar, but there is a difference in the wide melting endotherm to the right of the glass transition. Sample 1 shows a small melting peak, which is in the range of the T_m of Fenofibrate (see Table 9), whereas at sample 1_M and 1_R no peak is recognisable. Their difference in storage time might be the reason for the non-present peak in the range of 80.5°C (T_m Fenofibrate). Whereas, the sample from the model extruder was stored for 7 weeks until the DSC analysis were carried out. Sample 1_M and 1_R were stored for only 3 weeks. Thus it is concluded, that after a storage period of 3 weeks Fenofibrate did not recrystallized in the glassy solution, at least crystalline parts were not clear detectable by DSC analysis. [79]. In literature it was reported, that after 10 weeks of storage of HME pellets (Soluplus/Fenofibrate in the ratio 3:1) a recrystallization of Fenofibrate was detected by DSC analysis [70].

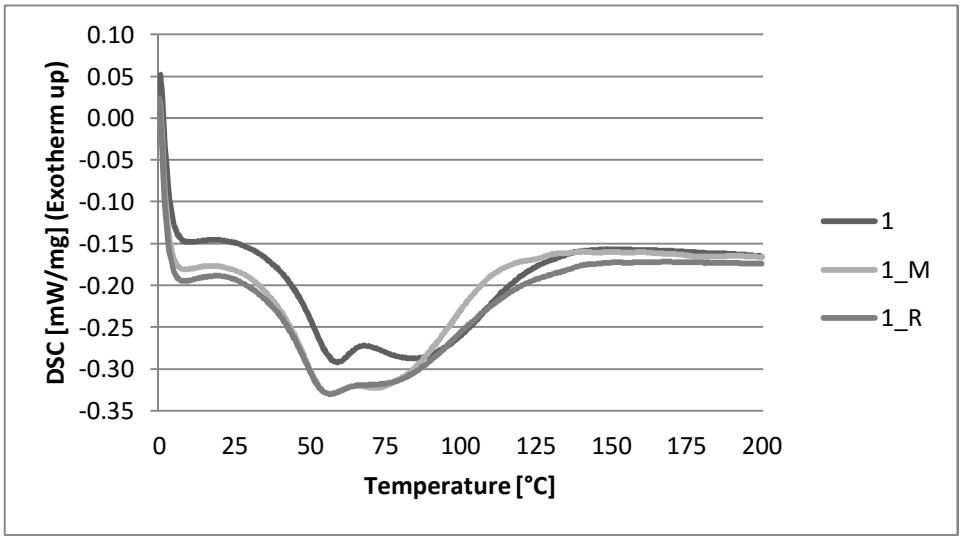

Figure 48: DSC thermograms of sample 1, 1_M and 1_R (1st heating cycle)

In order to investigate, if the glass transition temperature shift to higher temperatures is caused by the different storage times of the samples the DSC measurements of sample 1_M and 1_R were repeated after 7 weeks of storage (storage time of sample 1). The evaluation of the thermal analysis revealed the following results:

Table 37: Comparison of the glass transition temperature of sample 1, 1_M and 1_R with equal storage time (1st heating curve, n = 3)

Sample [-]		**T_g ± SD [°C]**		**Δc_p ± SD [J/(g*K)]**	
Model	*Target*	*Model*	*Target*	*Model*	*Target*
1	1_M	49.4 ± 0.6	49.4 ± 0.3	0.60 ± 0.03	0.63 ± 0.03
	1_R		48.4 ± 2.7		0.66 ± 0.08

By increasing the storage time of sample 1_M and 1_R from 3 to 7 weeks their glass transition temperature rises from 46.6°C to 49.4°C and from 45.8°C to 48.4°C, respectively (see Table 37). Thus the literature findings mentioned above are confirmed. In this case, the average T_g values of sample 1 and 1_M even get equal by analysing them after the same storage time. Regarding the course of the 1st heating run of sample 1_M and 1_R, there is again no peak in the range of the melting temperature of Fenofibrate or at least no recrystallized Fenofibrate parts are detectable by the DSC measurements (see Figure 49).

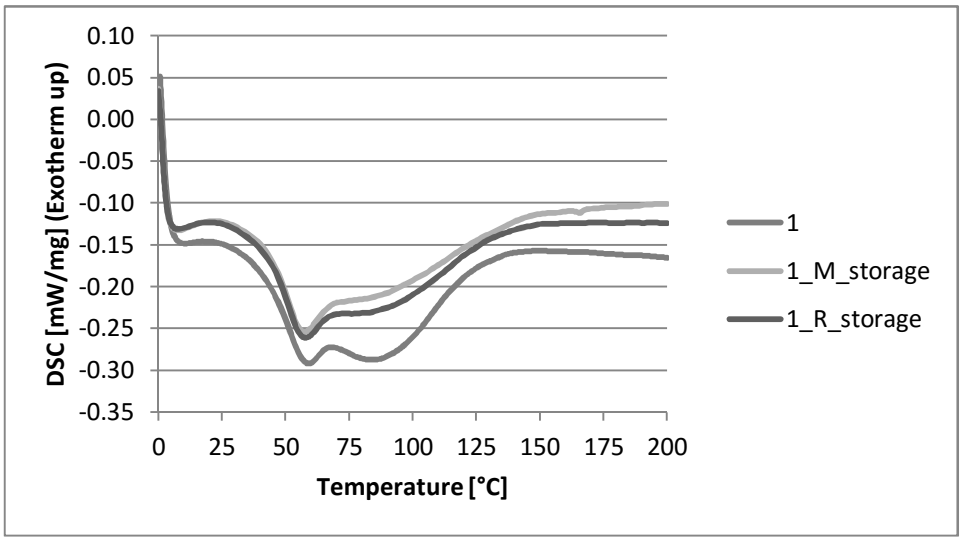

Figure 49: DSC thermograms of sample 1, 1_M and 1_R with equal storage time (1st heating cycle)

The representative DSC thermograms of sample 2, 2_M and 2_R are shown in Figure 50. The heating curve of sample 2 is shifted to the right. This was also the case for sample 1 (see Figure 48). Both samples have been extruded on the model extruder. Sample 2 has got a glass transition temperature of 52.5°C, sample 2_M one of 48.2°C and 2_R has got a glass transition temperature of 47.1°C. Thus the difference in their T_gs (average values) is more than 3°C. The storage time of sample 2 was 15 weeks until the DSC analysis were carried out and besides 12 weeks longer than the one of sample 2_M and 2_M. The physical aging effect can also be seen by comparing the (relaxation) enthalpies of the 3 curves. The one of sample 2 is obviously bigger. Furthermore, it has to be mentioned that the endotherm heat flux of sample 2_R is significant narrower than the one of sample 2 and 2_M.

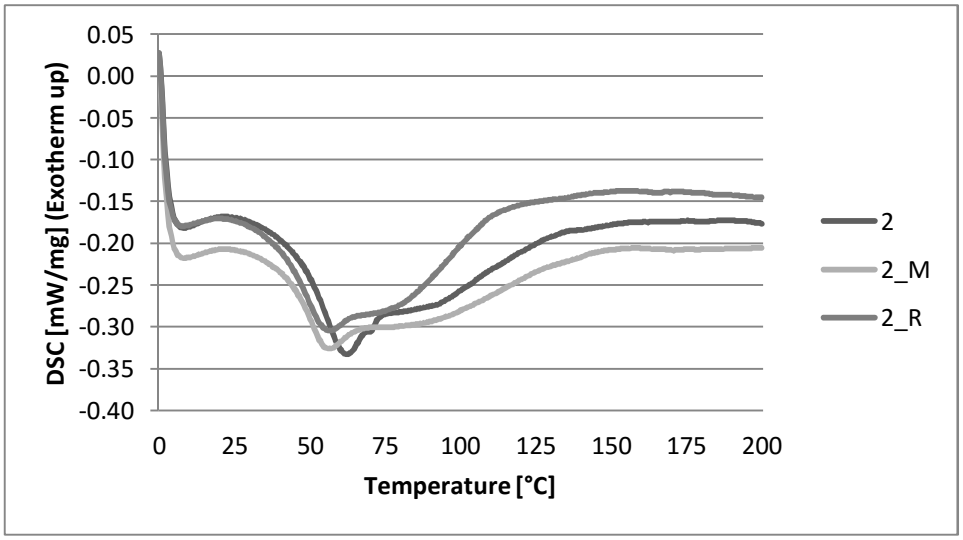

Figure 50: DSC thermograms of sample 2, 2_M and 2_R (1st heating cycle)

Figure 51 shows the 1st heating cycle of sample 5, 5_M and 5_R. The curve of the sample which was extruded on the model extruder is again slightly shifted to the right. The glass transition temperature of sample 5 is 47.9°C, the one of sample 5_M is 47.0°C and sample 5_R has got a T_g of 45.6°C. Regarding their average values (n = 3), the T_g of sample 5 and 5_M is even identical (47.3°C), although their difference in storage period is 4 weeks. In this case sample 5_M might have already reached a thermodynamically stable equilibrium state after a storage time of 3 weeks. Whereas the shape of the curves of sample 2, 2_M and 2_R does not look similar, these do. The heating run of sample 5_M and 5_R is nearly identical. The endotherm heat flux of sample 5_R is just a bit narrower again.

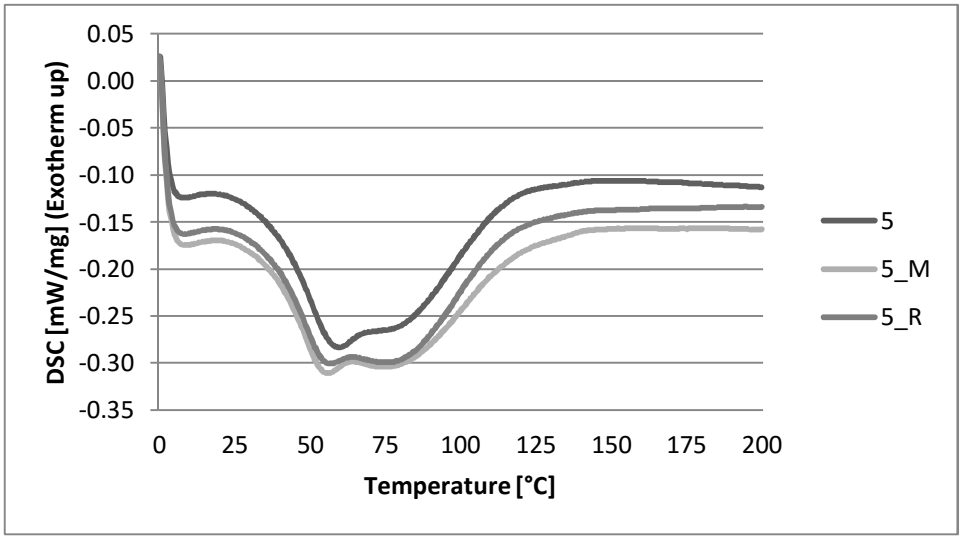

Figure 51: DSC thermograms of sample 5, 5_M and 5_R (1st heating cycle)

The 1st heating cycle of sample 6, 6_M and 6_R is shown in Figure 52. The endothermic heat flux of sample 6_R is again narrower than the one of the others. The curve of sample 6 shows a clearly peak right to the glass transition of the glassy solution of Soluplus® and Fenofibrate. The peak has its maximum around 100°C, leading to the assumption that there was moisture in the pellets. But by means of the electronic moisture analyser *MLS-N* from *KERN & Sohn GmbH*

it was shown, that the moisture content in the pellets from the model extruder, which generally had a longer storage time, do not show up a significantly higher moisture content than the samples from the target extruder (moisture content < 1 %). For closer investigations of the water content of the samples Karl Fischer titration might be the more accurate method.

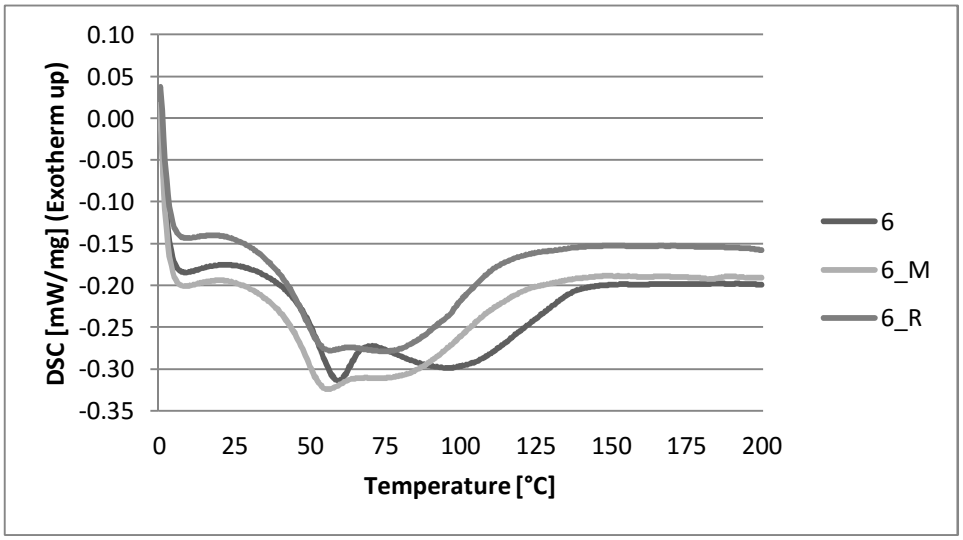

Figure 52: DSC thermograms of sample 6, 6_M and 6_R (1st heating cycle)

Regarding the glass transition temperatures of the samples, they are at 50.7°C, 47.3°C and 45.8°C respectively. That is a difference of almost 5°C. The T_g of sample 6 and 6_M are, however, closer to each other. This was the case for all "sample trios". The T_g of the sample whose process settings were calculated according to the method of Menges and Feistkorn was always closer to the T_g of the respective sample from the model extruder (see Table 36).

The storage time of sample 6 was 18 weeks until the DSC analysis were carried out and besides 15 weeks longer than the one of sample 6_M and 6_R. This can be seen by comparing the (relaxation) enthalpies of the 3 curves. The one of sample 6 is significantly greater. That effect was also visible for sample 2, 2_M and 2_R whose difference in storage period was 12 weeks (see Figure 54).

5.2.2 Dissolution behaviour

The dissolution rate of sample 1 and sample 1_M are almost identical until 30 minutes from the start of the measurement (see Figure 53). Whereas, the dissolution rate of sample 1_R is significantly smaller. Its initial dissolution rate is only 1.97 µg/(ml*min), which equates 29 % of total API content (see Table 38). By comparison, after ten minutes of dissolution testing, the amount of dissolved Fenofibrate of sample 1 and 1_M was 50 % and 47 %, respectively.

Table 38: Comparison of the initial dissolution rate and maximum concentration of dissolved API of sample 1 and the samples of respective scaled-down runs (n = 3)

Sample [-]		**Initial dissolution rate ± SD [µg/(ml*min)]**		**c_{max} ± SD [µg/ml]**		**t_{max} [min]**	
Model	*Target*	*Model*	*Target*	*Model*	*Target*	*Model*	*Target*
1	1_M	3.36 ± 0.17	3.20 ± 0.38	69.57 ± 4.18	60.74± 2.25	120	30

1_R	1.97 ± 0.34	58.73 ± 4.63	90

After 40 minutes of dissolution, the drug release profiles of sample 1_M and 1_R were approaching to each other. As the measurement is completed, they stagnate at a concentration of about 85 % dissolved API content in the dissolution medium. For sample 1, which was extruded on the model extruder, the concentration of dissolved API however rises until the measurement was ended. In the end, 104 % of the total API content is dissolved. Considering the maximum concentration of dissolved API, it was 69.57 µg/ml after 120 minutes for sample 1, it was 60.74 µg/ml after 30 minutes for sample 1_M and 58.73 µg/ml after 90 minutes for sample 1_R.

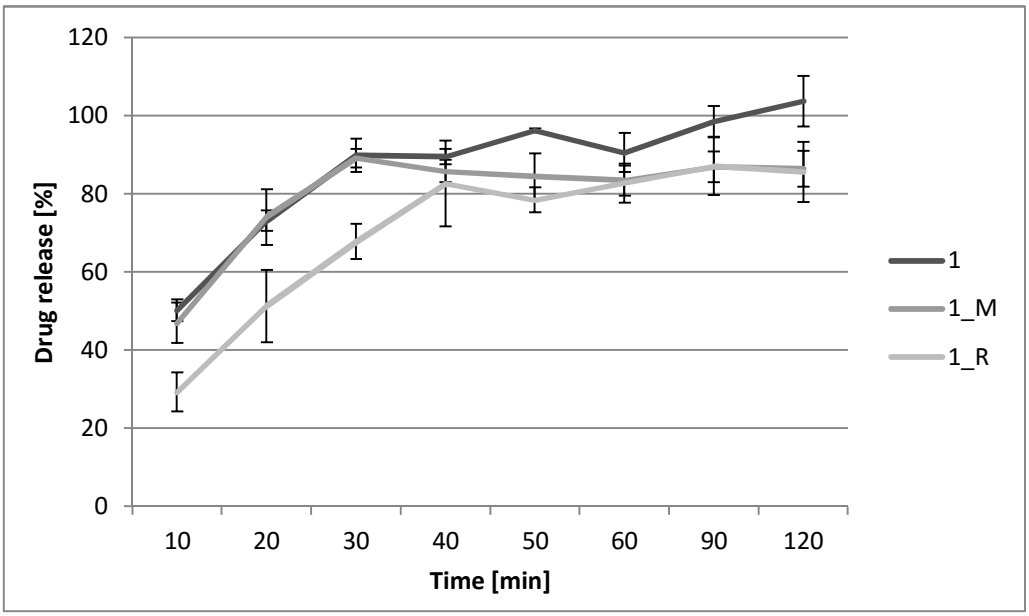

Figure 53: Dissolution profiles of sample 1, 1_M and 1_R (n = 3)

The respective dissolution behaviour of sample 2, 2_M and 2_R is shown in Table 39 and in Figure 54. Up to 50 minutes after the measurement was started, the three profiles differ significantly. Afterwards, the standard deviations of dissolved API concentration of sample 2_M and 2_R are overlapping, but not for sample 2.

Table 39: Comparison of the initial dissolution rate and maximum concentration of dissolved API of sample 2 and the samples of respective scaled-down runs (n = 3)

Sample [-]		**Initial dissolution rate ± SD [µg/(ml*min)]**		**c_{max} ± SD [µg/ml]**		**t_{max} [min]**	
Model	*Target*	*Model*	*Target*	*Model*	*Target*	*Model*	*Target*
2	2_M	4.06 ± 0.11	3.43 ± 0.33	72.76 ± 2.17	64.49 ± 4.39	90	120
	2_R		2.37 ± 0.34		60.36 ± 7.67		90

The differences in the dissolution profiles are especially found in the initial release rate. The initial dissolution rate of sample 2 is 4.06 µg/(ml*min), whereas sample 2_M has got an initial dissolution rate of 3.43 µg/(ml*min) and sample 2_R has got one of 2.37 µg/(ml*min). After ten minutes of dissolution, already 61 % of the total API content of sample 2 was dissolved. At

sample 2_R, however, only 35 % of the total API content was dissolved. In consideration of the drug release profiles over the whole dissolution testing time, it stands out that sample 2 always has got the highest dissolution rate. Its maximum concentration of dissolved Fenofibrate was 72.76 µg/ml after 90 minutes of dissolution (equal to 109 % of total API content). The maximum concentration of dissolved Fenofibrate was 64.49 µg/ml (drug release of 95 %) after 120 minutes for sample 2_M and 60.36 µg/ml (drug release of 90 %) after 90 minutes for sample 2_R.

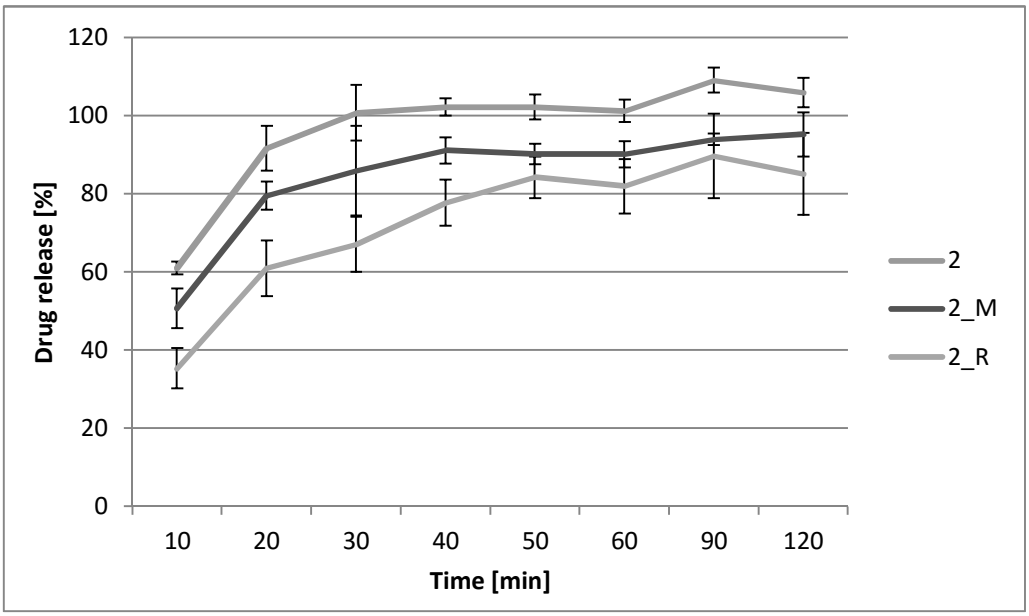

Figure 54: Dissolution profiles of sample 2, 2_M and 2_R (n = 3)

The initial dissolution rates and maximum concentrations of dissolved API of sample 5, 5_M and 5_R are listed in Table 40. With sample 5, a c_{max} of 76.02 µg/ml Fenofibrate was reached after 90 minutes, which corresponds to 113 % of the total API content. The maximum concentration of dissolved Fenofibrate was 63.94 µg/ml (93 % total API content) after 60 minutes for sample 5_M and 57.44 µg/ml (85 % total API content) after 120 minutes for sample 5_R.

Table 40: Comparison of the initial dissolution rate and maximum concentration of dissolved API of sample 5 and the samples of respective scaled-down runs (n = 3)

Sample [-]		**Initial dissolution rate ± SD [µg/(ml*min)]**		**c_{max} ± SD [µg/ml]**		**t_{max} [min]**	
Model	*Target*	*Model*	*Target*	*Model*	*Target*	*Model*	*Target*
5	5_M	3.16 ± 0.20	2.21 ± 0.16	76.02 ± 2.36	63.94 ± 7.78	90	60
	5_R		2.68 ± 0.59		57.44 ± 2.82		120

Looking at the dissolution profiles of the samples shown in Figure 55, it becomes apparent that sample 5 has got a higher dissolution rate than the others since Fenofibrate is faster dissolved in the dissolution medium. After ten minutes, the API concentration was 3.16 µg/ml at sample 5. This corresponds to 47 % of the total API content. The initial dissolution rate of sample 5_M is 2.21 µg/(ml*min) and the one of sample 5_R is 2.68 µg/(ml*min), a difference of

0.47 µg/(ml*min). Regarding the entire period of testing, their drug release behaviour is quite the same. After 120 minutes, 85 % of the total API content was dissolved of both samples. At the same time, 105 % of the total API content of sample 5 was dissolved.

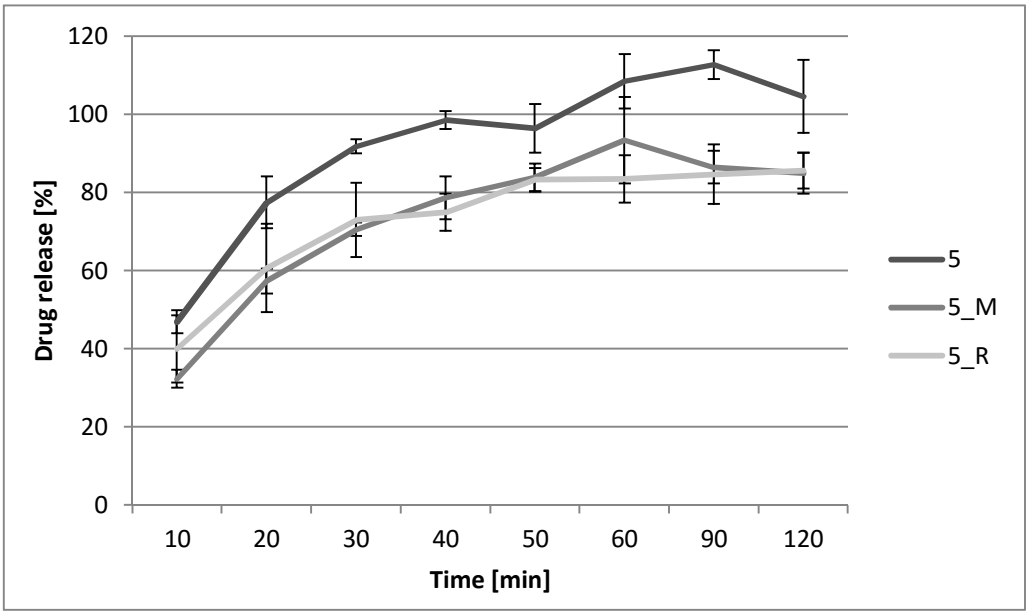

Figure 55: Dissolution profiles of sample 5, 5_M and 5_R (n = 3)

The initial dissolution rates of sample 6 and 6_R are almost the same, namely 3.41 µg/(ml*min) and 3.42 µg/(ml*min) for the latter. For sample 6_M the initial dissolution rate is, on the contrary, just 2.91 µg/(ml*min). It should, however, be mentioned here that the standard deviations of sample 6 and 6_M are greater than the difference in their mean values of the initial dissolution rate (see Table 41). Thus, there is no significant difference between those samples after ten minutes of dissolution. This state lasts for another ten minutes. After 30 minutes of dissolution testing, the drug release of sample 6 was considerably higher than the drug release of the samples of the respective scaled-down runs (6_M and 6_R; see Figure 56).

Table 41: Comparison of the **i**nitial dissolution rate and maximum concentration of dissolved API of sample 6 and the samples of respective scaled-down runs (n = 3)

Sample [-]		**Initial dissolution rate ± SD [µg/(ml*min)]**		**c_{max} ± SD [µg/ml]**		**t_{max} [min]**	
Model	*Target*	*Model*	*Target*	*Model*	*Target*	*Model*	*Target*
6	6_M	3.41 ± 0.83	2.91 ± 0.99	71.47 ± 2.51	60.02 ± 3.77	120	60
	6_R		3.42 ± 0.25		58.19 ± 3.68		60

The maximum concentration of dissolved Fenofibrate was 71.47 µg/ml (106 % of the total API content) after 120 minutes for sample 6, it was 60.02 µg/ml (89 % of the total API content) for sample 6_M and 58.19 µg/ml (86 % of the total API content) for sample 6_R. The samples of the scaled-down runs reached their c_{max} of dissolved Fenofibrate both after 60 minutes. Furthermore, there is no significant difference between their drug release profiles observed

over the entire dissolution testing (see Figure 56). After 120 minutes of testing, their amount of dissolved API in the dissolution medium reached a value of about 85 %.

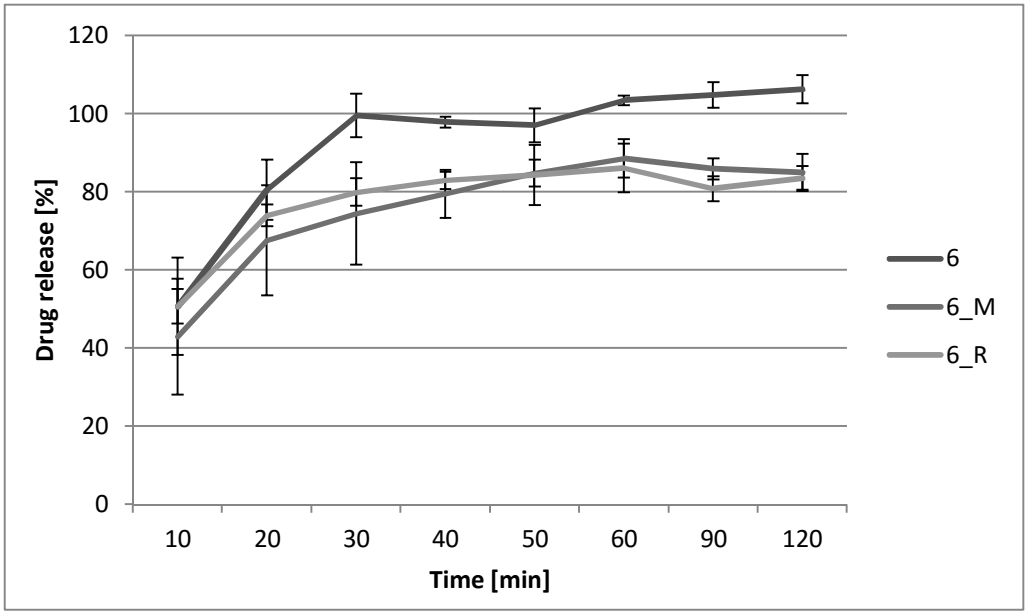

Figure 56: Dissolution profiles of sample 6, 6_M and 6_R (n = 3, except for sample 6_R after 50 minutes of dissolution: n = 2)

In summary, it can be said that after 40 minutes of dissolution testing, the drug release rate of the samples from the model extruder (1, 2, 5 and 6) were considerable higher than the ones from the target extruder. In some cases, there is still an overlap of the standard deviations of the respective samples, but the mean values of the dissolved Fenofibrate content from sample 1, 2, 5 and 6 are always larger. After 120 minutes of testing, the released API content was 104 % for sample 1, 106 % for sample 2, 105 % for sample 5 and it was 106 % for sample 6. Whereas almost all scaled- down samples stagnate at a drug release of 85 % in the end. The only exception is sample 2_M, it released 95 % of the total API content after 120 minutes of dissolution testing. The difference between the overall higher drug release of the samples from the model extruder and their respective scaled-down samples might be explained by their different mass temperatures during HME. The mass temperature of all samples which were manufactured on the target extruder was always more than 10°C higher than the mass temperature of the respective sample on the model extruder (see Table 35). As seen in Figure 31, the mass temperature has an adverse effect on the drug release of the samples from the model extruder. With an increasing mass temperature, the drug release of the samples decreased. It is assumed that the shorter the polymer chains, the better the entrapment of the API. Therefore, the drug release decreases.

In the beginning of the measurements, the initial dissolution rate of the samples from the model and target extruder is often the same - especially for sample 1 and 1_M. Their dissolution profiles are almost identical until 30 minutes of testing. In contrast, the initial dissolution rate of sample 2, 2_M and 2_R differs significantly as well as their entire dissolution profile. This difference, however, cannot be explained by dissimilar particle sizes because their

mean surface area is in the small range from 6.37 mm² to 6.91 mm². As shown by the dissolution profiles of sample 5_M/5_R (see Figure 55) and 6_M/6_R (see Figure 56), a difference in the mean surface area of about 1 mm² does not have a significant influence on the dissolution behaviour of the intermediate products (see Table 32).

Based on these findings, the storage time as possible cause of the occurring differences in the dissolution behaviour of sample 2, 2_M and 2_R remains. Sample 2 was stored for 11 weeks until the dissolution test was carried out, whereas the others were only stored for 2 weeks (Δt = 9 weeks). This was also the case for sample 6 and its scaled-down samples. Regarding the dissolution rates of sample 2 and 6 in comparison to the rates of their respective scaled-down runs, one would assume that by an increasing storage time, the drug release of the samples gets faster and further the maximum concentration of dissolved API content rises. However, literature does not confirm this assumption ([70], [80]). Kalivoda et al. observed a decrease in the dissolution rate from 0 to 10 weeks of storage period [70]. The HME pellets consist of the same binary material system, but the weight ratio is different: Soluplus®:Fenofibrate in the parts 3:1. Tian et al. showed that physical aging, caused by storage of the HME pellets, has an adverse effect on the dissolution behaviour [80]. The drug release decreases over storage time.

Sample 1 and 5 from the model extruder were stored for a couple of days less than their respective scaled-down samples until the dissolution tests were carried out. The main difference of these samples, apart from varying process parameters, which may cause the different dissolution profiles, is their mean surface area. The mean surface area of sample 1 (12.16 mm²) and 5 (11.42 mm²) is almost twice the one from their respective scaled-down runs (see Table 32). The dissolution rate of sample 1 and 5 is nevertheless higher, especially the one of sample 5 (see Figure 55). This effect, however, contradicts the *Nernst-Brunner equation* (see equation (29)), after which the drug release decreases with increasing pellet size and thus a decrease in the surface to volume ratio ([70], [86]).

Summarizing all possible reasons there remains one explanation for the different drug release in the beginning of the dissolution testing. During the measurements it has been observed, that pellets of some samples drop down right after pouring them into the dissolution medium. Other pellets, whereas stayed for more than 70 minutes at the surface of the dissolution medium. This is caused by a similar density of the pellets and the medium. The pellets which are located at the bottom of the vessels show up a higher drug release as the ones located at the surface of the medium because the rotating paddle shears the saturated liquid around the pellets away and “new” medium enables the dissolution of the API to continue again [87]. Thus for future investigations apparatus 1 – “basket” is recommended, since at this apparatus the pellets are all positioned at the same place and therefore this specific influence on the dissolution behaviour of the intermediate products could be avoided.

5.2.3 Content uniformity

The acceptance values of sample 1, 2, 5, 6 and the samples of the respective scaled-down runs are shown in Figure 57. As already mentioned in chapter 4.1.2.5 and 4.2.3.4 their AV is below the maximum allowed value "*L1*" (15.0). Thus, the content uniformity of all intermediate products is confirmed according to the European Pharmacopoeia – section 2.9.40 *Uniformity of Dosage Units* [68]. The lowest AV is reached by sample 5 (0.6), followed by sample 1 (2.7). Both were extruded on the model extruder. In comparison, sample 5_M and 5_R have got an AV of 4.4 and 2.8, respectively. The AV of sample 1_M and 1_R is 7.5 and 4.4, respectively. The AV of sample 1_M is at the same time, the highest one reached. This means, that the API is dispersed the "worst" in the pellets of this sample. However, its AV is still just the half of the maximum allowed value "*L1*". In general, no statement can be made if either the samples with the process settings calculated according to method from Menges and Feistkorn or the samples of the method from Rauwendaal yield to intermediate products with smaller AVs.

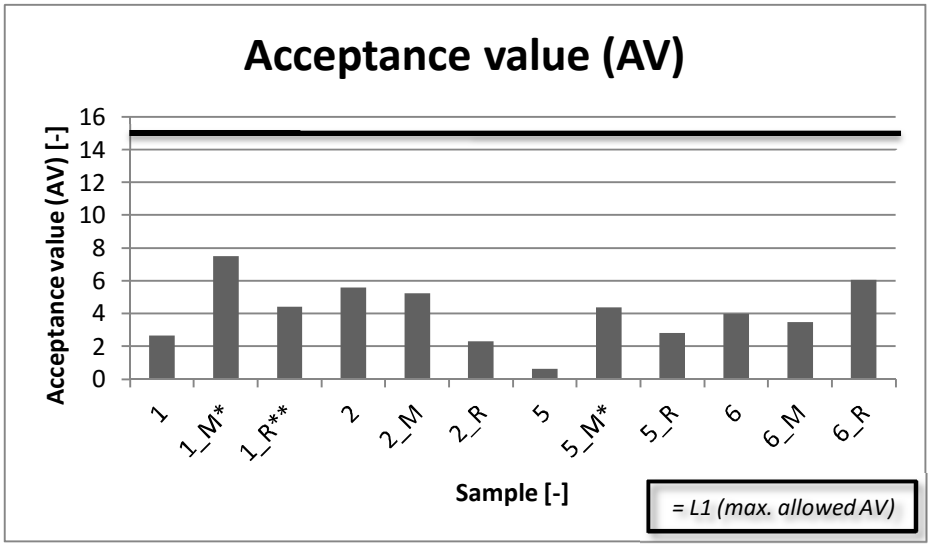

Figure 57: Acceptance values of sample 1, 2, 5, 6 and the samples of the respective scaled-down runs (*n = 9, **n = 8, all other samples: n = 10)

5.3 Summary

The comparison of the critical process parameters (mass temperature, SMEC and RTD) shows that there is only a correlation between the SMEC values of the model extruder and the samples whose process settings were calculated according to the method of Menges and Feistkorn (see Table 35). The samples from Rauwendaal do not show such correspondence. The other scale-independent process parameters of the model extruder also differ from the respective runs on the target extruder. The mass temperature of the runs on the target extruder is even more than 10°C higher than the respective one on the model extruder. The higher temperatures are caused by the single-start geometry of the discharge elements at the end of the screw from the target extruder as well as by their different die geometry ($K_{target\ extruder} < K_{model\ extruder}$). Both initiate a higher pressure build up in front of the die and therefore

the mass temperature increases (see equation (22)). The variations in the residence time distribution of the samples from the model extruder and their respective scaled-down samples are due to their different screw configuration. Since the portfolio of the available screw elements for the target extruder was limited, the optimum configuration could not be assembled. Regarding the conveying elements, there were significant differences in their pitch as well as in their overall D_o/D_i-ratio (see Table 28).

With regard to the thermal properties of the samples, there is a significant shift of the glass transition temperature of the samples from the model extruder to higher values compared to the ones from the target extruder. The only exception is sample 5, which has got an identical T_g to sample 5_M, namely 47.3°C. The shift in the glass transition temperature is due to different storage times of the samples, which was evidenced by repeated DSC measurements of sample 1_M and 1_R as their storage time was equal to the one of sample 1. This effect on the glass transition temperature was also reported in literature [80], [81]. However, it has to be mentioned that the T_g of the samples whose process settings were calculated according to the method of Menges and Feistkorn (M) are always closer to the T_g values of the samples from the model extruder than the samples from Rauwendaal (R) are (see Table 36).

By comparing the dissolution behaviour of the samples from the model and target extruder there is only in the beginning of the tests in some cases a correlation between the drug release rates (see Figure 53). The dissolution rate of sample 2, 2_M and 2_R does, however, not overlap over the whole testing time. The difference in the beginning of the measurement can be explained by the varying drop down behaviour of the pellets within the dissolution medium. The pellets of some samples dropped down far faster and thus the initial drug release of these samples is higher. The saturated liquid layer around them is sheared away by the rotating paddle and therefore new medium enables the dissolution of the API to continue again [87]. Whereas the saturated liquid layer of the pellets, which are positioned at the medium surface, do not experience this shearing of the paddle and thus their drug release stagnates until they also drop down to the bottom of the vessel. The differences in the overall drug release might be due to the varying mass temperatures of the samples during HME (see Table 35). After 120 minutes of dissolution testing, the drug release of the samples from the model extruder was about 105 % of the total API content, whereas the drug release of the samples from the target extruder stagnated at 85 % (only exception sample 2_M: after 120 minutes 95 % of the total API content was released). The mass temperature of the samples from the target extruder is always more than 10°C higher than the one at the model extruder and it is assumed, that shorter polymer chains are able to entrap the API better and are therefore decreasing the overall drug release.

The evaluation of the content uniformity test according to the European Pharmacopoeia – section 2.9.40 *Uniformity of Dosage Units* showed that all samples have got an acceptance value beneath the maximum allowed value “L1” [68]. Thus the API Fenofibrate is uniformly dispersed in every sample.

6 Conclusion and Prospect

Within this master´s thesis a procedure for transferring a hot melt extrusion process from an 18 mm co-rotating twin screw extruder to a 15.6 mm co-rotating twin screw extruder was established. Since both extruders already exist, the procedure was limited by the variation of the process input parameters and the assembly of the screw configuration.

The process analysis on the model extruder in the beginning was useful to understand how the input parameters affect the output parameters and how these on the other hand affect the product characteristics of the intermediate products (pellets). It was shown that the mass temperature was mainly affected by the die temperature set, since the temperature sensor was placed next to the die element and thus measured its thermal radiation. According to the results of 1D simulation, the actual mass temperature in front of the die was more than 40°C higher than the one measured by the sensor. The specific mechanical energy consumption and the residence time within the extruder were, as expected, mainly influenced by the screw speed set. By investigating the influence of the three scale-independent output parameters mentioned above on the product characteristics it was shown, that only the mass temperature of the samples during the HME process affects the dissolution behaviour of them negatively. Regarding the glass transition temperature, there was a decrease in the height of the glass transition recognizable by an increasing T_{mass}. A change in the SMEC value and in the RTD, however, revealed no significant difference in the glass transition temperature, the dissolution behaviour and in the content uniformity of the samples. Therefore, while transferring a HME process of the binary material system Soluplus® and Fenofibrate (9:1) the focus should be on the mass temperature of the extruded samples because it is critical regarding the dissolution behaviour of the intermediate products.

By comparing the process output parameters of the samples from the model extruder and their respective scaled-down samples, there was only a match of the SMEC values of the samples whose process settings were calculated according to the method of Menges and Feistkorn and the ones from the model extruder. Regarding the mass temperatures and the RTDs, there was no correlation. These differences are due to the different die geometries (dissimilar die conductance) and the non-optimum screw configuration of the target extruder. The evaluation of the DSC measurements revealed that the glass transition temperature of the samples from the model extruder is significantly shifted to higher temperatures compared to the samples from the target extruder. This change in T_g was caused by the different storage times of the samples and the physical aging which has taken place. Furthermore, it has to be mentioned, that the samples whose process settings were calculated according to the method of Menges and Feistkorn were, however, always closer to the T_g values of the samples from the model extruder than the ones from Rauwendaal. The dissolution profiles of the samples showed, except of some correlations in the beginning of the testing, no overlap. In addition,

the overall drug release of the samples from the model extruder was always higher than the one of the samples from the target extruder. These differences in the dissolution behaviour of the intermediate products can be explained by the varying drop down of the pellets in the dissolution medium and their different mass temperatures during HME. Therefore, for future investigations of the drug release of such HME pellets, the "basket"-apparatus is recommended in order to avoid the deviations in the beginning of the testing. The content uniformity tests showed that the API is uniformly dispersed in every intermediate product.

In conclusion it can be stated, that calculating the process input parameters according to the existing method from Menges and Feistkorn revealed more promising results. However, the aim of receiving intermediate products with similar thermal and dissolution properties was not completely achieved, since there were significant differences regarding the glass transition temperature (except sample 5 and 5_M: identical T_g) and the overall drug release. Some of these differences nevertheless occurred due to the given boundary conditions (e.g. D_o/D_i-ratio), because the die geometry of the target extruder and the extruder in general existed. Furthermore, the limited portfolio of screw elements has to be added as a restriction of the whole transfer procedure.

If one wants to receive intermediate products with similar properties, a complete transfer of the HME process must be possible. This means that the target extruder does not yet exist or at least where an unlimited assembly of the screw configuration and the die design is possible. However, before carrying out a transfer of the hot melt extrusion process, it is always necessary to have a good understanding of the process itself. This will help for subsequent iteration cycles by knowing which process input parameter needs to be adapted and how each individual parameter affects the product characteristics of the binary material system.

The established procedure for a transfer of the HME process within this thesis can nevertheless be used as guidance for a complete transfer of the HME process. It was shown where to put emphasis on while assembling the screw configuration of the target extruder – namely using the unrolled screw length as scale-factor and choosing screw elements with the same pitch or kneading blocks with the same offset-angle – and how to be sure that the die design reveals the same die conductance value in order to guarantee the same pressure build-up in front of the die. Since it was shown that calculating the process input parameters according to the existing method of Menges and Feistkorn yield more promising coinciding values, this method is recommended for calculating the input parameters. As this method is based on the model theory, it also enables calculating the extruder and screw dimensions for the target extruder in case it does not yet exist.

References

[1] M. Maniruzzaman, J. S. Boateng, M. J. Snowden, and D. Douroumis, “A review of hot-melt extrusion: process technology to pharmaceutical products,” *ISRN Pharm.*, vol. 2012, 2012.

[2] M. A. Repka, N. Langley, and J. DiNunzio, *Melt Extrusion: Materials, Technology and Drug Product Design*. Springer, 2013.

[3] A. Dreiblatt, “13 - Technological Considerations Related to Scale-Up of Hot-Melt Extrusion Processes,” in *Hot-melt Extrusion: Pharmaceutical Applications*, Chichester: John Wiley & Sons Ltd., 2012, pp. 285–300.

[4] M. M. Crowley, F. Zhang, M. A. Repka, S. Thumma, S. B. Upadhye, S. K. Battu, J. W. McGinity, and C. Martin, “Pharmaceutical Applications of Hot-Melt Extrusion: Part I,” *Drug Dev. Ind. Pharm.*, vol. 33, no. 9, pp. 909–926, 2007.

[5] J. Breitenbach, “Melt extrusion: from process to drug delivery technology,” *Eur. J. Pharm. Biopharm.*, vol. 54, no. 2, pp. 107 – 117, 2002.

[6] K. Kohlgrueber, *Co-rotating Twin-screw Extruders: Fundamentals, Technology, and Applications*. Munich: Carl Hanser Publishers, 2008.

[7] I. Ghebre-Selassie and C. Martin, *Pharmaceutical Extrusion Technology*. Marcel Dekker, Inc., 2003.

[8] D. Douroumis, *Hot-Melt Extrusion: Pharmaceutical Applications*. Chichester: John Wiley & Sons Ltd., 2012.

[9] Thermo Fisher Scientific Inc., Ed., “16 mm Screw Elements Portfolio.” 2012.

[10] L. Schenck, G. M. Troup, M. Lowinger, L. Li, and C. McKelvey, “Achieving a Hot Melt Extrusion Design Space for the Production of Solid Solutions,” in *Chemical Engineering in the Pharmaceutical Industry: R&D to Manufacturing*, D. J. am Ende, Ed. John Wiley & Sons, Inc., 2011, pp. 819–836.

[11] Bibliographisches Institut GmbH, “Bioverfuegbarkeit,” *DUDEN*, 2016. [Online]. Available: http://www.duden.de/rechtschreibung/Bioverfuegbarkeit.

[12] M. A. Repka, S. K. Battu, S. B. Upadhye, S. Thumma, M. M. Crowley, F. Zhang, C. Martin, and J. W. McGinity, “Pharmaceutical Applications of Hot-Melt Extrusion: Part II,” *Drug Dev. Ind. Pharm.*, vol. 33, no. 10, pp. 1043–1057, 2007.

[13] Abbott GmbH, “Datensicherheitsblatt für Kaletra Film-Coated Tablets.” 24-Sep-2015.

[14] Reckitt Benckiser Group plc., “RB: health, hygiene, home,” 29-Apr-2016. [Online]. Available: http://www.rb.com/brands/nurofen/.

[15] N.V. Organon, “Gebrauchsinformation NuvaRing.” Apr-2013.

[16] M. Zlokarnik, “Dimensionsanalyse,” in *Scale-up: Modelluebertragung in der Verfahrenstechnik*, Second Edition., Weinheim: Wiley-VCH Verlag GmbH & Co. KGaA, 2005, pp. 3–15.

[17] H. Herwig, “Dimensionsanalyse,” in *Stroemungsmechanik*, First Edition., Wiesbaden: Vieweg +Teubner, 2008, pp. 51–61.

[18] T. Szirtes and P. Rózsa, “Chapter 7 - Structure of physical relations,” in *Applied Dimensional Analysis and Modeling (Second Edition)*, Second Edition., T. S. Rózsa, Ed. Burlington: Butterworth-Heinemann, 2007, pp. 133 – 161.

[19] M. Zlokarnik, “Erarbeitung von pi-Sätzen mittels Matrizenumformung,” in *Scale-up: Modelluebertragung in der Verfahrenstechnik*, Second Edition., Weinheim: Wiley-VCH Verlag GmbH & Co. KGaA, 2005, pp. 17–24.

[20] M. Zlokarnik, “Typische Probleme und Fehler bei der Anwendung der Dimensionsanalyse,” in *Scale-up: Modelluebertragung in der Verfahrenstechnik*, Second Edition., Weinheim: Wiley-VCH Verlag GmbH & Co. KGaA, 2005, pp. 101–112.

[21] M. Zlokarnik, “Maßstabsinvarianz des pi-Raumes – Grundlage der Modelluebertragung,” in *Scale-up: Modelluebertragung in der Verfahrenstechnik*, Second Edition., Weinheim: Wiley-VCH Verlag GmbH & Co. KGaA, 2005, pp. 25–30.

[22] C. Rauwendaal, “Scale-up of Single Screw Extruders,” *Polym. Eng. Sci.*, vol. 27, no. 14, pp. 1059–1068, 1987.

[23] C. I. Chung, “5.5 - Scale-Up Methods,” in *Extrusion of Polymers: Theory and Practice*, Munich: Hanser Publishers, 2000, pp. 309–319.

[24] P. Karlinger, “Grundlagen der Kunststoffverarbeitung 2.” Hochschule Rosenheim, 20-Oct-2010.

[25] G. R. Langecker, “5 - Modelltheorie für Einschneckenmaschinen,” in *Extrusionstechnik*, Leoben: Montanuniversitaet Leoben, 2009, pp. 145–174.

[26] J. R. J. Wagner, E. M. I. Mount, and H. F. J. Giles, “7 - Scale-Up,” in *Extrusion: The definitive processing guide and handbook*, Second Edition., J. R. W. M. M. F. Giles, Ed. Oxford: William Andrew Publishing, 2014, pp. 101 – 104.

[27] B. H. Maddock, “Extruder Scale-Up by Computer,” *Polym. Eng. Sci.*, vol. 14, no. 12, pp. 853–858, 1974.

[28] J. F. Carley and J. M. McKelvey, “Extruder Scale-Up Theory and Experiments,” *Ind. Eng. Chem.*, vol. 45, no. 5, pp. 989–992, May 1953.

[29] G. Menges, J. Wortberg, and A. Mayer, “Model theory—an approach to design series of single-screw extruders,” *Adv. Polym. Technol.*, vol. 3, no. 2, pp. 157–165, 1983.

[30] G. Menges and W. Feistkorn, “Scale-Up of twin screw extruders application and verification with the example of PVC,” *Adv. Polym. Technol.*, vol. 4, no. 2, pp. 123–129, 1984.

[31] C. Conzen, *Numerische und experimentelle Untersuchungen zu Transportvorgängen in Schneckenmaschinen*. Kassel University Press, 2008.

[32] C. Rauwendaal, “10 - Twin Screw Extruders,” in *Polymer Extrusion (Fifth Edition)*, Fifth Edition., C. Rauwendaal, Ed. Hanser, 2014, pp. 697 – 761.

[33] J. R. J. Wagner, E. M. I. Mount, and H. F. J. Giles, “16 - Scale-Up,” in *Extrusion: The definitive processing guide and handbook*, Second Edition., J. R. W. M. M. F. Giles, Ed. Oxford: William Andrew Publishing, 2014, pp. 199 – 201.

[34] C. A. McKelvey, L. Schenck, M. Lowinger, and G. Troup, “Applying extrusion to pharmaceutical formulation design,” presented at the Society of Plastics Engineers Annual Technical Conference, 2007.

[35] J. Thiry, F. Krier, and B. Evrard, “A review of pharmaceutical extrusion: Critical process parameters and scaling-up,” *Int. J. Pharm.*, vol. 479, no. 1, pp. 227 – 240, 2015.

[36] C. Rauwendaal, *Polymer Extrusion*, Fifth Edition. Munich: Carl Hanser Verlag, 2014.

[37] W. Michaeli, *Extrusionswerkzeuge für Kunststoffe und Kautschuk: Bauarten, Gestaltung und Berechnungsmoeglichkeiten*, 2. Auflage. Munich, Vienna: Carl Hanser, 1991.

[38] H. Potente and S. Kramme, "Scale-Up in the Design of Extrusion Dies," *Macromol. Mater. Eng.*, vol. 287, no. 11, pp. 745–749, 2002.

[39] W. Ostwald, "Ueber die Geschwindigkeitsfunktion der Viskositaet disperser Systeme. I.," *Kolloid-Z.*, vol. 36, no. 2, pp. 99–117, 1925.

[40] G. R. Langecker, "12 - Verbindung der Rheologie zur Verarbeitungstechnik anhand von Parallel- und Hintereinanderschaltung von Düsen," in *Rheologie II*, Leoben: Montanuniversitaet Leoben, 2009, pp. 189–191.

[41] W. Geiger and W. Kotte, "Statistische Versuchsplanung," in *Handbuch Qualitaet*, Fifth Edition., Wiesbaden: Vieweg, 2008, pp. 457–461.

[42] J. Antony, "1 - Introduction to Industrial Experimentation," in *Design of Experiments for Engineers and Scientists*, Second Edition., J. Antony, Ed. Oxford: Elsevier, 2014, pp. 1 – 6.

[43] K. Siebertz, D. van Bebber, and T. Hochkirchen, *Statistische Versuchsplanung: Design of Experiments (DoE)*. Springer Berlin Heidelberg, 2010.

[44] J. Antony, "2 - Fundamentals of Design of Experiments," in *Design of Experiments for Engineers and Scientists*, Second Edition., J. Antony, Ed. Oxford: Elsevier, 2014, pp. 7 – 17.

[45] MKS Umetrics, Ed., "User Guide to MODDE." MKS Umetrics AB, 10-Feb-2014.

[46] J. Antony, "6 - Full Factorial Designs," in *Design of Experiments for Engineers and Scientists*, Second Edition., J. Antony, Ed. Oxford: Elsevier, 2014, pp. 63 – 85.

[47] J. Antony, "7 - Fractional Factorial Designs," in *Design of Experiments for Engineers and Scientists*, Second Edition., J. Antony, Ed. Oxford: Elsevier, 2014, pp. 87 – 112.

[48] W. Grellmann, *Polymer Testing*. München: Hanser, 2007.

[49] A. Frick and C. Stern, *DSC-Pruefung in der Anwendung*. Munich: Carl Hanser Verlag, 2006.

[50] T. A. Osswald and G. Menges, *Materials Science of Polymers for Engineers*. Carl Hanser Verlag GmbH & Company KG, 2012.

[51] European Pharmacopoeia 8.0, "Dissolution test for solid dosage forms." 2012.

[52] A. A. Noyes and W. R. Whitney, "THE RATE OF SOLUTION OF SOLID SUBSTANCES IN THEIR OWN SOLUTIONS.," *J. Am. Chem. Soc.*, vol. 19, no. 12, pp. 930–934, 1897.

[53] E. Brunner, "Reaktionsgeschwindigkeit in heterogenen Systemen," *Z Phys Chem*, vol. 43, pp. 56–102, 1904.

[54] W. Nernst, "Theorie der Reaktionsgeschwindigkeit in heterogenen Systemen," *Z Phys Chem*, vol. 47, pp. 52–55.

[55] A. Dokoumetzidis and P. Macheras, "A century of dissolution research: From Noyes and Whitney to the Biopharmaceutics Classification System," *Int. J. Pharm.*, vol. 321, no. 1–2, pp. 1 – 11, 2006.

[56] C. D. Herzfeldt and J. Kreuter, *Grundlagen Der Arzneiformenlehre*. Springer Berlin Heidelberg, 1999.

[57] Sigma-Aldrich Co. LLC, "F6020 - Fenofibrate," 2016. [Online]. Available: http://www.sigmaaldrich.com/catalog/product/sigma/f6020?lang=de&region=AT.

[58] S. Singh, R. J. Inamullah, N. Choudhary, and S. Sharma, "Stability-indicating UV-VIS spectrophotometric method for estimation of atorvastatin calcium and fenofibrate in tablet dosage form," *Bullerin Pharm. Res.*, vol. 2, no. 3, pp. 159–166, 2012.

[59] BASF SE, Ed., “Technical Information Soluplus®.” Jul-2010.

[60] BASF SE, Ed., “Safety Data Sheet Soluplus®.” 19-Dec-2014.

[61] Sigma-Aldrich Co. LLC., Ed., “Sicherheitsdatenblatt Fenofibrat.” 16-Jan-2015.

[62] D. Zhou, G. G. Z. Zhang, D. Law, D. J. W. Grant, and E. A. Schmitt, “Physical stability of amorphous pharmaceuticals: Importance of configurational thermodynamic quantities and molecular mobility,” *J. Pharm. Sci.*, vol. 91, no. 8, pp. 1863–1872, 2002.

[63] Sartorius AG, “Operating instructions: Sartorius Combics 1 plus.” 2004.

[64] Willy A. Bachofen AG Maschinenfabrik, “TURBULA®: Dreidimensionaler Schuettelmischer.” 2015.

[65] Coperion GmbH, “Datenblatt Verfahrensteil.” 2015.

[66] J. E. Agudo, P. J. Pardo, H. Sánchez, Á. L. Pérez, and M. I. Suero, “A Low-Cost Real Color Picker Based on Arduino,” *Sensors*, vol. 14, no. 7, p. 11943, 2014.

[67] Phenomenex Inc., “Luna: HPLC column.” 2015.

[68] European Pharmacopoeia 7.0, “Uniformity of dosage units.” 2008.

[69] D. J. Ende, *Chemical Engineering in the Pharmaceutical Industry: R&D to Manufacturing*. Wiley, 2011.

[70] A. Kalivoda, M. Fischbach, and P. Kleinebudde, “Application of mixtures of polymeric carriers for dissolution enhancement of fenofibrate using hot-melt extrusion,” *Int. J. Pharm.*, vol. 429, no. 1–2, pp. 58 – 68, 2012.

[71] K. Eggenreich, S. Windhab, S. Schrank, D. Treffer, H. Juster, G. Steinbichler, S. Laske, G. Koscher, E. Roblegg, and J. G. Khinast, “Injection molding as a one-step process for the direct production of pharmaceutical dosage forms from primary powders,” *Int. J. Pharm.*, vol. 505, no. 1–2, pp. 341 – 351, 2016.

[72] V. G. Rathod, V. Kadam, S. B. Jadhav, M. Zamiruddin, V. B. Bharkad, and S. P. Biradar, “IMMEDIATE RELEASE DRUG DELIVERY SYSTEM: A REVIEW,” *World J. Pharm. Pharm. Sci.*, vol. 3, no. 6, pp. 545–558, 2014.

[73] Thermo Fisher Scientific Inc., “Product specifications: Thermo Scientific PHARMA HME.” 2008.

[74] Pharmatech, “Pharmatech Multiblend.” 2016.

[75] J. J. Monaghan, “Simulating Free Surface Flows with SPH,” *J. Comput. Phys.*, vol. 110, no. 2, pp. 399 – 406, 1994.

[76] P. Cleary and M. Robinson, “Understanding viscous fluid transport and mixing in a twin screw extruder,” presented at the 8th International Conference on Metallurgical and Process Industry on Computational Fluid Dynamics in Oil & Gas, Metallurgical and Process Industries (CFD2011), Trondheim, Norway, 21-23 June 2011, Trondheim, 2011, p. 7.

[77] A. Eitzlmayr and J. Khinast, “Co-rotating twin-screw extruders: Detailed analysis of conveying elements based on smoothed particle hydrodynamics. Part 1: Hydrodynamics,” *Chem. Eng. Sci.*, vol. 134, pp. 861 – 879, 2015.

[78] A. Kalivoda, “Solubility enhancement of poorly water-soluble drugs by solid dispersion,” Heinrich-Heine-Universitaet Duesseldorf, Duesseldorf, 2012.

[79] S. Laske, A. Witschnigg, R. K. Selvasankar, and C. Holzer, “Measuring the residence time distribution in a twin screw extruder with the use of NIR-spectroscopy,” *J. Appl. Polym. Sci.*, vol. 131, no. 6, p. n/a–n/a, 2014.

[80] B. Tian, L. Zhang, Z. Pan, J. Gou, Y. Zhang, and X. Tang, “A comparison of the effect of temperature and moisture on the solid dispersions: Aging and crystallization,” *Int. J. Pharm.*, vol. 475, no. 1–2, pp. 385 – 392, 2014.

[81] V. K. Kakumanu and A. K. Bansal, “Enthalpy Relaxation Studies of Celecoxib Amorphous Mixtures,” *Pharm. Res.*, vol. 19, no. 12, pp. 1873–1878, 2002.

[82] D. Cangialosi, V. M. Boucher, A. Alegria, and J. Colmenero, “Physical aging in polymers and polymer nanocomposites: recent results and open questions,” *Soft Matter*, vol. 9, no. 36, pp. 8619–8630, 2013.

[83] D. J. Hourston, M. Song, A. Hammiche, H. M. Pollock, and M. Reading, “Modulated differential scanning calorimetry: 2. Studies of physical ageing in polystyrene,” *Polymer*, vol. 37, no. 2, pp. 243 – 247, 1996.

[84] K. Liao, D. Quan, and Z. Lu, “Effects of physical aging on glass transition behavior of poly(dl-lactide),” *Eur. Polym. J.*, vol. 38, no. 1, pp. 157 – 162, 2002.

[85] L. C. E. Struik, “Physical aging in plastics and other glassy materials,” *Polym. Eng. Sci.*, vol. 17, no. 3, pp. 165–173, 1977.

[86] M. K. SARFRAZ, M. AKHTAR, N. RAHMAN, and K. H. Yuen, “Influence of Drug Solubility, Binders and Pellet Size in Formulating Sustained Release Pellets,” *Lat. Am. J. Pharm*, vol. 29, no. 8, pp. 1352–7, 2010.

[87] SMI-LabHut Ltd., “Shear Rate & Sink Conditions,” *Labhut*, 14-Jun-2016. [Online]. Available: http://www.labhut.com/education-centre/about-dissolution-testing/shear-rate-sink-conditions.html.